공학박사학위논문

Synthesis and Characterization of Sulfonated Poly(arlyene ether sulfone) based Polymeric Materials and Their Application in Fuel Cells Operating at High-Temperature and Low Humidity Conditions

술폰산 폴리(아릴렌 에테르 술폰)을 기반으로 한 고분자 물질의 합성 및 분석과 이의 고온, 저가습 구동용 연료전지 적용에 관한 연구

2017년 2월

서울대학교 대학원

화학생물공학부

김 기 현

술폰산 폴리(아릴렌 에테르 술폰)을 기반으로 한 고분자 물질의 합성 및 분석과 이의 고온, 저가습 구동용 연료전지 적용에 관한 연구

Synthesis and Characterization of Sulfonated Poly(arlyene ether sulfone) based Polymeric Materials and Their Application in Fuel Cells Operating at High-Temperature and Low Humidity Conditions

지도교수 이 종 찬 박사

이 논문을 공학박사학위 논문으로 제출함.

2017 년 2 월

서울대학교 대학원

화학생물공학부

김 기 현

김기현의 박사학위논문을 인준함.

2017 년 2 월

위 원 장 (인)

부위원장 (인)

위 원 (인)

위 원 (인)

위 원 (인)

Synthesis and Characterization of Sulfonated Poly(arlyene ether sulfone) based Polymeric Materials and Their Application in Fuel Cells Operating at High-Temperature and Low Humidity Conditions

by

Kihyun Kim

Adviser: Professor Jong-Chan Lee, Ph. D.

Submitted in Partial Fulfillment
of the Requirements for the Degree of
DOCTOR OF PHILOSOPHY

February, 2017

School of Chemical and Biological Engineering
College of Engineering
Graduate School
Seoul National University

Abstract

This study presents synthesis and characterization of sulfonated poly(arylene ether sulfone) (SPAES) based polymeric materials for application in polymer electrolyte membrane fuel cells operating at high-temperature and low humidity conditions. Especially, SPAES-based polymer electrolyte membranes having various structures have been described in detail. Firstly, semi-interpenetrating polymer network (semi-IPN) membranes based on SPAES are developed for application in polymer electrolyte membrane fuel cells operating at high temperature (> 80 ℃) and low relative humidity (< 50% RH) conditions. Two types of semi-IPN membranes using different cross-linkers are simply prepared by *in-situ* casting and thermal-initiated radical polymerization of vinyl phosphonic acid (VPA) and two kinds of cross-linkers such as diethylene glycol dimethacrylate (DEGDMA) and bis(2-(methacryloyloxy)ethyl) phosphate (BMAEP), respectively, in *N*,*N*-dimethylacetamide solutions of SPAES. The incorporation of VPA units into the SPAES based membrane system improves the proton conductivity especially at high temperature and low humidity conditions. In addition, all the cross-linkers such as DEGDMA and BMAEP, prevent the decrease in the mechanical and chemical stabilities by the presence of aliphatic linear poly(vinyl phosphonic acid)

chains in the semi-IPN membranes. Furthermore, the semi-IPN membrane using BMAEP as the cross-linker can prevent the decrease of the proton conductivity by the formation of cross-linked structures because the additional phosphonic acid group in BMAEP can make the additional proton conducting pathways in the semi-IPN membrane. The fuel cell performances of membrane-electrode assemblies (MEAs) prepared with the semi-IPN membranes using DEGDMA (180 mW cm^{-2} at 120 ℃ and 40% RH) and BMAEP (187 mW cm^{-2} at 120 ℃ and 40% RH) are found to be superior to that of the MEA from the SPAES membrane (145 mW cm^{-2} at 120 ℃ and 40% RH). Durability test results at the operating conditions indicate that all the semi-IPN membranes are electrochemically very stable maintaining the low hydrogen crossover and high power densities.

Secondly, a series of pore-filling membranes are prepared by impregnating porous cross-linked benzoxazine-benzimidazole copolymer P(*p*BUa-*co*-BI) substrates with SPAESs having different degree of sulfonation for polymer electrolyte membrane fuel cells operating at high-temperatures (> 80 ℃) and low-humidity (< 50% RH) conditions. The SPAESs are synthesized by reacting 4,4'-dihydroxybiphenyl with the mixtures of disulfonate-4,4'-difluorodiphenylsulfone and 4,4'-difluorodiphenylsulfone in different ratios. The porous P(*p*BUa-*co*-BI) substrates are prepared by extracting dibutyl phthalate (DBP) included in P(*p*BUa-*co*-BI) films using methanol. The P(*p*BUa-*co*-BI) films are prepared by stepwise

heating the casted *N*,*N*-dimethylacetamide solution containing the mixtures of poly[2,2′-(*m*-phenylene)-5,5′-bibenzimidazole] (PBI), 3-phenyl-3,4- dihydro-6-*tert*-butyl-2*H*-1,3-benzoxazine (*p*BUa), and DBP to 220 ℃. The pore-filling membranes are found to have much improved dimensional stability and mechanical strength compared with the SPAES membranes. Although the proton conductivity values of the pore-filling membranes are slightly smaller than those of the SPAES membrane, their cell performance is superior to that of the SPAES membrane at 120 ℃ and 40% RH conditions because ultrathin pore-filling membranes (15-20 μm) having high mechanical strength can be prepared and they can contain a larger content of chemically-bound water

Thirdly, proton conductive porous substrates consisting of cross-linked benzoxazine-benzimidazole copolymers are developed for practical application of reinforced pore-filling membranes in polymer electrolyte membrane fuel cells operating at high-temperatures (> 80 ℃) and low relative humidity (< 50% RH) conditions. The porous proton conductive substrates are prepared by casting solution mixtures of sodium 3-(4-sulfonatophenyl)-3,4-dihydro-2*H*-1,3 benzoxazine-6-sulfonate (*p*S) and poly[2,2′-(*m*-phenylene)-5,5′-bibenzimidazole] (PBI) with dibutyl phthalate (DBP) as a porogen in *N*,*N*-dimethylacetamide, followed by subsequent stepwise heating to 220 ℃ and extraction of DBP from the P(*p*S-*co*-BI) films using methanol. The resulting porous substrates are found

to have mechanically robust cross-linked structures, tunable hydrophilicity, and reasonably high proton conductivity. A pore-filling membrane is prepared by impregnating the porous substrate with SPAES having the degree of sulfonation of 70 mol%. The pore-filling membrane exhibits much improved dimensional stability and mechanical strength compared to the linear SPAES membrane and its proton conductivity and cell performance are found to be superior to the pore-filling membrane prepared using the porous substrate based on cross-linked benzoxazine-benzimidazole copolymers without any proton conductive acid groups.

Finally, we propose a simple and effective cross-linking technology for the design of a high performance cross-linked SPAES (C-SPAES) membrane using perfluoropolyether (PFPE) as a novel cross-linker for fuel cell applications. The C-SPAES membrane is prepared by *in-situ* casting and heating the polymer mixture solution of SPAES with chloromethyl side groups and PFPE. The C-SPAES membrane shows much improved physicochemical stability and comparable proton conductivity compared with the SPAES membrane due to the finely phase-separated morphology induced from the cross-linked polymer network structure using PFPE. Under practical operating conditions of automotive fuel cells (90 ℃, 50% RH, and 150 kPa), membrane electrode assembly from the C-SPAES membrane shows an outstanding cell performance (1.17 W cm^{-2} at 0.65

V) compared with that from the SPAES membrane (0.85 W cm^{-2} at 0.65 V) mainly due to the enhanced interfacial compatibility between the C-SPAES membrane and electrode surfaces.

Keyword: Sulfonated poly(arylene ether sulfone), Polymer electrolyte membrane fuel cell, Semi-interpenetrating polymer network membrane , pore-filling membrane, cross-linked membrane.

Student Number: 2013-30277

TABLE OF CONTENT

Chapter 2

Semi-Interpenetrating Network Electrolyte Membranes Based on Sulfonated Poly(arylene ether sulfone) for Fuel cells at High Temperature and Low Humidity Conditions

Chapter 3

Sulfonated Poly(arlyene ether sulfone) Based Semi-Interpenetrating Polymer Network Membranes Containing Cross-Linked Poly(Vinyl Phosphonic Acid) Chains for Fuel Cell Applications at High Temperature and Low Humidity Conditions

Chapter 4

Highly Reinforced Pore-Filling Electrolyte Membranes from Sulfonated Poly(arylene ether sulfone)s for High-Temperature Fuel Cell Applications

Chapter 5

Proton Conductive Porous Substrate Supported Sulfonated Poly(arylene ether sulfone) Pore-Filling Membrane for High-Temperature Fuel Cell Applications

Chapter 6

A Simple and Effective Cross-Linking Technology for the Design of a High-Performance Proton Exchange Membrane for Automotive Fuel Cell Applications

List of Tables

List of Figures

Chapter 1

Introduction

1.1. Polymers Electrolyte Membrane Fuel Cells

Fuel cell technology has received much attention due to its great potential as a clean and efficient energy conversion system [1]. A Fuel cell is a device that can convert chemical energy in fuels directly into electrical energy, and the efficiency of the fuel cell reaches as high as 60% in electrical energy conversion and overall 80% in the co-generation of thermal and electrical energies with the more than 90% of major pollutants reduction [2]. Fuel cells are categorized as follows: 1) polymer electrolyte membrane fuel cells (PEMFC), solid oxide fuel cells (SOFCs), alkaline fuel cells (AFCs), phosphoric acid fuel cells (PAFCs) and molten carbonate fuel cells (MCFCs) (**Table 1.1)** [3]. PEMFCs, among these types of fuel cells, are being developed as electrical power sources for portable devices and automobile transportations. Compared with other type of fuel cells, PEMFCs are well-suited for these applications for the following reasons: operating at relatively low-temperature ranges (50-200 ℃), short start-up, and transient-response times etc. (**Figure 1.1**) [4]. PEMFCs are composed of polymer electrolyte membrane, catalyst layer with carbon support, gas diffusion layer and bipolar plate. Polymer electrolyte membrane is a key component restricting the overall performance of the PEMFC systems. Polymer electrolyte membranes is designed to conduct

protons (from the anode to the cathode), while acting as a barrier preventing the mixing of fuels. This was done so that the polymer electrolyte membrane should meet the following characteristics: high proton conductivity, good mechanical properties, high thermo-oxidative stability, low permeability of fuels and oxidants, and excellent physical stability during the operation, as well as low cost of production [5]. More specifically, the U.S. Department of Energy (DOE) has established a guideline of 120 °C and 50% relative humidity as the target operating conditions for automobile applications [6]. Therefore, recent studies about the polymer electrolyte membranes have focused on the design of better performing polymer electrolyte membranes under operating conditions of high temperatures (> 80 °C) and low humidity (< 50%RH).

1.2. Sulfonated Poly(arylene ether sulfone)

Poly(arylene ether sulfone) and its derivatives (**Figure 1.2(a)**) are well-known engineering thermoplastics that have been widely used in industries due to their high thermal stabilities and excellent mechanical properties, as well as resistance to thermo-oxidation and hydrolysis by acids and bases [7]. In addition, structure diversity of these polymers through various chemical modifications makes it possible to use modified polymers in advanced industrial fields such as electronic and energy devices. Particularly, the development of modified poly(arylene ether sulfone)s without deterioration of their excellent physicochemical properties is one of the great attention in the field of polymer electrolyte membranes for fuel cell applications [8]. Sulfonated poly(arylene ether sulfone)s prepared by attaching sulfonic acid groups through chemical modification (post-sulfonation method) have been studied intensively since the pioneering work of Noshay and Robeson, who developed a mild sulfonation method for the bisphenol-A based poly(arylene ether sulfone)s [9]. Various sulfonation agents have been used for this modification method such as chlorosulfonic acid and a sulfur trioxide–triethyl phosphate complex [9]. In these post-sulfonation reactions, however, the sulfonic acid group is usually attached to the activated *ortho* position to the aromatic ether

linkage, as shown in **Figure 1.2(b).** In the case of the bisphenol-A-based poly(ether sulfone) systems, no more than one sulfonic acid group per repeating unit could be attached. Kerres *et al*. reported an alternative sulfonation procedure based on a series of modification steps including metalation–sulfonation–oxidation using commercial polysulfone [10]. This research had great attention because it is the first report of sulfonation effect on the deactivated sites of the polysulfone repeating unit (**Figure 1.2(c)**). The first report of the synthesis of sulfonated poly(arylene ether sulfone)s using a sulfonated monomer such as 4,4'-dichlorodiphenylsulfone was from McGrath *et al*. and they provided general procedures for direct polymerization of sulfonated poly(arylene ether sulfone) random copolymers (**Figure 1.3)** [8]. Based on a modification of this process, we have synthesized sulfonated poly(arylene ether sulfone)s having a different degree of sulfonation and have utilized these polymers as membrane components for the design of better-performing polymer electrolyte membranes in fuel cells operating at high temperature and low humidity conditions. Although the currently important polymer electrolyte membranes in fuel cells are the perfluorinated ionomer based membranes such as Nafion®, they are known to have some significant technical limitations at high temperature operation such as low thermal and mechanical stabilities at the temperature above 80 ℃ as well as high fuel permeability (**Figure 1.4**) [11].

1.3. Polymer Electrolyte Membrane Fuel Cells Operating at High-Temperature and Low Humidity Conditions

As water is essential to transport protons in the fuel cell systems, the performance of PEMFCs using both perfluorinated membranes and sulfonated poly(arylene ether sulfone) based membranes can dramatically deteriorate at high temperature (above 80 ^{o}C) and low RH conditions. Considering the cell performance of PEMFCs, low temperatures (typically run at ≤ 80 ℃ because of the working temperature limitation of Nafion®) with the fully humidified state is the best operating conditions. However, working at low temperatures and fully humidified conditions brings about several disadvantages for PEMFC systems, especially for automotive fuel cell applications: 1) Operating temperatures below 80 ℃ requires larger radiators than for internal combustion engine vehicles to maintain adequate heat rejection. 2) Maintaining the fully hydrated state of the polymer electrolyte membrane requires additional complex water management (air and fuel humidifiers, back pressure supplying systems, sensors, water re-circulators, etc.), adding cost and complexity to the fuel cell system. 3) A Small amount of carbon oxide (CO) and other possible byproduct gases can poison Pt catalyst in electrodes easily because such gases can be easily absorbed on Pt below 80 ℃. Therefore, as

mentioned in chapter 1.1, the U.S. Department of Energy has identified the key conditions that must be improved for PEMFCs; these include increasing the temperature up to 120 ℃ and lowering the humidification requirements of the fuel cell stack. Lowering the humidification and increasing the operating temperature will decrease the cost and complexity of the fuel cell power systems by allowing the simplification of the water and thermal management systems. In addition to reducing the cost and complexity, the susceptibility of Pt-based catalysts to fuel contaminants decreases at higher temperatures, relaxing the need for the highest quality fuel. Therefore, great efforts have strived to increase the operating conditions of PEMFCs at high-temperatures (80 - 130 ℃) and low humidity (< 50% RH).

1.4. Motivation

The development of polymer electrolyte membranes operating at high temperatures (80-130 ℃) and low relative humidity (< 50% RH) conditions is one of the important issues for the practical application of polymer electrolyte membrane fuel cells in the automobile transportation [12]. Since the currently used radiators in automobiles are designed to be operated at the high temperatures, it is highly desirable for polymer electrolyte membrane to be applicable at the same temperature conditions. However the optimized operating temperature for the commonly used perfluorinated ionomer membrane such as Nafion® is lower such as from 60 to 80 ℃ [6]. There have been a series of researches on the fabrication of alternative PEMs based on sulfonated aromatic polymers, such as sulfonated poly(arylene ether sulfone), for the possible operation at high temperatures due to their high thermal stability and excellent mechanical strength, as well as inexpensive product processing and easy functionalization. However, high electrochemical performance such as proton conductivity and fuel cell performance of polymer electrolyte membranes based on sulfonated poly(arylene ether sulfone) can be only achieved when the polymer has high enough degree of sulfonation (DS), while the sulfonated poly(arylene ether sulfone) with high DS does not have high enough physicochemical stability to have the desirable

performance required for polymer electrolyte membrane fuel cell. In this study, we propose very effective strategies to improve the electrochemical performance of the sulfonated poly(arylene ether sulfone) based membrane systems at high temperatures and low RH conditions by incorporation of semi-interpenetrating polymer network structure, pore-filling structure and cross-linked polymer network structure.

In the first part of the thesis (Chapter 2 and 3), we have described facile strategies to improve the proton conductivity and fuel cell performance of the sulfonated poly(arylene ether sulfone)-based electrolyte membrane without deterioration of the mechanical stability by the incorporation of vinyl phosphoric acid (VPA) and cross-linker into SPAES. In the second part of the thesis (Chapter 4 and 5), the effective methods for the development of ultra-thin and high proton conductive reinforced pore-filling electrolyte membranes based on sulfonated poly(arylene ether sulfone)s having high DS have been described. In the last part of the thesis (Chapter 6), the simple but effective cross-linking technology for the design of better performing cross-linked sulfonated poly(arlyene ether sulfone) has been described.

1.5. References

[1] B.C. Steele, A. Heinzel, Materials for fuel-cell technologies, Nature, 414 (2001) 345-352.

[2] S. Shamim, K. Sudhakar, B. Choudhary, J. Anwar, A review on recent advances in proton exchange membrane fuel cells: Materials, technology and applications.

[3] A.-C. Dupuis, Proton exchange membranes for fuel cells operated at medium temperatures: Materials and experimental techniques, Progress in Materials Science, 56 (2011) 289-327.

[4] R. Borup, J. Meyers, B. Pivovar, Y.S. Kim, R. Mukundan, N. Garland, D. Myers, M. Wilson, F. Garzon, D. Wood, Scientific aspects of polymer electrolyte fuel cell durability and degradation, Chemical reviews, 107 (2007) 3904-3951.

[5] H. Zhang, P.K. Shen, Recent development of polymer electrolyte membranes for fuel cells, Chemical reviews, 112 (2012) 2780-2832.

[6] M.A. Hickner, H. Ghassemi, Y.S. Kim, B.R. Einsla, J.E. McGrath, Alternative polymer systems for proton exchange membranes (PEMs), Chemical reviews, 104 (2004) 4587-4612.

[7] R.J. Cotter, Engineering plastics: a handbook of polyarylethers, Taylor & Francis, 1995.

[8] F. Wang, M. Hickner, Y.S. Kim, T.A. Zawodzinski, J.E. McGrath, Direct polymerization of sulfonated poly (arylene ether sulfone) random (statistical) copolymers: candidates for new proton exchange membranes, Journal of Membrane Science, 197 (2002) 231-242.

[9] A. Noshay, L. Robeson, Sulfonated polysulfone, J Appl Polym Sci, 20 (1976) 1885-1903.

[10] J. Kerres, W. Cui, S. Reichle, New sulfonated engineering polymers via the metalation route. I. Sulfonated poly (ethersulfone) PSU Udel® via metalation-sulfination-oxidation, Journal of Polymer Science Part A: Polymer Chemistry, 34 (1996) 2421-2438.

[11] B. Bae, K. Miyatake, M. Watanabe, Sulfonated poly (arylene ether sulfone ketone) multiblock copolymers with highly sulfonated block. Synthesis and properties, Macromolecules, 43 (2010) 2684-2691.

[12] C. Houchins, G. Kleen, J. Spendelow, J. Kopasz, D. Peterson, N. Garland, D. Ho, J. Marcinkoski, K. Martin, R. Tyler, D. Papageorgopoulos, U.S. DOE Progress Towards Developing Low-Cost, High Performance, Durable Polymer Electrolyte Membranes for Fuel Cell Applications, Membranes, 2 (2012) 855-878.

[13] S.J. Peighambardoust, S. Rowshanzamir, M. Amjadi, Review of the proton exchange membranes for fuel cell applications, Int J Hydrogen Energ, 35 (2010) 9349-9384.

Table 1.1 Major types of fuel cells [3].

	PEMFC	DMFC	AFC	PAFC	MCFC	SOFC
Electrolyte	Polymer or solid acid	Polymer	KOH in H_2O	Phosphoric acid	Molten carbonate in $LiAlO_2$	Yttrium-stabilized ZrO_2
Operating temperature	50–200 °C	0–60 °C	50–200 °C	150–220 °C	600–700 °C	700–1000 °C
Charge carrier	H^+	H^+	OH^-	H^+	CO_3^{2-}	O^{2-}
Primary fuel	H_2	Methanol	H_2	H_2	H_2, CO, CH_4	H_2, CO

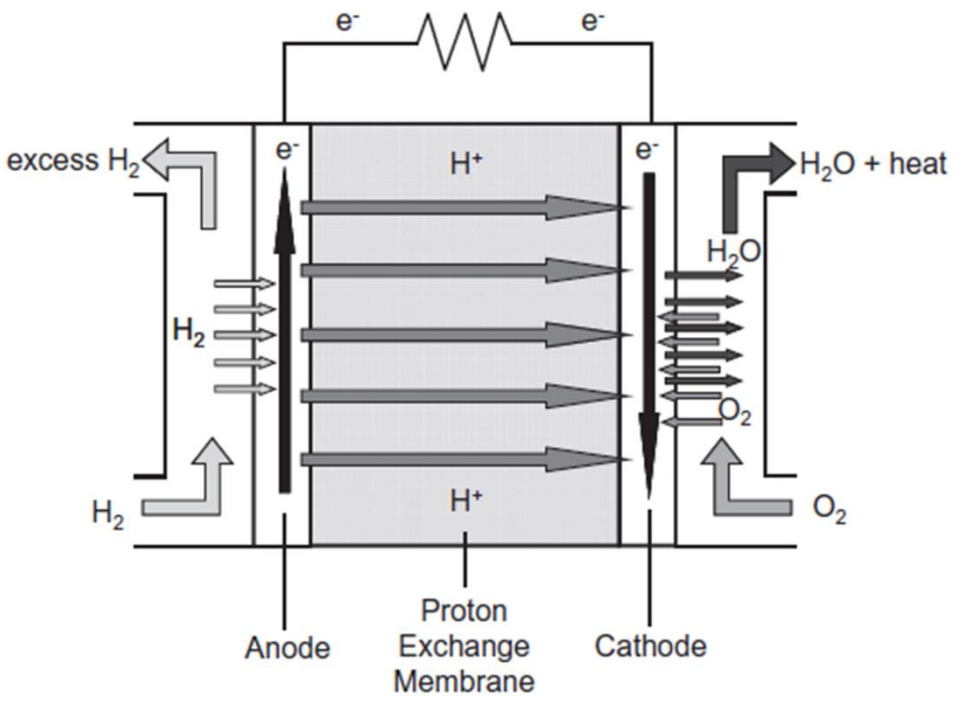

Figure 1.1 Schematic illustration of polymer electrolyte membrane fuel cell [3].

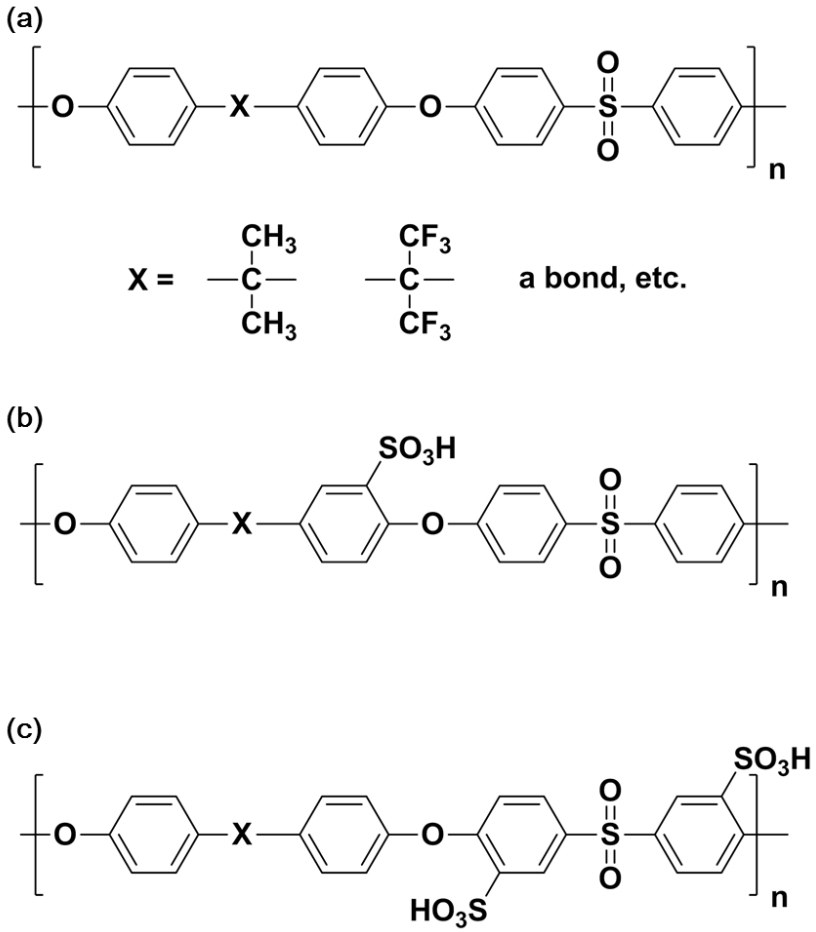

Figure 1.2 Chemical structures of (a) poly(arylene ether sulfone) and its derivatives, (b) products of bisphenol-A-based sulfonated poly(ether sulfone)s using post sulfonation method and (c) products of bisphenol-A-based sulfonated poly(ether sulfone)s followed by metalation–sulfination–oxidation processes.

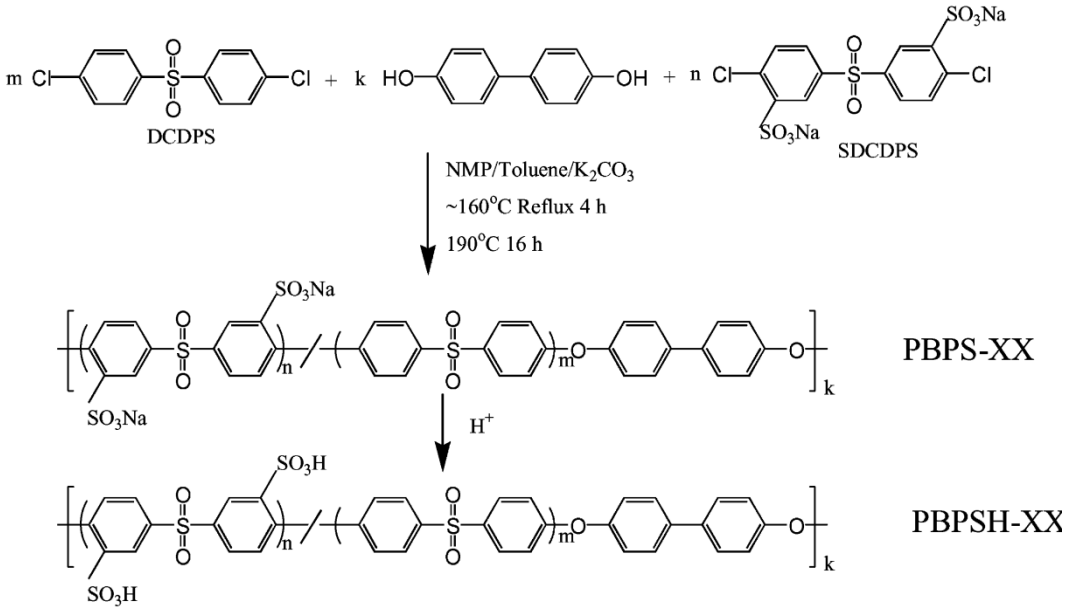

(n+m)/k = 1.01 (in mole); XX = 100n/(n+m)

Figure 1.3 Chemical structure and synthesis method of sulfonated poly(arylene ether sulfone)s using sulfonated monomer [8].

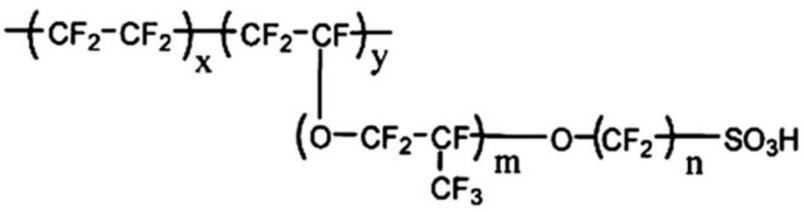

Nafion®117	m≧1, n=2, x=5-13.5, y=1000
Flemion®	m=0, 1; n=1-5
Aciplex®	m=0, 3; n=2-5, x=1.5-14
Dow membrane	m=0, n=2, x=3.6-10

Figure 1.4 Chemical structure of perfluorinated ionomer based polymer electrolyte membranes [13].

Chapter 2

Semi-Interpenetrating Network Electrolyte Membranes Based on Sulfonated Poly(arylene ether sulfone) for Fuel cells at High Temperature and Low Humidity Conditions

2.1. Introduction

The development of polymer electrolyte membranes (PEMs) operating at high temperatures (>90 ℃) and low relative humidity (< 50% RH) is one of the most important issues for the practical applications in polymer electrolyte membrane fuel cells (PEMFCs) in automobile transportations [1,2]. Since the automotive radiators currently used in automobiles are designed to be operated at high temperatures (>90 ℃), it is also desirable for PEM operating at the high temperatures, while lower temperatures from 60 to 80 ℃ have been known to be the optimum operation temperatures for the commonly used PEM based on pure Nafion® [3]. There have been studies on the fabrication of alternative PEMs based on sulfonated aromatic polymers, such as sulfonated poly(arylene ether sulfone) (SPAES), for possible applications at high temperatures due to their thermal stability and excellent mechanical properties as well as inexpensive product process [4]. However, PEMs based on SPAES can have high enough proton conductivity only at a high degree of sulfonation (DS), while SPAES with high DS do not have high enough physicochemical stability for the desirable performance of PEMFC. In this study, we demonstrate a very facile approach to the fabrication of new semi-interpenetrating network (semi-IPN) membranes

based on SPAES showing much improved proton conductivity and electrochemical performance compared with pristine SPAES membrane, without any deterioration of the mechanical stability. The semi-IPNs are composed of cross-linked polymer networks and linear polymer chains penetrated into the polymer matrix (**Figure 2.1(a)**). They can show the combined chemical properties of the component polymers having the improved physical properties and high conductivities.

A series of semi-IPN membranes were prepared by a simple one step process using the mixtures of vinyl phosphonic acid (VPA), diethylene glycol dimethacrylate (DEGDMA), and SPAES (**Figure 2.1(b)**). VPA containing a phosphonic acid group was used as a monomer to improve the proton conductivity of SPAES, and DEGDMA was used as a cross-linker to impart the physicochemical stability of VPA. We found that the content of the cross-linker affected the proton conductivity and mechanical strength of the semi-IPN membranes, and the membrane electrode assemblies (MEAs) prepared using the semi-IPN membranes obtained from the optimum cross-linker showed much improved fuel cell performance compared with those prepared using the SPAES membranes.

2.2. Experimental

Synthesis of sulfonated poly(arylene ether sulfone) (SPAES)

Sulfonated poly(arylene ether sulfone) (SPAES) was synthesized *via* nucleophilic aromatic substitution polymerization [5]. SPAES with an ion exchange capacity (IEC) of 1.97 mequiv./g and a degree of sulfonation of 50 mol% was used (M*n*: 43,100, M*w*: 106,000).

Preparation of semi-interpenetrating network (semi-IPN) and pristine SPAES membranes

1.0 g of SPAES, 1.0 g of VPA, and DEGDMA were dissolved in 13 g of dimethylacetamide (DMAc), where the amounts of DEGDMA were 0.22, 0.34, or 0.45 g corresponding to 10, 15 or 20 mol% of VPA, respectively. Then, azobisisobutyronitrile (1 wt. % of the total amount of VPA and DEGDMA) was injected into the polymer solution, and the mixture was spread onto a glass plate. The thickness of the solution could be controlled by a doctor blade applicator. The casted solution was heated stepwise from 25 to 80 ℃, then kept at 80 ℃ for 24 h in a vacuum oven. Flexible polymer films were obtained by the thermal treatment

because polymerization of VPA, cross-linking reaction of DEGDMA, and solvent evaporation of DMAc occurred simultaneously. When the amounts of DEGDMA are 10, 15 and 20 mol% of VPA, the obtained semi-IPN membranes were noted as D10 (IEC = 2.15 mequiv./g), D15 (2.09 mequiv./g) and D20 (2.01 mequiv./g), respectively. Pristine SPAES membranes were also prepared as a control by the same preparation method. The thicknesses of all the membranes were about 20 μm.

Characterization and PEMFC tests

Proton conductivity of the samples were measured at 120 ℃ under different relative humidity (RH) conditions using a conductivity measurement system (BekkTech, BT-552MX) and water uptake was measured at 80 ℃ under different RH using a temperature and humidity controllable chamber (Espec, SH-241). Mechanical properties of the membranes were measured using a universal testing machine (Lloyd, LR-10K). Membrane electrode assemblies (MEAs) were fabricated by a decal method. Catalyst layers were comprised of catalyst (50 wt. % Pt/C, Tanaka Kikinzoku Kogyo) and Aquivion^{TM} ionomer (EW750, Solvay). The Pt catalyst and ionomer loadings were 0.4 and 0.35 mg/cm^2, respectively. The membranes with catalyst layers (10 cm^2 of active area) were sandwiched and hot

pressed at 120 ℃ and 100 kgf cm^{-2} for 5min, then gas diffusion layers (25BC, SGL) were placed on both sides of the catalyst layers. The cell performance and durability tests were executed on a fuel cell test station (Scribner Associates Inc., 850e). Single cells were operated in galvanostatic mode at 120 ℃ and 40% RH by feeding hydrogen and air (humidified at 93.3 ℃) into the anode and cathode, respectively, at a flow rate of 100 and 200 cc/min, without back pressures. Activation of the MEAs was performed at constant current density of 0.2 A cm^{-2} for 24 h. In the durability test, open circuit voltages (OCVs) of the MEAs were monitored and recorded for 100 h at an interval of 10 min, along with the repetitive measurements of cell performance. For a measurement of H_2 leak current through the membranes, a stepwise DC voltage was applied between the electrodes, while supplying hydrogen and nitrogen into the anode and cathode, respectively [6].

2.3. Results and Discussion

Figure 2.2(a) shows the proton conductivities of the membranes as a function of RH at 120 ℃. The proton conductivities of D10 and D15 were found to be larger than those of SPAES membrane, while those of D20 were smaller than those of SPAES membrane for RHs above 30%. The larger proton conductivity values of D10 and D15 could be ascribed to the existence of the additional phosphonic acid groups from VPA monomer. Since the molecular weight of VPA is smaller than the monomeric unit of SPAES, the semi-IPN membranes can have higher content of the acid groups which can form the dynamic hydrogen-bonded chains facilitating the long-range proton transport [7]. Especially at lower RH conditions, D10 and D15 showed much larger proton conductivities than SPAES; the proton conductivity ratio of D10 to SPAES at 90% RH was 1/0.85 and that at 40% RH was 1/0.53. Therefore, the incorporation of the phosphonic acid groups into the membrane can further increase the proton conductivity at low RH conditions. Others also reported the increase of proton conductivity of VPA-based polymers because of the self-condensation equilibrium behavior of phosphonic acid groups, especially at high temperature and low RH conditions [8,9]. Since water molecules are generated by self-condensation reactions of the phosphoric acid

groups at these conditions, larger proton conductivity is expected [9,10].

The smaller proton conductivity values of D20 compared to SPAES membrane could be ascribed to the larger content of the cross-linker (DEGDMA). The larger DEGDMA content can increase the cross-linking density of the polymers, which in turn decrease the chain mobility and the size of the acid clusters that facilitate proton transport. Furthermore, since DEGDMA does not contain any acid groups, the increase of DEGDMA content can further decrease the size of the acid clusters. The water uptake result (**Figure 2.2(b)**) well agrees with the proton conductivity behavior of the semi-IPN membranes.

Figure 2.2(c) shows the tensile strength behavior of the semi-IPN and SPAES membranes. The tensile strength values of the semi-IPNs were found to be smaller than that of the SPAES, because VPA and DEGDMA moieties in the semi-IPN decreased the mechanical strength of the membrane. Polymeric backbones of VPA and DEGDMA are composed of aliphatic hydrocarbons, and they have less effective intermolecular interactions than the aromatic polar backbone of SPAES. However, the increase of the DEGDMA content increased the tensile strength of the semi-IPN membrane, due to the increase of the cross-linking density [11]. Although the elongation at break values for the semi-IPNs (19, 17, and 14% for D10, D15 and D20, respectively) were found to be slightly smaller than that of the SPAES membrane (28%), they are still larger than those of most sulfonated

aromatic membranes [12,13]. By comparing the proton conductivities and mechanical properties of the semi-IPN membranes, D15 was selected for the further investigation of the PEMFC performance and durability test. Although the proton conductivity of D15 was slightly smaller than that of D10, it displayed superior tensile strength compared to D10. While, D20 displayed a higher tensile strength than D15, it was not chosen because of its lower proton conductivity.

Fuel cell performance tests of the MEAs using D15 and SPAES membranes were conducted at 120 ℃ and 40% RH, the possible fuel cell operating conditions for automobiles suggested by the U.S. Department of Energy [14]. **Figure 2.3(a)** shows the current-voltage and current-power density curves of the H_2/air cells of the MEAs. D15 showed smaller voltage drop at the same current density and higher peak power density than SPAES membrane. The maximum power density values of D15 and SPAES were 171 and 145 mW cm^{-2}, respectively. Therefore, the incorporation of VPA moieties into the SPAES increased the cell performance because VPA can increase the proton conductivity. Since the cell performance of PEMFC has been known to be affected by the membrane thickness [15], MEAs from D15's having different thickness were also tested (**Figure. 2.3(b)**). First of all, the OCVs of the MEAs prepared with D15 were found to be larger than 900 mV, suggesting that gas permeation through the membrane is negligible. The maximum current density increased with a decrease of thickness, and a maximum

power density of 180 mW cm^{-2} was obtained from D15 with a thickness of 10 μm, the thinnest membrane. Therefore, the ohmic resistance could be decreased by decreasing the membrane thickness. However, when the thickness of D15 was decreased below 10 μm, the OCVs dropped under 900 mV due to the formation of microstructures and pin-holes in the very thin films [16]. The long term durability of the MEAs is very important for practical applications. The OCV holding method involving repetitive I-V measurements was used to evaluate the electrochemical durability of the MEAs from D15 (**Figure 2.3(c)**). Only a very small decrease of the OCV values from 935 to 905 mV was observed after 100 h of operations and the peak power density values did not change much in the range of 167-171 mW cm^{-2}. The durability test was also performed using the MEAs from SPAES and recast-Nafion. SPAES showed the similar OCV values ranged from 960 to 925 mV, while quite smaller the peak power densities ranged from 140-145 mW cm^{-2} were observed due to the smaller proton conductivity. The initial cell performance of the MEA from recast-Nafion was similar to that of D15 (**Figure 2.3(a)**). However, it showed very poor durability performance (**Figure 2.3(c)**): the OCV values decreased from 918 mV to 600 mV after 42 h possibly due to the well-known disadvantages of Nafion such as poor physical properties causing the gas leakage [3,17,18]. On the contrary D15 showed the very small H_2 leak current densities (0.18, 0.25, and 0.38 mA cm^{-2} at 200, 500, and 800 mV,

respectively) even at the high constant voltage mode. Therefore the MEA prepared using D15 has high electrochemical stability under the harsh experimental conditions.

2.4. Conclusions

A series of semi-IPN membranes were prepared by the simple one step process using a linear polymer, SPAES, and polymer matrix comprised of vinyl phosphonic acid (VPA) and cross-linker (DEGDMA). The incorporation of the polymer matrix into SPAES could improve the proton conductivity without any deterioration of the mechanical stability, resulting in highly improved cell performance at high temperature and low humidity conditions. Detailed fuel cell tests demonstrated the feasibility of the semi-IPN membrane as an electrolyte for high temperature and low humidity PEMFCs: (1) the ohmic loss was reduced by decreasing the membrane thickness; (2) the variation in OCV and cell performances was constant during the operation. Therefore, the semi-IPN membranes prepared by the incorporation of the conventional linear polymer into VPA-based polymer matrix have the advantages such as easy fabrication, improved proton conductivity and cell performance for the practical applications in PEMFCs.

2.5. References

[1] S. K. Kim, T. Ko, S. W. Choi, J. O. Park, K. H. Kim, C. Pak, H. Chang, J. C. Lee, J. Mater. Chem. 22 (2012) 7194-7205.

[2] S. K. Kim, S. W. Choi, W. S. Jeon, J. O. Park, T. Ko, H. Chang, J. C. Lee, Macromolecules 45 (2012) 1438-1446.

[3] M. A. Hickner, H. Ghassemi, Y. S. Kim, B. R. Einsla, J. E. McGrath, Chem. Rev. 104 (2004) 4587-4612.

[4] K. Xu, H. Oh, M. A. Hickner, Q. Wang, Macromolecules 44 (2011), 4605-4609.

[5] F. Wang, M. Hickner, Y. S. Kim, T. A. Zawodzinski, J. E. McGrath, J. Membrane. Sci. 197 (2002) 231-242.

[6] S. Nakamura, E. Kashiwa, H. Sasou, S. Hariyama, T. Aoki, Y. Ogami, H. Nishikawa, Electr. Eng. Jpn. 174 (2011) 1-9.

[7] R. Tayouo, G. David, B. Ameduri, J. Roziere, S. Roualdes, Macromolecules 43 (2010) 5269-5276.

[8] J. Parvole, P. Jannasch, J. Mater. Chem. 18 (2008) 5547-5556.

[9] Z. Florjanczyk, E. Wielgus-Barry, Z. Poltarzewski, Solid State Ionics 145 (2001) 119-126.

[10] H. Steininger, M. Schuster, K. D. Kreuer, A. Kaltbeitzel, B. Bingol, W. H.

Meyer, S. Schauff, G. Brunklaus, J. Maier, H. W. Spiess, Phys. Chem. Chem. Phys. 9 (2007) 1764-1773.

[11] D. S. Jones, G. P. Andrews, S. P. Gorman, J. Pharm. Pharmacol. 57 (2005) 1251-1259.

[12] Y. Gao, G. P. Robertson, M. D. Guiver, G. Wang, X. Jian, S. D. Mikhailenko, X. Li, S. Kaliaguine, J. Membrane. Sci. 278 (2006) 26-34

[13] H. Dai, H. M. Zhang, Q. T. Luo, Y. Zhang, C. Bi, J. Power Sources 185 (2008) 19-25

[14] J. Fenton, D. Slattery, FY 2012 Annual Progress Report 2012, PP. 68-70

[15] Y. B. Shen, P. Heo, C. Pak, H. Chang, T. Hibino, Electrochem. Commun. 24 (2012) 82-84.

[16] S. K. Kim, K. H. Kim, J. O. Park, K. Kim, T. Ko, S. W. Choi, C. Pak, H. Chang, J. C. Lee, J. Power Sources 226 (2013) 346-353.

[17] T. Miyahara, T. Hayano, S. Matsuno, M. Watanabe, K. Miyatake, ACS Appl. Mater. Interfaces 4 (2012) 2881-2884

[18] M. Marrony, R. Barrera, S. Quenet, S. Ginocchio, L. Montelatici, A. Aslandies, J. Power Sources 182 (2008) 469-475

(a)

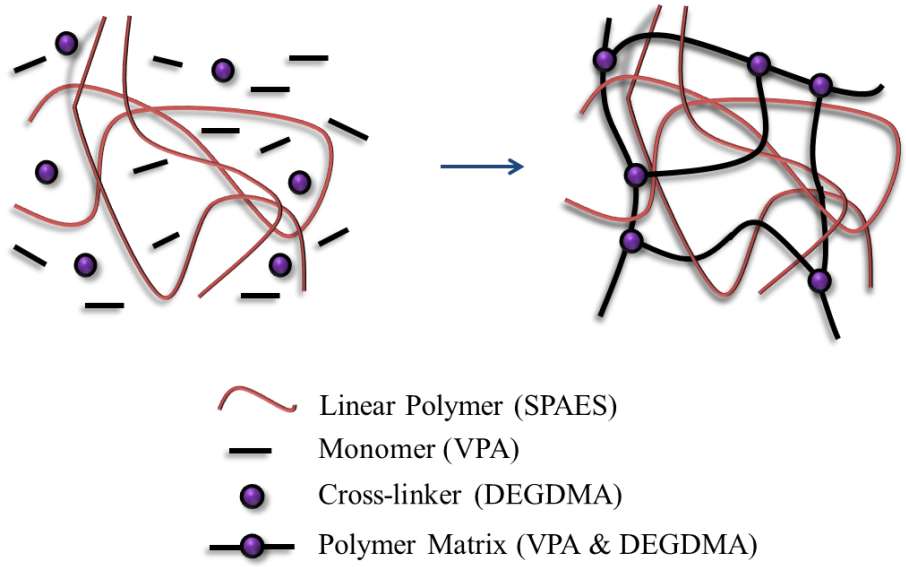

(b)

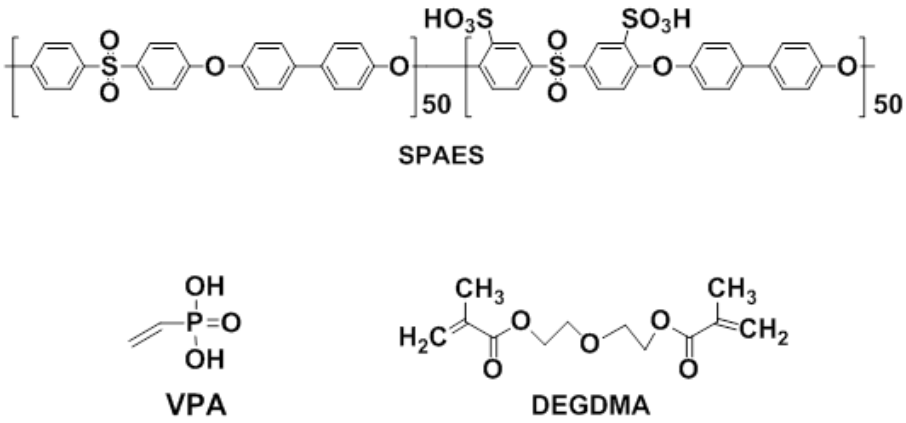

Figure 2.1 Schematic illustration of (a) semi-IPN structure and (b) chemical structure of SPAES, VPA and DEGDMA.

(a)

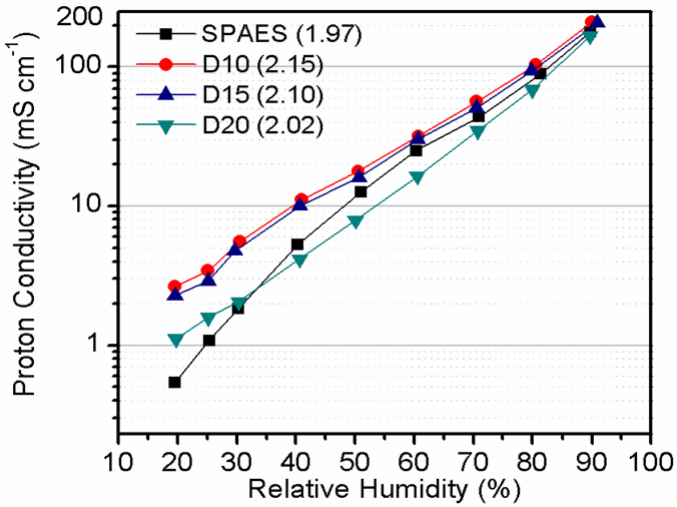
SPAES (1.97)
D10 (2.15)
D15 (2.10)
D20 (2.02)
Proton Conductivity (mS cm-1)
Relative Humidity (%)
200
100
10
1
10 20 30 40 50 60 70 80 90 100

(b)

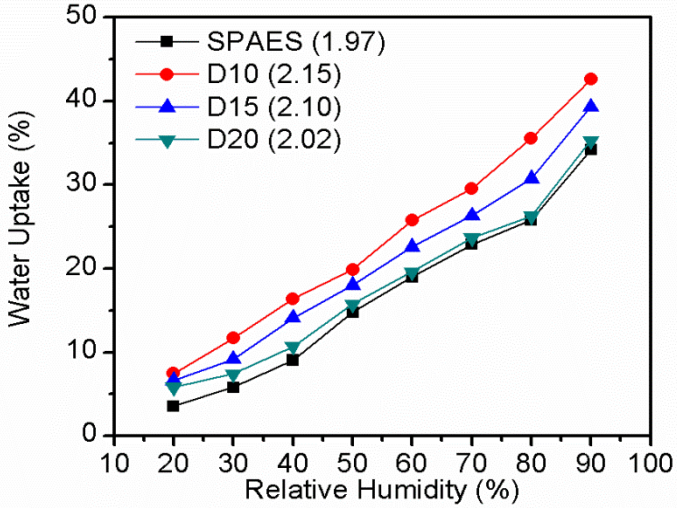
SPAES (1.97)
D10 (2.15)
D15 (2.10)
D20 (2.02)
Water Uptake (%)
Relative Humidity (%)
50
40
30
20
10
0
10 20 30 40 50 60 70 80 90 100

(c)

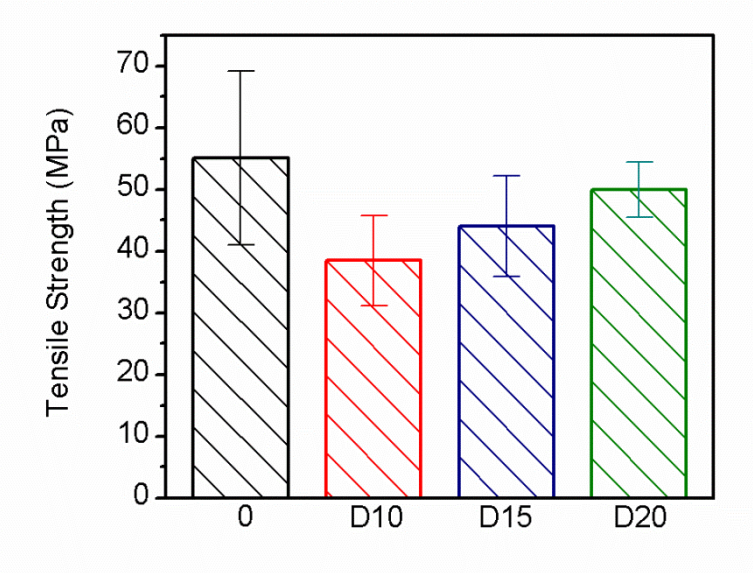

Figure 2.2 (a) proton conductivities at 120 °C, (b) water uptake at 80 °C as a function of RH and (c) tensile strength as a function of DEGDMA content.

(a)

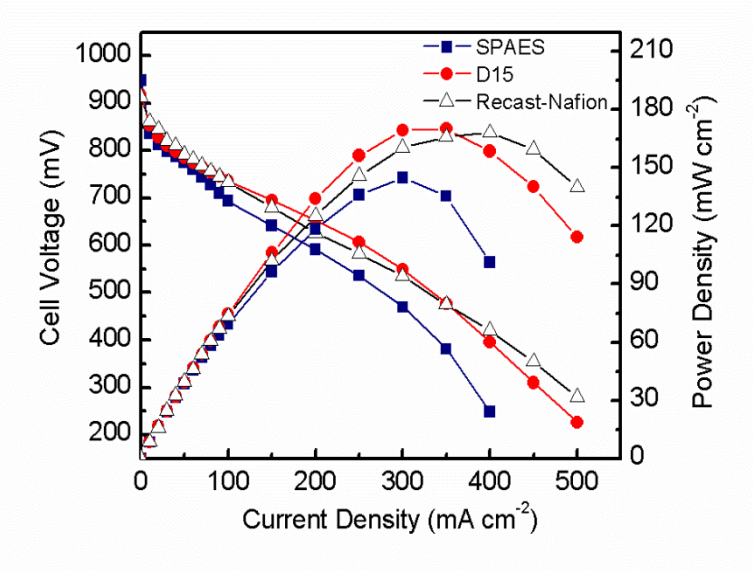
SPAES
D15
Recast-Nafion
Cell Voltage (mV)
Power Density (mW cm-2)
Current Density (mA cm-2)
1000
900
800
700
600
500
400
300
200
210
180
150
120
90
60
30
0
0
100
200
300
400
500

(b)

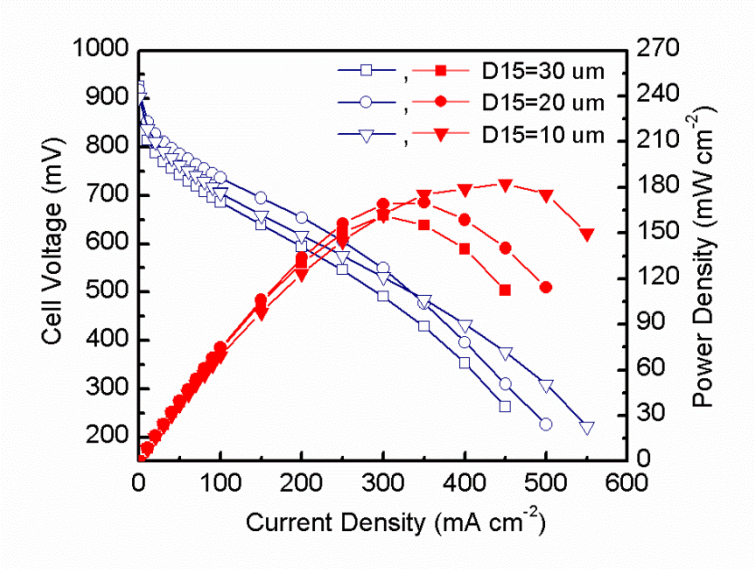
D15=30 um
D15=20 um
D15=10 um
Cell Voltage (mV)
Power Density (mW cm-2)
Current Density (mA cm-2)
1000
900
800
700
600
500
400
300
200
270
240
210
180
150
120
90
60
30
0
0
100
200
300
400
500
600

(c)

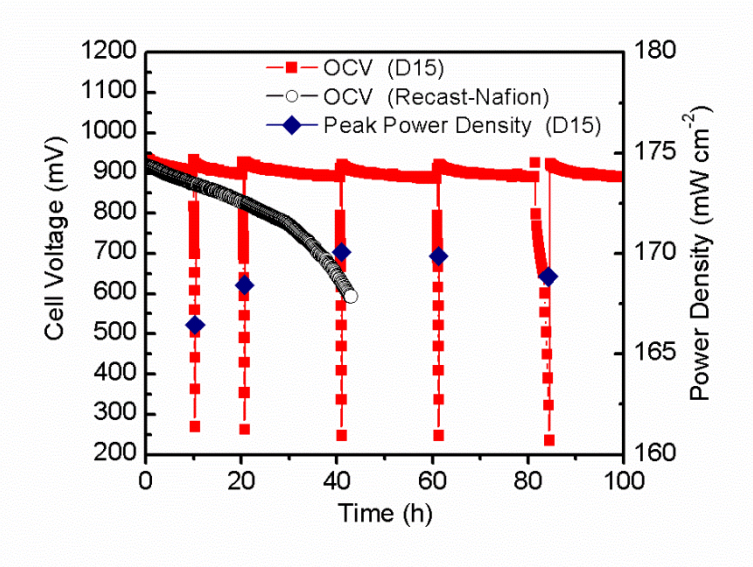

Figure 2.3 Cell voltage and power density as a function of the current density for (a) MEAs prepared using D15, SPAES and recast-Nafion (thicknesses of all membranes are 20 µm.) and (b) MEAs prepared using D15's having different thicknesses. (c) Durability test of the MEAs prepared using D15 and recast-Nafion. All the tests were conducted at 120 °C and 40 % RH.

Chapter 3

Poly(Arlyene Ether Sulfone) based Semi-Interpenetrating Polymer Network Membranes Containing Cross-Linked Poly(Vinyl Phosphonic Acid) Chains for Fuel Cell Applications at High Temperature and Low Humidity Conditions

3.1. Introduction

Polymer electrolyte membrane fuel cells (PEMFCs) have been studied widely due to their great potential as a clean and efficient energy conversion system for automotive, residential, and portable applications [1-3]. Especially, considerable attention has been paid to the development of PEMFCs operating at high temperatures (above 90 ℃) and low relative humidity (below 50% RH) conditions because of their numerous advantages such as rapid electrode kinetics, suppressed CO poisoning, better heat utilization, and simple water management systems [4-6]. However, the pure perfluorosulfonic acid membranes (*e.g.*, Nafion® and Flemion®) themselves without any further modification processes are not practical for PEMFC applications operating at high temperatures because of their low glass transition temperatures, poor thermo-mechanical properties, and the poor water maintaining ability above 80 ℃ [7-9].

The drawbacks of the perfluorosulfonic acid membranes have prompted the development of alternative polymer electrolyte membranes (PEMs) based on hydrocarbon polymers. For example, several aromatic polymers such as sulfonated polyimide (SPI) [10], sulfonated poly(ether ether ketone) (SPEEK) [11,12], sulfonated poly(arylene ether sulfone) (SPAES) [13], and

polybenzimidazole (PBI) [14-17] have been investigated as the alternative polymers for the PEMFC applications. Among these hydrocarbon polymers, SPAES has been widely studied for high-temperature PEMs due to its high thermal stability, excellent mechanical strength, and its relatively low cost [18]. Still the direct application of pure SPAES has been limited because the SPAES having these advantages normally has lower proton conductivity than the perfluorosulfonic acid polymers [19,20]. The proton conductivity of SPAES could be increased by increasing the degree of sulfonation (DS), while the SPAES with high DS do not have high enough physical and chemical stability for PEMFC operation. Therefore, several approaches have been performed to prepare SPAES-based membranes having high proton conductivities with good physicochemical properties by preparing block copolymers [21], comb-likes polymers [22], and pore-filling structures based on SPAES with high DS [23]. Although they showed the improved properties, the drawbacks of these approaches includes the tedious synthetic procedures for the preparation of the polymers and the complicated process for the fabrication of the membranes.

Our group found a very facile approach to improve the proton conductivity and fuel cell performance of the SPAES-based membrane systems at high temperature and low RH conditions using semi-interpenetrating polymer network (semi-IPN) structures and it was reported as a short communication [24]. Recently we found

that the proton conductivity and fuel cell performance could be further improved in the SPAES-based membrane systems by the incorporation of vinyl phosphonic acid (VPA) and bis(2-(methacryloyloxy)ethyl) phosphate (BMAEP) units into the semi-IPN structures. Especially BMAEP, the newly selected cross-linker, can increase the flexibility of the rigid cross-linked VPA-based polymer networks by the flexible oxyethylene linkages and the phosphate group in the middle of BMAEP structure can provide additional path for proton transport in the semi-IPN structure. The detailed synthesis procedure for the preparation of the semi-IPN membranes containing optimum content of BMAEP and their membrane properties including morphology, thermal and mechanical stabilities, ion exchange capacity and proton conductivity are fully discussed for the first time here. Furthermore the fuel cell performance and long-term durability of membrane-electrode assemblies prepared using the semi-IPN membranes were also compared with those prepared using the linear SPAES and recast-Nafion® membranes under the high temperature and low humidity conditions, especially at 120 ℃ and 40% RH. The operating conditions of 120 ℃ and 40% RH were intentionally used because the operating temperature up to 120 ℃ is the technical target operating temperature for commercialization of the fuel cell vehicles suggested by U.S. Department of Energy (DOE) [25,26] and 40% RH is a maximum humidity that we could practically control at 120 ℃ under atmospheric

pressure without the back pressure supply system using only humidified reactant gases.

3.2. Experimental

Materials

4,4’-Dihydroxybiphenyl (BP, 97.0%, Aldrich) and 4,4’-dichlorodiphenylsulfone (DCDPS, 98.0%, Aldrich) were recrystallized from methanol and toluene, respectively, prior to use. 3,3’-Disulfonate-4,4’-dichlorodiphenylsulfone (SDCDPS) was synthesized from DCDPS according to a previous literature [27]. 2,2’-Azobis(isobutyronitrile) (AIBN, Junsei) was recrystallized from ethanol. Toluene (99.5%, Junsei) was refluxed over calcium hydride and distilled. *N*-Methyl-2-pyrrolidone (NMP, 99.0%, Junsei) and *N*,*N*-dimethylacetamide (DMAc, 99.0%, Junsei) were stored over molecular sieves at nitrogen atmosphere. Potassium carbonate (K_2CO_3, 99.0+%, Aldrich) was dried in vacuum prior to use. Fuming sulfuric acid (65% SO_3, Merck), sodium chloride (NaCl, 99.5%, Daejung), sodium hydroxide (NaOH, 98.0%, Daejung), vinylphosphonic acid (VPA, 95.0+%, TCI), and bis(2-(methacryloyloxy)ethyl) phosphate (BMAEP, 100.0%, Aldrich) were used as received. Nafion® (DE 2021, DuPont) was obtained from Nano Getters, Co., as a 20 wt. % solution in a mixture of aliphatic alcohols and water. Aquivion^{TM} ionomer (EW750) was purchased from Solvay as a 20.1 wt. % dispersion in a water.

Synthesis of Sulfonated Poly(arylene ether sulfone) (SPAES)

SPAES was prepared by the condensation polymerization using the 4,4'-dihydroxybiphenyl (BP) and two kinds of dichloro monomers such as 3,3'-Disulfonate-4,4'-dichlorodiphenylsulfone (SDCDPS) and 4,4'-dichlorodiphenylsulfone (DCDPS). A three-neck flask equipped with nitrogen inlet and outlet, mechanical stirrer, condenser, and Dean-Stark trap was charged with 5.00 g (26.9 mmol) of BP, 3.86 g (13.4 mmol) of DCDPS, 6.60 g (13.4 mmol) of SDCDPS, and 4.27 g (30.9 mmol) of K_2CO_3 in 45.2 mL of NMP (~25 wt. %). Then 22.6 mL of toluene (NMP/toluene = 2/1 v/v) was added as an azeotroping agent. The reaction mixture was heated at 145 ^oC for 4 h to ensure the complete dehydration. After the removal of the toluene completely, the temperature was raised to 190 ℃ for another 48 h to obtain a viscous solution. After the solution was cooled to room temperature, 10.0 mL of NMP was added to dilute the solution. The homogeneous solution was filtered to remove the salt produced by the polymerization, and then poured into *iso*-propylalcohol (1000 mL) to precipitate the polymer. The precipitate was rinsed several times with *iso*-propylalcohol, and then dried overnight under vacuum. The product having the sodium sulfonate ($-SO_3Na$) group was treated with 1 M H_2SO_4 aqueous solution at 80 ℃ for 6 h to produce SPAES having sulfonic acid ($-SO_3H$) group. The product was thoroughly washed with distilled water several times. Considering the amount

of the monomer mixtures used for the polymerization, product polymer was obtained in 92% of yield after being dried in a vacuum oven for 12 h.

Preparation of semi-IPN Membranes (B10, B15, and B20)

1.0 g of SPAES, 1.0 g of VPA, BMAEP, and AIBN was dissolved in 13 g of DMAc, where the amounts of BMAEP were 0.29 g, 0.45 g, or 0.59 g and 1 wt. % of AIBN to the total amount of VPA and BMAEP used. The mixture was spread onto a glass plate and its thickness was controlled by a doctor blade film applicator. The casted solution was heated stepwise from 25 to 80 ℃ for 1 h and then kept at 80 ℃ for 24 h in a vacuum oven. The obtained film was rinsed with distilled water several times to remove the unreacted monomer and any remaining DMAc, and then semi-IPN membranes having thickness of about 20 μm were obtained after drying in a vacuum oven for 24 h. The semi-IPN membranes prepared using 0.29, 0.45, and 0.59 g of BMAEP were denoted as B10, B15, and B20, respectively, because the molar ratios of VPA *vs* BMAEP in these membranes are 100: 10, 100: 15, and 100: 20, respectively.

Preparation of Pristine SPAES and Recast-Nafion® Membranes

Pristine SPAES and recast-Nafion® membranes were prepared as the benchmark samples by casting the 15 wt. % SPAES solution in DMAc and 20 wt. % Nafion® solution in a mixture of aliphatic alcohols and water, respectively, onto a glass plate. The same film preparation method used for the semi-IPN membranes including the solution casting, thermal treatment, and drying processes was employed. The film thicknesses of the pristine SPAES and the recast-Nafion® membranes were controlled by use of the doctor blade film applicator and samples with a thickness of about 20 μm were prepared.

Preparation of Membrane Electrode Assemblies (MEAs)

Membrane electrode assemblies (MEAs) were fabricated by the decal method [24]. The catalyst ink was prepared by mixing catalyst powder (50 wt. % Pt/C, Tanaka Kikinzoku Kogyo), Aquivion™ ionomer dispersion (EW750, Solvay), and solvent mixture comprising 1: 4 weight ratio of water: dipropylene glycol. The catalyst layer was prepared by coating the ink on a decal substrate and drying it at 60 °C. The amounts of Pt catalyst and Aquivion™ ionomer were 0.4 mg cm^{-2} and 0.35 mg cm^{-2} in the catalyst layers for anode and cathode, respectively. The membrane with the catalyst layers (10 cm^2 of active area) was sandwiched and hot pressed at

120 ℃, and gas diffusion layers (25BC, SGL) were placed on both sides of the catalyst layers.

Characterization

The ^{1}H-NMR spectra was collected on Avance 400 (Bruker, Germany) with a proton frequency of 400 MHz using deuterated dimethylsulfoxide as the solvent and tetramethylsilane (TMS) as the internal standard. Molecular weights (M_n and M_w) were measured at 35 ℃ by gel permeation chromatography (GPC) consisting of a Waters 510 HPLC pump, three columns PLgel 5 μm guard, MIXED-C, MIXED-D, and a Viscoter T60A dual detector. HPLC grade DMF was used as an eluent and flow rate was 1.0 mL min^{-1}. Calibration was performed with polystyrene standards. FT-IR spectra of samples were recorded in the attenuated total reflectance (ATR) mode in the frequency range of 4000 to 650 cm^{-1} on a Nicolet 6700 instrument (Thermo Scientific, USA). The spectra were recorded as the average of 32 scans with the resolution of 8 cm^{-1}. The samples were put in equal physical contact with the sampling plate of the spectrometer accessory to avoid differences caused by pressure and penetration depth. The morphological characterization of the membranes was analyzed using a field-emission scanning electron microscopy (FE-SEM, Carl Zeiss SUPRA 55VP, Germany), operated at an accelerating voltage of 15 kV. All samples were coated with platinum under

vacuum prior to the test. The cross-sectional specimens of the membranes were prepared by breaking the membrane manually after cooling in liquid nitrogen.

Thermo-gravimetric analysis (TGA) was carried out using Q5000IR (TA instruments, USA). The samples were heated from 35 to 800 ℃ with a heating rate of 10 ℃ min^{-1} under air atmosphere. The mechanical properties were measured using a universal testing machine (Lloyd LR-10K, UK) at room temperature (~20 ℃) and RH in the range of 38-42% with a gauge length and cross head speed of 15 mm and 5 mm min^{-1}, respectively. The samples were equilibrated for 5 h at room RH before measurement. Dumbbell specimens were prepared using the ASTM standard D638 (Type V specimens). For each measurement, at least seven samples were used and their average value was calculated.

Ion-exchange capacity (IEC) of the membranes was measured by back-titration method [28]. The membranes were soaked in 1 M NaCl aqueous solution for 24 h, and then the solution was titrated with 0.01 M NaOH aqueous solution. The value of IEC was calculated using the following equation:

$$IEC\ [mequiv.g^{-1}] = (C_{NaOH} \cdot \Delta V_{NaOH} / W_s)\ X\ 1000$$

where C_{NaOH}, ΔV_{NaOH}, and W_s are the concentration of NaOH (aq), the consumed volume of NaOH (aq), and the weight of the dry membrane, respectively.

Proton conductivities of the membranes were measured at 120 ℃ and different RH conditions. The sample was fixed to a four-point conductivity cell and connected to the test stand (BekkTech, BT-552MX) for the continuous control of the humidity and temperature. The RH in the cell was controlled by feeding with hydrogen gas which was humidified by passing the gas flow through a humidification column. The test was carried out at 120 ℃ of H_2 at 230 kPa under an input flow rate of 500 cm^3 min^{-1}. The membrane was pre-equilibrated at 120 ℃ and 70% RH for 2 h, and then the conductivity measurement was started from 70%. The conductivity measurement was continued by lowering the humidity to 20% RH and then by raising to 90% RH at 10% intervals with a 15 min equilibration time for each measurement. The oxidative stability of the membranes was evaluated by Fenton's test, i.e. the determination of the sample weight change after being exposed to a Fenton's reagent (3 wt.% H_2O_2 aqueous solution containing 4 ppm Fe^{2+}). Pre-weighed dry membranes were soaked in a 50 ml of Fenton solution at 80 ℃. After 1 h, the membranes were taken out, washed thoroughly with distilled water, and dried at 80 ℃ for 24 h in vacuum before the weight was measured.

Cell performance and long-term durability test were executed on a fuel cell test station (Scribner Associates Inc., 850e Fuel Cell Test Station). Unit cells were operated in galvanostatic mode at 120 ℃ and 40% RH conditions by feeding

humidified hydrogen and air (at 93.3 ℃) into the anode and cathode, respectively, at the flow rate of 100 and 200 cm^3 min^{-1},respectively, without any back pressure. The activation of the MEAs was performed at a constant current density of 0.2 A cm^{-2} for 24 h. In the durability test, open circuit voltages (OCVs) of the MEAs were monitored and recorded for 100 h at an interval of 10 min along with the continual measurements of the cell performance. Gas cross-over through the membranes was measured by hydrogen cross-over measurements [29]. During the hydrogen cross-over measurements, the cell performance test was interrupted and stepwise DC voltages (at 200, 500, and 800 mV) were applied between the electrodes, while hydrogen and nitrogen were supplied into the anode and cathode, respectively.

3.3. Results and Discussion

Synthesis of Sulfonated Poly(arylene ether sulfone) (SPAES)

SPAES was synthesized *via* nucleophilic step-growth polymerization [30] using the monomer mixture of 4,4'-dihydroxybiphenyl (BP), 4,4'-dichlorodiphenylsulfone (DCDPS), and 3,3'-disulfonate-4,4'-dichlorodiphenylsulfone (SDCDPS) as shown in **Figure 3.1(a)**. The weight-average molecular weight (M_w) and number average molecular weight (M_n) of the SPAES calculated from the GPC measurement were 106,000 and 43,100, respectively. The chemical structure of the resulting copolymer was confirmed by ^{1}H-NMR spectroscopy (**Figure 3.1(b)**). The DS calculated from the peak integration in the ^{1}H-NMR spectrum was found to be about 47 mol% although DS of 50 mol% was expected because the feed molar ratio of sulfonated (SDCDPS) and nonsulfonated (DCDPS) dichloro monomers is 1:1. Possibly slightly different reactivity between SDCDPS and DCDPS caused this result as reported by others [9,31]. Since high fuel cell performance has been observed when the membranes have high proton conductivity, it is highly desirable to use SPAES films having high DS [18]. However when SPAES films having the DS larger than 50 mol% were used, their proton conductivities could not be obtained at the high

temperature and low humidity conditions (120 ℃ and 40% RH), the desirable fuel cell operating condition, due to their poor dimensional stability at the pre-equilibrium condition at 120 ℃ and 70% RH for 2 h and the conductivity measurement conditions at 120 ℃ and various RH. We found that 50 mol% is about the maximum DS maintaining the physicochemical stability of the membranes at the operating condition. Therefore, we intentionally prepared the semi-IPN membranes using the SPAES with DS of 50 mol% to show the effect of the semi-IPN structures from the monomer (VPA) and the cross-linker (BMAEP) for the fuel cell membrane and the SPAES with the DS of 50 mol% was used as the benchmark membrane for the systematical study, although we recently found that the semi-IPN membranes from the SPAES with DS larger than 50 mol% are also quite stable and the MEAs from these membranes show excellent fuel cell performance and durability.

Preparation of semi-Interpenetrating Polymer Network (semi-IPN) Membranes (B10, B15, and B20)

A series of semi-IPN membranes were prepared simply by *in-situ* casting and heating the mixture of SPAES, VPA, and BMAEP in DMAc. The polymerization of VPA and BMAEP forming the cross-linked interpenetrating networks in the

SPAES matrix and the evaporation of the solvent, DMAc, occur simultaneously. The polymerization and cross-linking reactions of the monomer (VPA) and the cross-linker (BMAEP) could be confirmed by the FT-IR spectra of the solution mixtures of VPA, BMAEP, and AIBN (thermal initiator) before and after heating the mixture at 80 ℃ for 24 h (the same heat treatment condition used for the preparation of the semi-IPN membrane) as a separate experiment (**Figures 3.2(a)** and **3.2(b)**). After the thermal treatment, the characteristic vinyl (C=C) stretch peak at 1615 cm^{-1} disappear and the intensities of the peaks at 932, 815, and 725 cm^{-1}, corresponding to the out-of-plane bending modes (–$CH=CH_2$) of VPA and BMAEP, decrease. The polymerization and the cross-linking reaction could be further confirmed by the observation of the change from the clear transparent solution of VPA and BMAEP into the cross-linked hydrogels insoluble in water as shown in the **Figure 3.2(c)**.

Figure 3.3 shows the FT-IR spectra of the SPAES and semi-IPN membranes obtained by the heating process. P=O vibration peak at 1040 cm^{-1}, P-O vibration peaks at 1000-910 cm^{-1}, and phosphonic acid bands at 1740- 1590 cm^{-1} were observed from the semi-IPN membranes [32, 33]. In addition, the intensities of the C-H stretching vibration peaks at 2975 and 2894 cm^{-1} from the cross-linked networks and the broad band at 3700-3000 cm^{-1} from the hydrogen bonded network necessary for the proton conduction in the semi-IPN membranes were

found to be larger than those observed in the SPAES membrane, the benchmark sample [33,34].

The miscibility of the matrix and the interpenetrating polymers is very important for the formation of physically stable semi-IPN membranes because the semi-IPN membranes having phase-separated domains are physically unstable and normally very brittle, thus they cannot be used as electrolyte membranes in fuel cells [35]. The semi-IPN membranes prepared using 1.0: 1.0 weight ratios of VPA to SPAES such as B10, B15, and B20 were found to be transparent from their photo images and smooth surface images were observed from their SEM images similar to that of SPAES membrane (**Figure 3.4**), indicating that the SPAES, the matrix polymer, and the polymer networks formed by VPA and BMAEP are more or less miscible in the molecular level [36-38]. When VPA to SPAES weight ratios were larger than 1.0: 1.0 such as 1.5: 1.0 and 2.0: 1.0, phase separation forming hazy films and non-uniform surface SEM images were observed (**Figure 3.5**), indicating that there are the phase-separated domains [37,38]. It is quite common for the polymer mixtures being miscible at certain compositions, while immiscible at the different composition ranges [39-41]. Based on the performed preliminary studies it is assumed that the SPAES and the polymeric chains formed by VPA and BMAEP are miscible when the ratio is 1.0: 1.0, while they are immiscible when they are 1.5: 1.0 and 2.0: 1.0. Therefore, the weight ratio of VPA to SPAES in 1.0: 1.0 was

used for the preparation of the semi-IPN membrane to investigate the improvement of the proton conductivity and electrochemical performance. It was also tried to prepare semi-IPN membranes using divinyl benzene having fully aromatic structure as the cross-linker. However, the resulting membranes were found to be very brittle and cracks were formed very easily due to the phase separation forming fragile network structure (**Figure 3.6**). Therefore, it was found that BMAEP, the aliphatic cross-linker having extra phosphonic acid group, is much more effective than the hydrophobic aromatic cross-linker in the preparation of the semi-IPN membranes.

Thermal Stability

The high thermo-oxidative stability of PEMs is one of the most important properties for the fuel cell systems operating at high temperature for a long period of time [42]. **Figure 3.7** shows the TGA traces recorded up to 800 ℃ for the SPAES and the semi-IPN membranes and the hydrogel prepared by heating at 80 ℃ for 24 h using 1.0: 0.15 molar ratio of VPA and BMAEP without SPAES. The hydrogel comprising VPA and BMAEP units shows a small initial weight loss at 130 ℃ from the reversible self-condensation and desorption of water [43] and a larger weight loss at around 300 ℃ associated with the cleavage of the C-P bonds

[42]. The SPAES shows the backbone degradation at around 500 ℃ [21]. The degradation temperature (T_{d10}, 10 wt. % of weight loss from the initial weight) of SPAES, B10, B15, and B20 were found to be 380, 360, 356, and 348 ℃, respectively. The lower degradation temperature of the semi-IPN membranes than that of SPAES could be ascribed to the aliphatic chain structure of the VPA-based polymer networks having the same chemical structures of the hydrogel. Since the degradation temperature of the VPA-based polymer network is lower than that of the SPAES linear polymer, the increase in BMAEP content decreases the thermal stability of the semi-IPN membranes. However, the degradation temperature of the semi-IPN membranes is still high enough to be used as PEM because the operating temperature for the high-temperature and low humidity PEMFC system is around 100-150 ℃ [9,44-46].

Mechanical Stability

Figure 3.8 shows the mechanical properties of SPAES and the semi-IPN membranes and these values are listed in **Table 3.1**. Since the fuel cell test using the MEAs from these membranes was performed at 120 ℃ and 40% RH, the mechanical properties of the SPAES and semi-IPN membranes measured at room temperature condition might not represent the actual mechanical stability of the

fuel cell membranes. However it is also true the mechanical properties at room temperature have been commonly used to estimate the polymer stability at high temperatures in various of fields [26,47-49]. The SPAES membrane has the tensile strength and the elongation at break values of 55 MPa and 30%, respectively. The semi-IPN membranes have the tensile strength values in the range of 41-48 MPa, and an elongation at break values in the range of 20-13%. The mechanical properties of the semi-IPN membranes were found to be affected by the chemical composition and the degree of the cross-linking [34]. The increase of BMAEP content can decrease the mechanical strength because the content of physically weaker aliphatic chain increases, while it can also increase the mechanical property because it can increase content of the mechanically robust cross-linked structures. Since such positive and negative effects of the BMAEP units are combined, as the BMAEP content increase from 0 to 10 mol% (from SPAES to B10), the tensile strength decreases, while when it changes from 10 to 20 mol% (B10 to B20), the tensile strength starts to increase. Still the tensile strength values of the semi-IPN membranes are smaller than that of SPAES membrane, because the aliphatic linkages formed by VPA and BMAEP lower the mechanical strength. Since the elongation at break values are most largely dependent on the cross-linking density, the increase of BMAEP content decreases the elongation at break value as reported by others for other cross-linked polymers [50-55]. Still the

tensile strength and the elongation at break values of the semi-IPN membranes are in the range of those of membranes showing good fuel cell performance [5, 56-58]

Ion Exchange Capacity

Since the IEC directly reflects the number of ion exchangeable groups such as sulfonic and phosphonic acid groups in the membrane, the proton conductivity of fuel cell membrane is closely related to IEC values. The semi-IPN membranes can have larger amount of the acid groups because the molecular weight of VPA (108.03 g mol^{-1}) and BMAEP (322.25 g mol^{-1}) having two and one phosphonic acid groups, respectively, are much smaller than that of the SPAES monomeric unit (1005.11 g mol^{-1}) having two sulfonic acid group. Therefore, the IEC values of the semi-IPN membranes are larger than that of the SPAES membrane (**Table 3.1**). Still BMAEP can decrease the IEC value because the increase of the cross-linker content increases the cross-linking density and decreases the chain mobility, which in-turn decreases the water absorbing ability [47,59-60]. Therefore as the BMAEP content increases from 0 to 20 mol%, the IEC value increases from 1.97 to 2.30 mequiv. g^{-1}, then decreases to 2.07 mequiv. g^{-1}.

Proton Conductivity

Figure 3.9 shows the proton conductivities of the membranes measured at 120 ℃ by changing the RH from 20 to 90%. The proton conductivity values of all the semi-IPN membranes were found to be larger than those of SPAES membrane. The larger proton conductivity values of the semi-IPN membranes could be ascribed to the larger content of acid groups (phosphonic and sulfonic acid groups) and the larger IEC values. Therefore, the order of the proton conductivity values of the membranes follows the order of the IEC values, B10> B15> B20> SPAES. The larger content of the acid groups can form the more and larger dynamic hydrogen-bonded domains that can facilitate the long-range proton transport [61-63]. Especially, the difference of the proton conductivities between the semi-IPN and the SPAES membranes at the low RH range below 50% is larger than that between the membranes at the high RH range above 50% in **Figure 3.9**. For example, the proton conductivity values of B10 at 40% and 90% RH are 15.0 and 230.6 mS cm^{-1}, respectively, and those of the SPAES are 5.3 and 178.3 mS cm^{-1}, respectively. Therefore, the conductivity value ratios of B10 to SPAES at 40% RH and at 90% RH are 2.8 and 1.3, respectively. The incorporation of extra phosphonic acid groups by VPA and BMAEP can increase the proton conductivity of the semi-IPN membranes especially at the low RH conditions possibly due to the self-condensation equilibrium of the phosphonic acid groups at high

temperature such as 120 ℃, the operation temperature in this study, which can generate the water molecules at high temperature and low RH conditions [43,64-65]. In general, the increase of the cross-linker content in the membranes decreases the conductivity of the proton conducting membranes as reported by others and us from the previous works because the increase of the cross-linking density of the polymers decreases the chain mobility and the size of the acid clusters [24,47,66]. However, when relatively small amount of BMAEP (the molar ratio of VPA to BMAEP is 100 to 10 for B10) was used as the cross-linker into the semi-IPN membrane, the increase of the proton conductivity was observed because the extra phosphonic acid groups are added into the membrane. However the further increase of BMAEP content (the molar ratios of VPA to BMAEP is 100 to 15 and 100 to 20 for B15 and B20, respectively) decreases the proton conductivity slightly by the increase of the cross-linking density, still their proton conductivity values are larger than those of SPAES membrane at the same relative humidity.

Cell Performance

Considering the mechanical properties and proton conductivities of the semi-IPN membranes, B15 membrane was selected for further studies such as cell

performance, long-term durability, and hydrogen cross-over behaviors. Although the proton conductivity of B15 is slightly smaller than that of B10, the tensile strength of B15 is superior to that of B10. Although B20 has a slightly larger tensile strength value than B15, it was not chosen because of its lower proton conductivity and elongation at break values. The cell performance of the MEAs using B15, SPAES, and recast-Nafion® membranes was measured at 120 ℃ and 40% RH conditions. **Figure 3.10** shows current-voltage (polarization) and power density curves for the H_2/air cells of the MEAs based on SPAES, B15, and recast-Nafion® membranes. The operating voltages and power densities of the cell based on B15 was found to be larger than those based on SPAES over the entire range of current density. Although there is not much differences of the initial cell voltages in the low current density region (0-100 mA cm^{-2}, see insert in **Figure 3.10**) of the MEAs from B15 and SPAES membranes, the limit current density value (550 mA cm^{-2}) of the MEA from B15 was found to be much larger than that (400 mA cm^{-2}) of the MEA from SPAES. In addition, the maximum power density values of the MEAs from B15 and SPAES are 187 and 145 mW cm^{-2}, respectively. Possibly the larger proton conductivity of B15 membrane led to the better cell performance. Although the initial cell voltages in the low current density region of the MEA from B15 are smaller than those from the recast-Nafion® membrane, larger cell voltage values in the ohmic resistance and high current density regions, in the

range of about 100-550 mA cm^{-2}, were observed from the MEA from B15 membrane. The initial voltage drop of polarization curves has been ascribed to the retardation of the oxygen reduction reaction (in the electrochemical activation process) at the cathode [2,67-68]. Since the same electrodes were used for the cell performance measurements of the two MEAs from B15 and recast-Nafion® membranes, the initial cell voltage drops should be attributed to the difference of the interfacial resistance at the membrane-electrode interfaces of the two MEAs [69]. It was reported that the interfacial resistance between the membrane and electrode is highly affected by the fluorine concentration of the membrane when the electrode were fabricated using perfluorinated polymer as the electrode components such as ionomer and binder [13,69-71]. Therefore smaller initial voltage drop was observed when the recast-Nafion® membrane was used because Nafion® is the perfluorinated polymer. However, when B15 was used, larger initial voltage drop was observed possibly due to the increase of resistance between the membrane and electrode because B15 based on hydrocarbon structures has poor compatibility with the perfluorinated ionomer. However, the MEA from B15 membrane shows larger cell voltage values in the ohmic resistance and high current density regions, in the range of about 100-550 mA cm^{-2}, than the MEA from the recast-Nafion® membrane. This better cell performance in these regions could be attributed to the higher proton conductivity of B15 and

lower physical stability of Nafion® at high temperatures. For example, the proton conductivity of B15 and the recast-Nafion® membrane at 120 ℃ and 40% RH are 15 and 10 mS cm^{-1} measured by us and others [72], respectively, and poor physical properties of the recast-Nafion® could be estimated by the hydrogen cross-over current density shown in **Table 3.2**. It was also found that the recast-Nafion® is not practical to use as an electrolyte membrane in high temperature fuel cell. The operating voltage of the MEA with the recast-Nafion® membrane decreased gradually during the activation process used in this study. Thus, it was difficult to obtain reproducible cell performance data of the MEA with the recast-Nafion® membrane during the repetitive cell performance measurements.

Durability Test

In addition to the improvement of the cell performance, the long-term durability of the MEAs is a very important factor to predict the feasibility of the practical fuel cell applications [45,71]. OCV holding test involving the continual cell performance measurements were used to evaluate the electrochemical stability of the MEAs prepared using B15, recast-Nafion®, and SPAES membranes (**Figure 3.11**). The MEA from B15 shows the good electrochemical stability under the operating conditions at 120 ℃ and 40% RH: small decrease of the OCV values from 940 to 904 mV was observed after 100 h operations, and the peak power

density values were maintained in the range of 187-183 mW cm^{-2}. The MEA from the recast-Nafion® membrane shows very poor durability performance as shown in Supplementary Materials: the OCV values decreased from 918 to 600 mV after only 42 h operation possibly due to the well-known disadvantages of Nafion® at high temperatures [56, 73-74]. The durability test under the same experimental condition was also performed using the MEA from SPAES membrane. The peak power density values of the MEA with SPAES membrane, ranging from 140 to 145 mW cm^{-2}, were found to be much smaller than those of the MEA with B15 membrane possibly because of the lower proton conductivity values of the SPAES membrane. The oxidative stability of the membranes was evaluated using the Fenton's test by measuring the residual weight after 1 h using 3 wt.% H_2O_2 aqueous solution containing 4 ppm Fe^{2+} (**Table 3.2**). Although the test results showed that the recast-Nafion® membrane is more stable than SPAES and B15 membranes because the residual weight of the recast-Nafion® membrane was found to be larger than those of SPAES and B15 membranes. However, such Fenton's test result has been known not to represent the cell durability result proportionally as reported by others [2,75]. We also found the MEA from B15 membrane has better cell durability than that from the recast-Nafion® membrane at the operating condition.

The Hydrogen cross-over, one of the most important parameter for the fuel cell membranes, was estimated by measuring the hydrogen cross-over current density [28,76-77]. **Figure 3.12** shows the hydrogen cross-over current density of the MEA from B15 membrane obtained at the beginning and at the end of the operation after 100 h. The hydrogen cross-over values at the beginning are 0.2, 0.3, and 0,5 mA cm^{-2} at 200, 500 and 800 mV, respectively, and those at the end of the operation after 100 h are 0.5, 1.5, and 2.8 mA cm^{-2} at 200, 500 mV, and 800 mV, respectively. B15 membrane possesses quite small hydrogen cross-over values even at the high constant voltage mode after 100 h of operation possibly due to the chemically stable cross-linked structure of the semi-IPN membrane. The hydrogen cross-over values of the MEA from the recast-Nafion® membrane are much larger than those of the MEA from B15 as listed in **Table 3.2**.

3.4. Conclusions

The semi-IPN membranes prepared simply by *in-situ* casting and heating the mixtures of sulfonated poly(arlyene ether sulfone) (SPAES), vinyl phosphonic acid (VPA), and bis(2-(methacryloyloxy)ethyl) phosphate (BMAEP) exhibit much higher proton conductivities than the SPAES membrane without much deterioration of physicochemical stabilities such as thermal and mechanical stabilities. Subsequently, the cell performance of the MEAs with the semi-IPN membranes is much better than that with the SPAES membrane at the high temperature and low humidity condition (120 ℃ and 40% RH). Durability tests demonstrate the feasibility of the semi-IPN membranes as electrolytes for high temperature and low humidity PEMFCs: (1) the OCVs and the cell performances were stable during the long-term operation; (2) extremely small hydrogen cross-over values were observed. Therefore, we strongly believe that this study can provide the insight into the modification of conventional hydrocarbon-based polymer electrolyte membranes and the semi-IPN structures for practical application in high temperature and low humidity PEMFCs.

3.5. References

[1] B.C.H. Steele, A. Heinzel, Nature 414 (2001) 345-352.

[2] Y.Y. Shao, G.P. Yin, Z.B. Wang, Y.Z. Gao, J. Power Sources 167 (2007) 235-242.

[3] S.K. Kim, T. Ko, S.W. Choi, J.O. Park, K.H. Kim, C. Pak, H. Chang, J.C. Lee, J. Mater. Chem. 22 (2012) 7194-7205.

[4] S.K. Kim, S.W. Choi, W.S. Jeon, J.O. Park, T. Ko, H. Chang, J.C. Lee, Macromolecules 45 (2012) 1438-1446.

[5] K.D. Papadimitriou, F. Paloukis, S.G. Neophytides, J.K. Kallitsis, Macromolecules 44 (2011) 4942-4951.

[6] Y.Z. Fu, A. Manthiram, M.D. Guiver, Electrochem. Commun. 8 (2006) 1386-1390.

[7] J. Roziere, D.J. Jones, Annu. Rev. Mater. Res. 33 (2003) 503-555.

[8] B. Bae, K. Miyatake, M. Watanabe, Macromolecules 43 (2010) 2684-2691.

[9] W.L. Harrison, M.A. Hickner, Y.S. Kim, J.E. McGrath, Fuel Cells 5 (2005) 201-212.

[10] Y. Woo, S.Y. Oh, Y.S. Kang, B. Jung, J. Memb. Sci. 220 (2003) 31-45.

[11] P. Xing, G.P. Robertson, M.D. Guiver, S.D. Mikhailenko, K. Wang, S. Kaliaguine, J. Memb. Sci. 229 (2004) 95-106.

[12] L.L. Nie, H. Dong, X. Han, G.W. He, H. Wu, Z.Y. Jiang, J. Power Sources 240 (2013) 258-266.

[13] K.B. Wiles, C.M. de Diego, J. de Abajo, J.E. McGrath, J. Memb. Sci. 294 (2007) 22-29.

[14] J.W. Jung, S.K. Kim, J.C. Lee, Macromol. Chem. Physic. 211 (2010) 1322-1329.

[15] S.-K. Kim, T.-H. Kim, T. Ko, J.-C. Lee, J. Memb. Sci. 373 (2011) 80-88.

[16] S.K. Kim, T.H. Kim, J.W. Jung, J.C. Lee, Polymer 50 (2009) 3495-3502.

[17] S.K. Kim, T.H. Kim, J.W. Jung, J.C. Lee, Macromol. Mater. Eng. 293 (2008) 914-921.

[18] F. Wang, M. Hickner, Y.S. Kim, T.A. Zawodzinski, J.E. McGrath, J. Memb. Sci. 197 (2002) 231-242.

[19] N.W. Li, D.S. Hwang, S.Y. Lee, Y.L. Liu, Y.M. Lee, M.D. Guiver, Macromolecules 44 (2011) 4901-4910.

[20] K.D. Kreuer, J. Memb. Sci. 185 (2001) 29-39.

[21] H.-S. Lee, A. Roy, O. Lane, J.E. McGrath, Polymer 49 (2008) 5387-5396.

[22] M. Ingratta, E.P. Jutemar, P. Jannasch, Macromolecules 44 (2011) 2074-2083.

[23] N. Hara, H. Ohashi, T. Ito, T. Yamaguchi, J. Phys. Chem. B 113 (2009) 4656-4663.

[24] K. Kim, P. Heo, T. Ko, J.-C. Lee, Electrochem. Commun. 48 (2014) 44-48.

[25] J.Fenton, D. Slattery, DOE Hydrogen Program, FY 2012 Annual Progress Report 2012, PP.68-70

[26] C. Houchins, G. Kleen, J. Spendelow, J. Kopasz, D. Peterson, N. Garland, D. Ho, J. Marcinkoski, K. Martin, R. Tyler, D. Papageorgopoulos, Membranes 2 (2012) 855-878.

[27] M. Ueda, H. Toyota, T. Ouchi, J.I. Sugiyama, K. Yonetake, T. Masuko, T. Teramoto, J. Polym. Sci. Pol. Chem. 31 (1993) 853-858.

[28] E.A. Weiber, S. Takamuku, P. Jannasch, Macromolecules 46 (2013) 3476-3485.

[29] S. Nakamura, E. Kashiwa, H. Sasou, S. Hariyama, T. Aoki, Y. Ogami, H. Nishikawa, Electr. Eng. Jpn. 174 (2011) 1-9.

[30] Odian, G. In Principles of Polymerization, 4th ed., Wiley-Interscience, Hoboken, NJ, 2004, pp 149-150.

[31] W.L. Harrison, F. Wang, J.B. Mecham, V.A. Bhanu, M. Hill, Y.S. Kim, J.E. McGrath, J. Polym. Sci. Pol. Chem. 41 (2003) 2264-2276.

[32] A. Bozkurt, W.H. Meyer, Solid State Ionics 138 (2001) 259-265.

[33] A. Aslan, S.U. Celik, A. Bozkurt, Solid State Ionics 180 (2009) 1240-1245.

[34] S.U. Celik, U. Akbey, R. Graf, A. Bozkurt, H.W. Spiess, Phys. Chem. Chem. Phys. 10 (2008) 6058-6066.

[35] L. Chikh, V. Delhorbe, O. Fichet, J. Memb. Sci. 368 (2011) 1-17.

[36] Y.S. Guan, H.T. Pu, H.Y. Pan, Z.H. Chang, M. Jin, Polymer 51 (2010) 5473-5481.

[37] A.K. Kulshreshtha, C. Vasile, Handbook of Polymer Blends and Composites Vol.3A, Rapra Technology Ltd.,Shawbury, UK, 2003, pp 286

[38] L. Sperling, V. Mishra, Polym. Adv. Technol. 7 (1996) 197-208.

[39] T. Ko, K. Kim, B.-K. Jung, S.-H. Cha, S.-K. Kim, J.-C. Lee, Macromolecules 48 (2015) 1104−1114.

[40] L.J. Chen, Y.S. Qin, X.H. Wang, X.J. Zhao, F.S. Wang, Polymer 52 (2011) 4873-4880.

[41] Y.M. Ren, R.Z. Yang, X.L. Liu, F.Q. Liu, Eur. Polym. J. 47 (2011) 2016-2021.

[42] J. Parvole, P. Jannasch, Macromolecules 41 (2008) 3893-3903.

[43] J. Parvole, P. Jannasch, J. Mater. Chem. 18 (2008) 5547-5556.

[44] E. Chalkovaa, C. Wang, S. Komarneni, J. Lee, M. Fedkin, S. Lvov, ECS Trans. 25 (2009) 1141-1150.

[45] M. Marrony, R. Barrera, S. Quenet, S. Ginocchio, L. Montelatici, A. Aslanides, J. Power Sources 182 (2008) 469-475.

[46] D.W. Shin, N.R. Kang, K.H. Lee, D.H. Cho, J.H. Kim, W.H. Lee, Y.M. Lee, J. Power Sources 262 (2014) 162-168.

[47] K. Si, R. Wycisk, D.X. Dong, K. Cooper, M. Rodgers, P. Brooker, D. Slattery, M. Litt, Macromolecules 46 (2013) 422-433.

[48] C. Gao, S.L. Zhang, X.J. Li, S.S. Zhu, Z.H. Jiang, Polymer 55 (2014) 119-125.

[49] O.S. Taskin, B. Kiskan, Y. Yagci, Macromolecules 46 (2013) 8773-8778.

[50] K.S. Lee, M.H. Jeong, Y.J. Kim, S.B. Lee, J.S. Lee, Chem. Mater. 24 (2012) 1443-1453.

[51] N. Zhang, G. Zhang, D. Xu, C.J. Zhao, W.J. Ma, H.T. Li, Y. Zhang, S. Xu, H. Jiang, H.C. Sun, H. Na, Int. J. Hydrogen Energ. 36 (2011) 11025-11033.

[52] Y. Zhang, X. Fei, G. Zhang, H.T. Li, K. Shao, J. Zhu, C.J. Zhao, Z.G. Liu, M.M. Han, H. Na, Int. J. Hydrogen Energ. 35 (2010) 6409-6417.

[53] S.L. Zhong, X.J. Cui, H.L. Cai, T.Z. Fu, C. Zhao, H. Na, J. Power Sources 164 (2007) 65-72.

[54] S. Ray, S.K. Ray, J. Memb. Sci. 270 (2006) 132-145.

[55] P. Gode, A. Hult, P. Jannasch, M. Johansson, L.E. Karlsson, G. Lindbergh, E. Malmstrom, D. Sandquist, Solid State Ionics 177 (2006) 787-794.

[56] H. Dai, H.M. Zhang, Q.T. Luo, Y. Zhang, C. Bi, J. Power Sources 185 (2008) 19-25.

[57] Y. Gao, G.P. Robertson, M.D. Guiver, G. Wang, X. Jian, S.D. Mikhailenko, X. Li, S. Kaliaguine, J. Memb. Sci. 278 (2006) 26-34.

[58] H.P. Bi, J.L. Wang, S.W. Chen, Z.X. Hu, Z.L. Gao, L.J. Wang, K. Okamoto, J. Memb. Sci. 350 (2010) 109-116.

[59] B.P. Tripathi, V.K. Shahi, J. Phys. Chem. B 112 (2008) 15678-15690.

[60] C.Y. Tseng, Y.S. Ye, K.Y. Kao, J. Joseph, W.C. Shen, J. Rick, B.J. Hwang, Int. J. Hydrogen Energ. 36 (2011) 11936-11945.

[61] R. Tayouo, G. David, B. Ameduri, J. Roziere, S. Roualdes, Macromolecules 43 (2010) 5269-5276.

[62] A. Aslan, A. Bozkurt, J. Power Sources 217 (2012) 158-163.

[63] G.W. He, J. Zhao, S. Hu, L.Q. Li, Z.Y. Li, Y.F. Li, Z. Li, H. Wu, X.L. Yang, Z.Y. Jiang, Acs Appl. Mater. Inter. 6 (2014) 15291-15301.

[64] Z. Florjanczyk, E. Wielgus-Barry, Z. Poltarzewski, Solid State Ionics 145 (2001) 119-126.

[65] H. Steininger, M. Schuster, K.D. Kreuer, A. Kaltbeitzel, B. Bingol, W.H. Meyer, S. Schauff, G. Brunklaus, J. Maier, H.W. Spiess, Phys. Chem. Chem. Phys. 9 (2007) 1764-1773.

[66] L.C. Fu, G.Y. Xiao, D.Y. Yan, J. Mater. Chem. 22 (2012) 13714-13722.

[67] B.J. Yao, X.L. Yan, Y. Ding, Z.J. Lu, D.X. Dong, H. Ishida, M. Litt, L. Zhu, Macromolecules 47 (2014) 1039-1045.

[68] J. Zhang, Z. Xie, J. Zhang, Y. Tang, C. Song, T. Navessin, Z. Shi, D. Song, H. Wang, D.P. Wilkinson, Z.-S. Liu, S. Holdcroft, Journal of Power Sources 160 (2006) 872-891.

[69] C.H. Lee, S.Y. Lee, Y.M. Lee, S.Y. Lee, J.W. Rhim, O. Lane, J.E. McGrath,

ACS Appl. Mater. Interfaces 1 (2009) 1113-1121.

[70] Y.S. Kim, M.J. Sumner, W.L. Harrison, J.S. Riffle, J.E. McGrath, B.S. Pivovar, J. Electrochem. Soc. 151 (2004) A2150-A2156.

[71] S.K. Kim, K.H. Kim, J.O. Park, K. Kim, T. Ko, S.W. Choi, C. Pak, H. Chang, J.C. Lee, J. Power Sources 226 (2013) 346-353.

[72] D.H. Hadis Zarrin, Yu Jun, Zhongwei Chen, Michael Fowler, J. Phys. Chem. C 115 (2011) 20774-20781.

[73] M.A. Hickner, H. Ghassemi, Y.S. Kim, B.R. Einsla, J.E. McGrath, Chem. Rev. 104 (2004) 4587-4611.

[74] T. Miyahara, T. Hayano, S. Matsuno, M. Watanabe, K. Miyatake, Acs Appl. Mater. Inter. 4 (2012) 2881-2884.

[75] Vijay A. Sethuraman, John W. Weidner, Andrew T. Haug, Sathya Motupally, a.L.V. Protsailo, , Journal of The Electrochemical Society, 155 (2008) b50-b57.

[76] S. Lu, R. Xiu, X. Xu, D. Liang, H. Wang, Y. Xiang, J. Membr. Sci. 464 (2014) 1-7.

[77] Y. Fu, A. Manthiram, M.D. Guiver, Electrochem. Commun. 9 (2007) 905-910.

Table 3.1 Mechanical properties, and IEC of SPAES and semi-IPN membranes (B10, B15 and B20).

Membrane	Tensile Strength (MPa)	Elongation at break (%)	IEC_w[a] (mequiv. g^{-1})
SPAES	55.0 ± 0.4	30.4 ± 7.8	1.97
B10[b]	41.6 ± 2.1	19.9 ± 0.8	2.30
B15[b]	44.6 ± 2.7	14.8 ± 5.1	2.20
B20[b]	48.6 ± 4.1	13.0 ± 3.3	2.07

[a] Calculated by back titration method.

[b] B10, B15, and B20 are the semi-IPN membranes prepared using the molar ratios of VPA vs BMAEP of 100: 10, 100: 15, and 100: 20, respectively.

Table 3.2 Results of oxidative stability test and hydrogen cross-over measurement.

Membrane	Residual weight[a] (%)	Hydrogen cross-over[b] (mA cm^{-2})	
		200[c] (mV)	500[c] (mV)
SPAES	83	0.2	0.3
B15	83	0.2	0.3
Recast-Nafion®	98	1.3	1.8

[a] Obtained by Fenton's test.

[b] Measured at the beginning of the operation at 120 ℃ and 40% RH.

[c] Applied DC voltages between the electrodes.

(a)

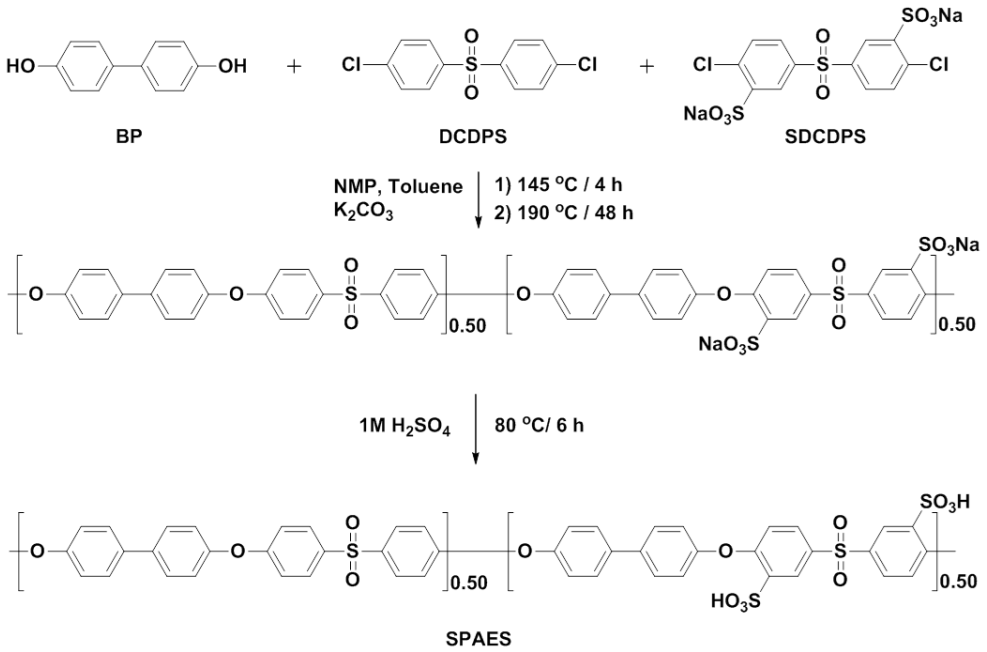

(b)

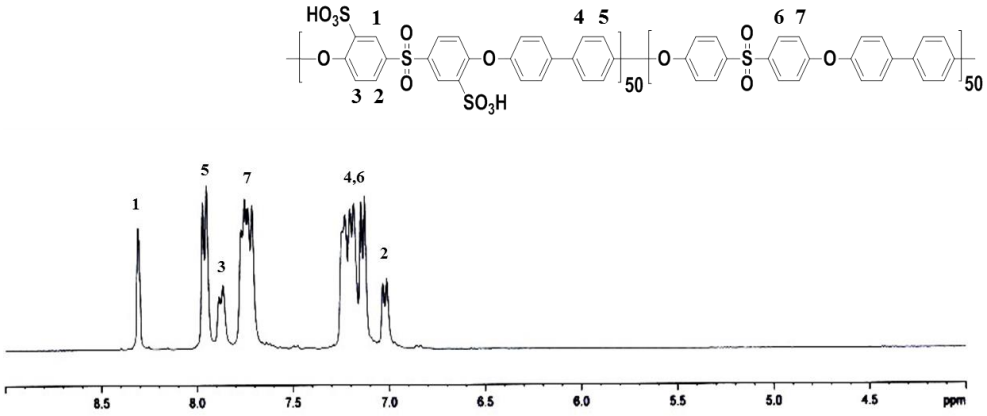

Figure 3.1 (a) Synthesis of SPAES and (b) ^{1}H-NMR spectrum of SPAES.

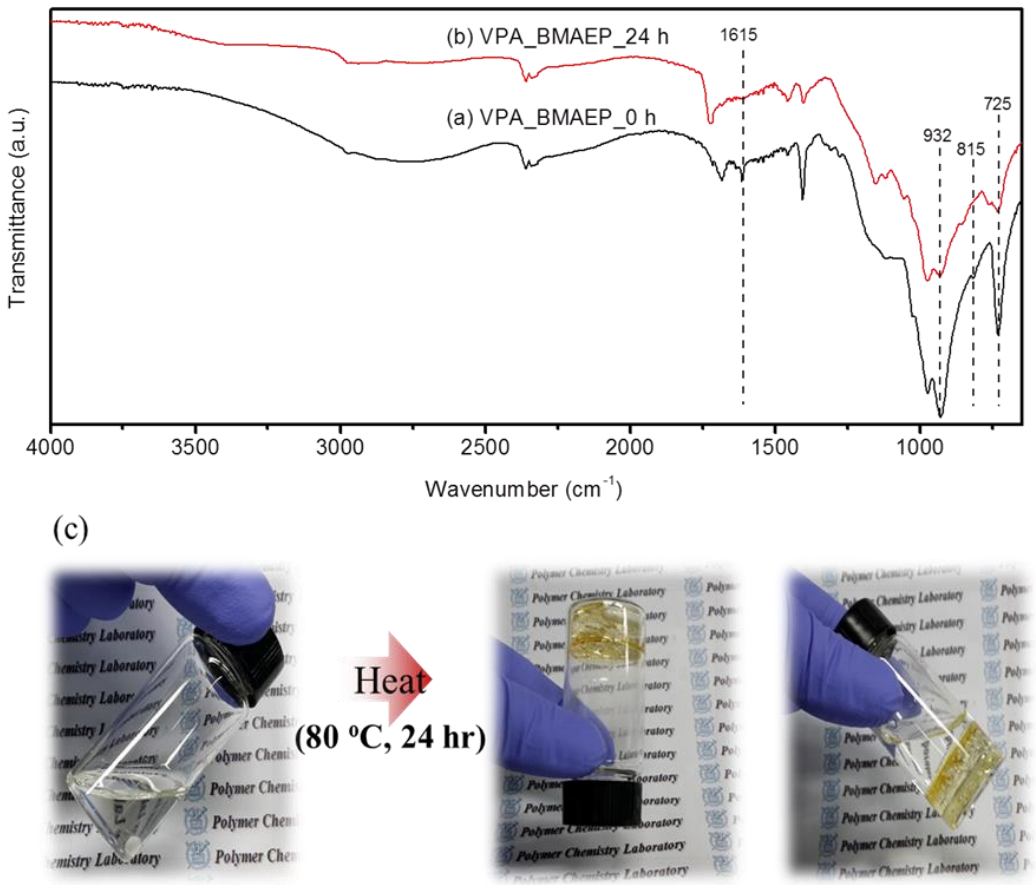

Figure 3.2 Infrared spectra of VPA-based solution containing BMAEP and thermal initiator (AIBN). (a) Before thermal treatment (b) after thermal treatment at 80 ℃ for 24 h. (c) Photo images of VPA-based solution after thermal treatment at 80 ℃ for 24 h.

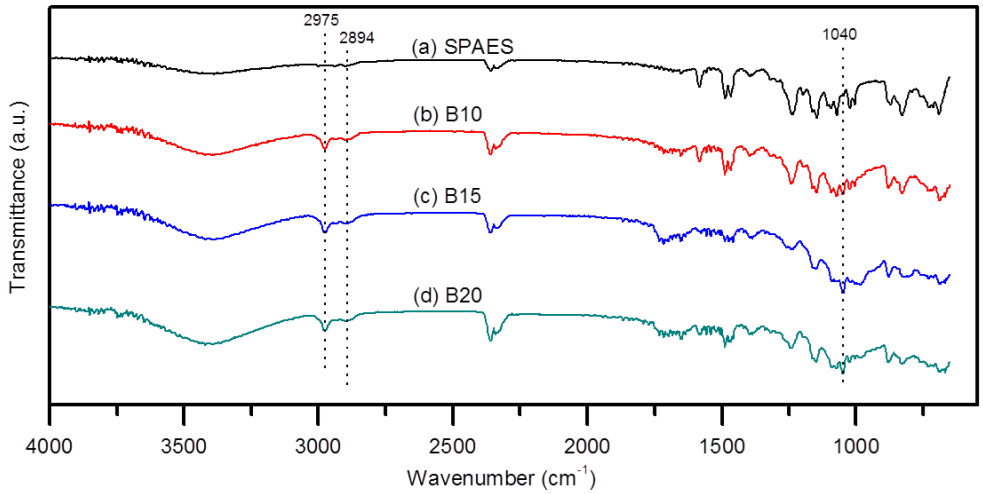

Figure 3.3 Infrared spectra of (a) SPAES, (b) B10, (c) B15, and (d) B20 membranes.

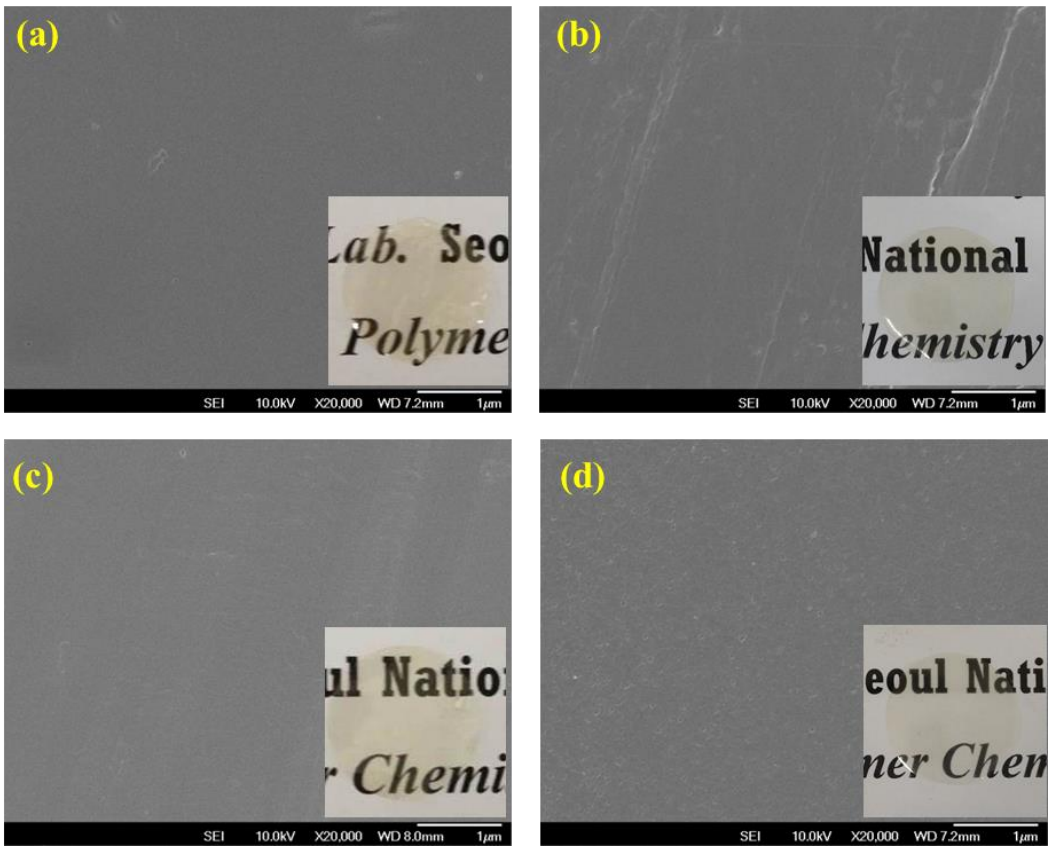

Figure 3.4 SEM and photo (inset) images of (a) SPAES, (b) B10, (C) B15, and (d) B20 membranes.

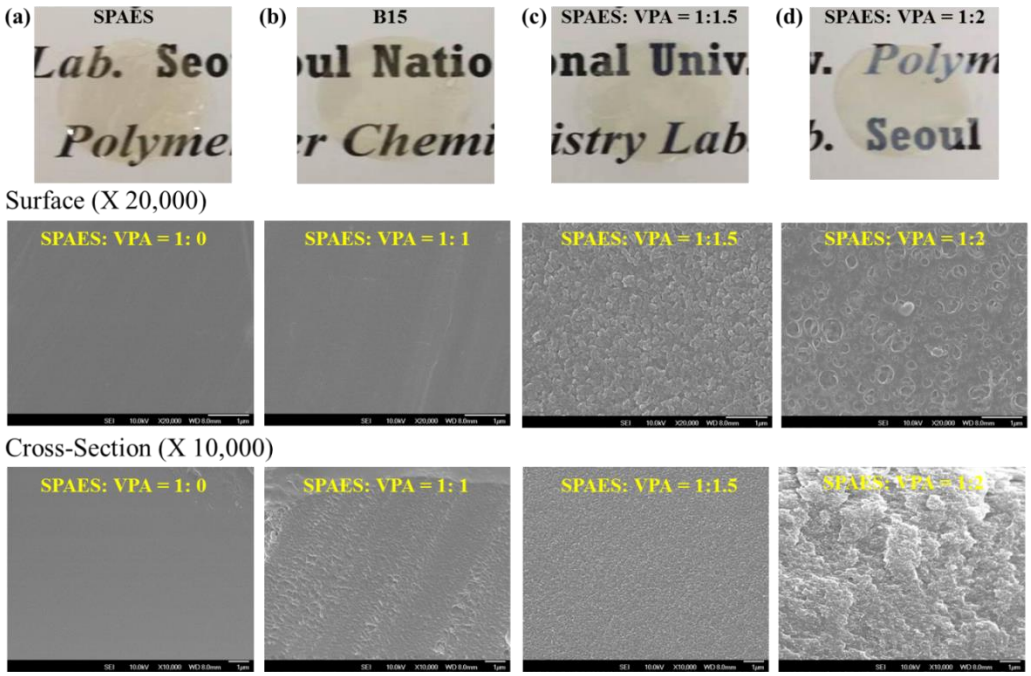

Figure 3.5 Photo and SEM images (surface and cross-section) of the membranes with various weight ratios of SPAES to VPA. (a) VPA 0 (SPAES: VPA = 1: 0, SPAES) (b) VPA 1.0 (SPAES: VPA = 1: 1, B15) (c) VPA 1.5 (SPAES: VPA = 1: 1.5) (d) VPA 2.0 (SPAES: VPA = 1: 2). Molar content of BMAEP in the all semi-IPN membranes is 0.15 mol of VPA.

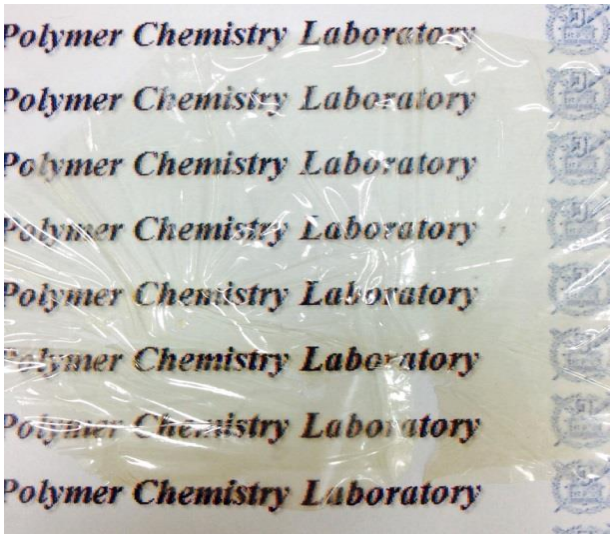

Figure 3.6 Photo image of semi-IPN membrane using divinyl benzene as a cross-linker.

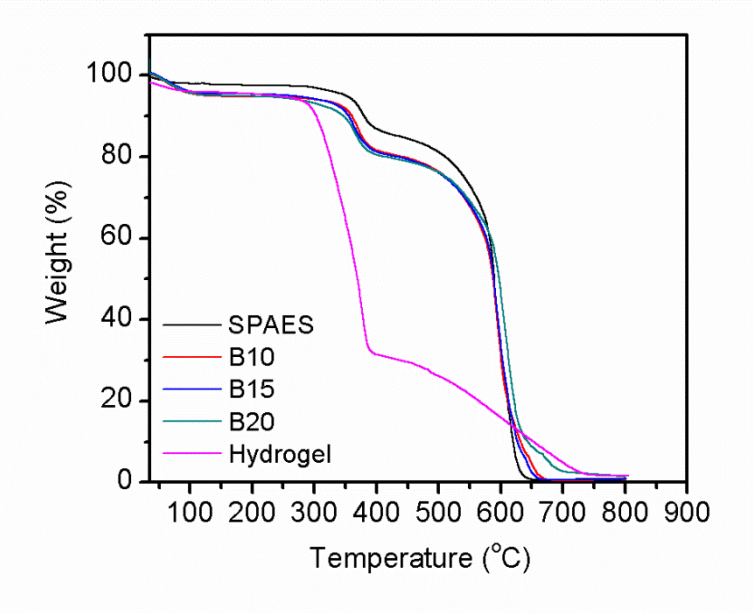

Figure 3.7 TGA curves of SPAES and semi-IPN membranes (B10, B15, and B20), and the hydrogel prepared by heating at 80 °C for 24 h using 1.0: 0.15 molar ratio of VPA to BMAEP (the same composition used for B15) without SPAES.

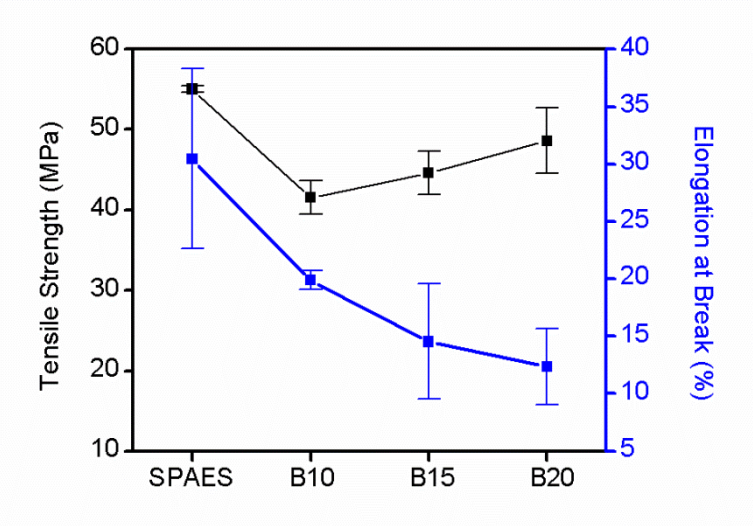

Figure 3.8 Tensile strength and elongation at break of SPAES and semi-IPN (B10, B15, and B20) membranes.

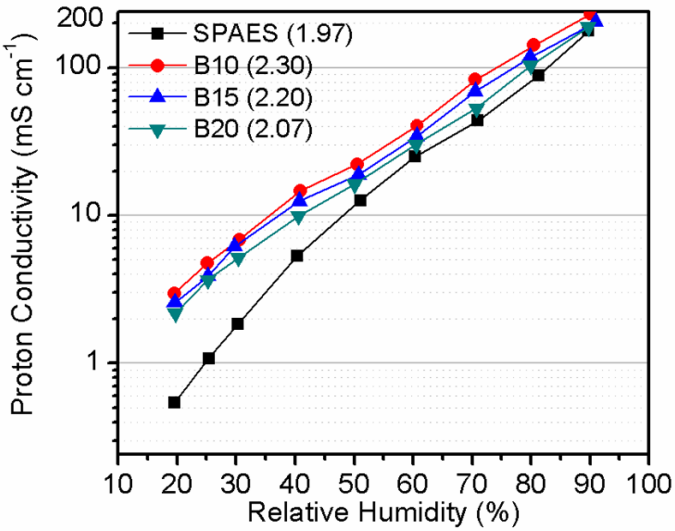

Figure 3.9 Proton conductivities of SPAES and semi-IPN (B10, B15, and B20) membranes at 120 °C as a function of relative humidity.

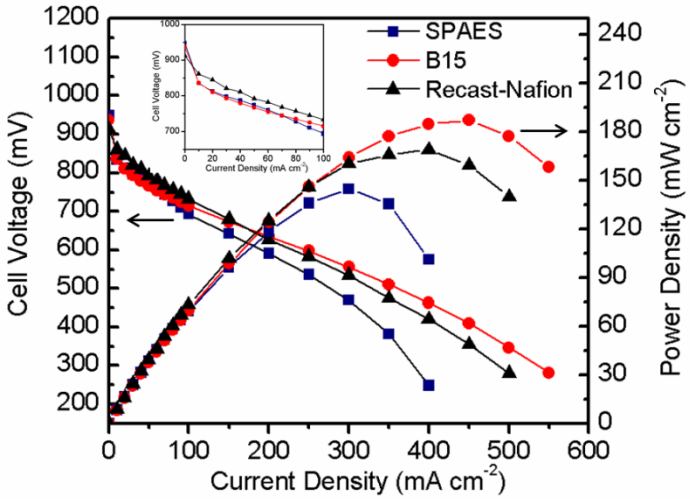

Figure 3.10 Cell voltage and power density as a function of the current density for MEAs prepared using SPAES, B15, and recast-Nafion® membranes at 120 °C and 40% RH. The thicknesses of these membranes are about 20 μm and their active areas are 10 cm^2. (Inset) enlargement of polarization curves in the range of 0-100 mA cm^{-2}.

(a)

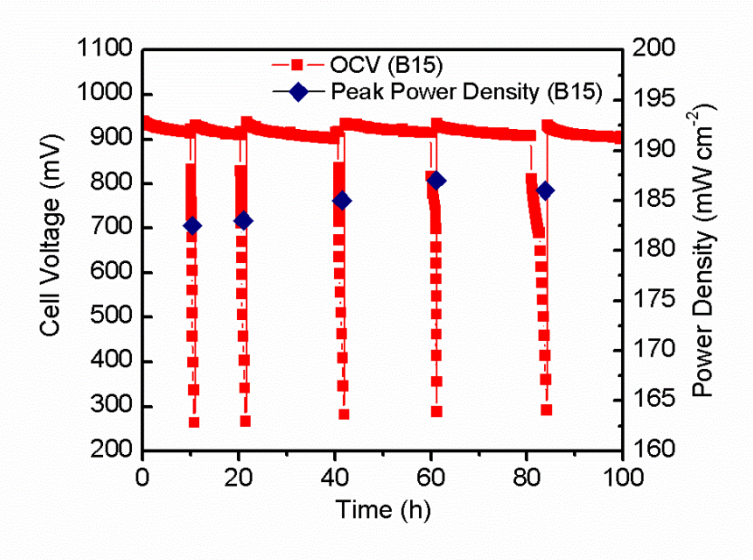
OCV (B15)
Peak Power Density (B15)
Cell Voltage (mV)
Power Density (mW cm-2)
Time (h)
1100
1000
900
800
700
600
500
400
300
200
200
195
190
185
180
175
170
165
160
0
20
40
60
80
100

(b)

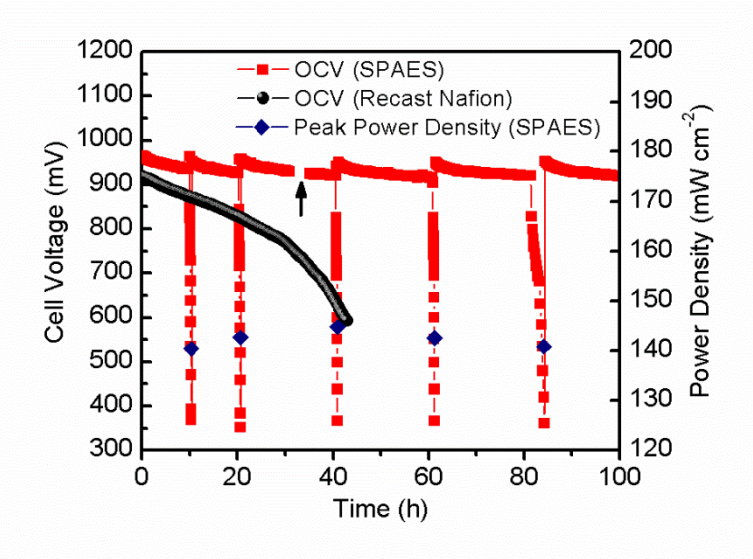
OCV (SPAES)
OCV (Recast Nafion)
Peak Power Density (SPAES)
Cell Voltage (mV)
Power Density (mW cm-2)
Time (h)
1200
1100
1000
900
800
700
600
500
400
300
200
190
180
170
160
150
140
130
120
0
20
40
60
80
100

Figure 3.11 Durability test (OCV holding method involving the continual I-V measurements) of the MEAs prepared using (a) B15 membrane (b) at 120 °C and 40% RH for 100 h. recast-Nafion® and SPAES membranes at 120 °C and 40% RH for 100 h. Arrow on figure denotes the region induced by temporary recording error.

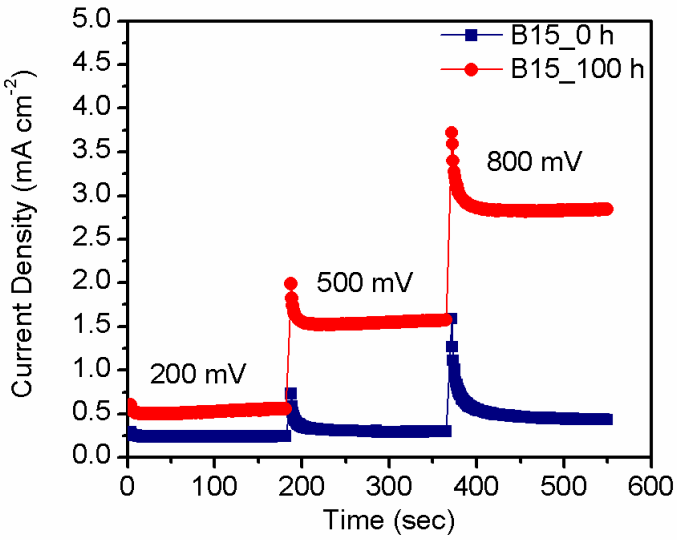

Figure 3.12 Hydrogen cross-over current density of the MEA prepared using B15 membrane at 120 °C and 40% RH obtained by applying step-wise DC voltages (at 200, 500, and 800 mV) between the electrodes with supplying hydrogen and nitrogen into the anode and cathode, respectively.

Chapter 4

Highly Reinforced Pore-Filling Electrolyte Membranes from Sulfonated Poly(Arylene Ether Sulfone)s for High-Temperature Fuel Cell Applications

4.1. Introduction

Polymer electrolyte membranes (PEMs) have been studied intensively due to their potential application in chemical energy conversion devices such as polymer electrolyte membrane fuel cells (PEMFCs) [1,2]. Especially, recent studies have focused on the development of PEMs operating at high temperatures (above 100 ℃) and low relative humidity (< 50% RH) for the practical application of PEMFCs to automobile transportation [3,4]. In particular, thin and high-conductive PEMs are strongly preferred in automotive application, necessitating high-power density [5]. A formidable challenge in developing thin membranes is the accompanying loss of their mechanical strength and dimensional stability. In order to overcome these limitations, numerous approaches including the preparation of composite and cross-linked membranes have been suggested [6-9]. Recently pore-filling electrolyte membranes, a kind of hybrid membranes consisting of mechanically reinforcing porous substrate and proton conducting electrolyte, have attracted considerable attention because reasonably thin membranes with high mechanical strength and good dimensional stability can be prepared [10-14]. The physicochemical stability of the reinforcing porous substrate and the compatibility between the porous substrate and the impregnated

proton conducting electrolyte have been found to be very important for pore-filling membrane systems to show good cell performance [15,16]. Representative examples of the porous substrates most widely used in industries are poly(tetrafluoroethylene) (PTFE) and polyimide (PI). Although these porous substrates exhibit high physical, mechanical, and thermal stabilities, there are more challenges to improve the cell performance of the pore-filling membrane systems by improving the interactions between the porous substrates and the impregnated proton conducting polymers. Intrinsically the hydrophilic proton conducting polymers such as Nafion® are not comparable with the hydrophobic porous PTFE or PI substrates [5,17]. The compatibility could be improved by pre-treatments including solvent boiling or SiO_2 coating on the PTFE or PI substrates, while these pre-treatment processes can decrease the stability and pore-size of the porous substrates [5,17-19].

We previously prepared phosphoric acid doped cross-linked polybenzimidazole (PBI) and polybenzoxazine (PBOA) copolymer membranes which showed outstanding cell performances and long-term durability at elevated temperatures due to their good compatibility with hydrophilic phosphoric acid and high mechanical strength [20-22]. In this study, porous cross-linked PBOA–PBI substrates with tunable pore-size and porosity as well as high physical stability were prepared by mixing and heating the mixture of 3-phenyl-3,4- dihydro-6-*tert*-

butyl-2*H*-1,3-benzoxazine (*p*BUa), PBI, and dibutyl phthalate (DBP) as a porogen in *N*,*N*-dimethylacetamide followed by an extraction process. The detailed synthesis procedure and properties of the porous substrates are provided in this paper, including their morphology and mechanical properties. A series of sulfonated poly(arylene) ether sulfone (SPAES) with high degree of sulfonation (DS, mol%) from 60 to 80 mol% were used as the proton conducting polymer electrolytes filling the pores of the substrates because of their high proton conductivity [17,23]. Although SPAESs with such high DS have high proton conductivity, they have not been able to be used as polymer membranes for fuel cell application because their physical and mechanical stability is very poor at the hydrated state [8,9,24]. However, they could be used in this study as pore-filling materials because the porous cross-linked substrates can maintain the physical and dimensional stability of the membrane systems.

The detailed synthesis procedure for the preparation of the pore-filling membranes consisting of porous cross-linked PBOA–PBI substrate and SPAES is discussed, including their properties such as morphology, water absorption behavior, dimensional and mechanical stabilities, and proton conductivity. Furthermore, the cell performances of membrane electrode assemblies from the pore-filling membranes are compared with that from the pristine SPAES membrane at 120 ℃ and 40% RH.

4.2. Experimental

Materials

Isophthalic acid (99%, Aldrich), 4,4'-difluorodiphenylsulfone (DFDPS, 99.0%, Aldrich) and 4,4'-dihydroxybiphenyl (BP, 97.0%, Aldrich) were recrystallized from ethanol, toluene, and methanol, respectively. Disulfonate-4,4'-difluorodiphenylsulfone (SDFDPS) was synthesized from DFDPS as described by Harrison *et al* [25]. The yield of SDFDPS after recrystallization was 86%. *N*-Methyl-2-pyrrolidone (NMP, 99.0%, Junsei) and *N*,*N*-dimethylacetamide (DMAc, 99.0%, Junsei) were stored over molecular sieves under nitrogen and toluene (99.5%, Junsei) was refluxed over calcium hydride and distilled. Potassium carbonate (K_2CO_3, 99.0+%, Aldrich) was dried under vacuum at 80 ^oC for 48 h, prior to use. Fuming sulfuric acid (65% SO_3, Merck), sodium chloride (NaCl, 99.5%, Daejung), sodium hydroxide (NaOH, 98.0%, Daejung), 3,3'–diaminobenzidine (97%, Tokyo Kasei, TCI), polyphosphoric acid (PPA, 116% H_3PO_4, Junsei), and phosphorous pentoxide (97%, Aldrich), 4–*tert*–butylphenol (99%, Aldrich), *p*–formaldehyde (95%, Aldrich), aniline (99%, Aldrich) and dibutyl phthalate (DBP, 99%) were used without further purification.

Synthesis of sulfonated poly(arylene ether sulfone) (SPAES-X)

A series of sulfonated poly(arylene ether sulfone) (SPAES-X), where X is the feed monomer ratio of SDFDPS, were synthesized by the condensation polymerization of the dihydroxy monomer (BP) with the mixture DFDPS and SDFDPS. The degree of sulfonation (DS, mol%) of the SPAES was controlled by changing the ratio of SDFDPS to DFDPS. When the molar ratios of SDFDPS to DFDPS were 60: 40, 70: 30, and 80: 20, they are respectively represented herein by SPAES-60, SPAES-70, and SPAES-80. The following procedure was used for the preparation of SPAES-60 in potassium form (K^+). A 250 mL three-neck flask equipped with an overhead mechanical stirrer, a nitrogen inlet and outlet, a condenser, and a Dean-Stark trap was charged with 5.0 g (26.9 mmol) of BP, 2.7 g (10.8 mmol) of DFDPS, 7.4 g (16.1 mmol) of SDFDPS, and 4.5 g (32.3 mmol) of K_2CO_3 in 60.0 mL of NMP (~25 wt%). Then 30.0 mL of toluene (NMP/toluene = 2/1 v/v) was used as an azeotrope agent. The reaction mixture was heated at 145 ℃ for 4 h to ensure complete dehydration. The temperature was raised slowly to 190 ℃ for the complete removal of the toluene. The reaction was allowed to proceed for another 24 h. During the polymerization, the reaction mixture turned to a viscous brown-colored solution. The solution was cooled to room temperature and diluted with 10.0 mL of NMP. The diluted solution was filtered to remove the salts and decanted into *iso*-propyl alcohol (1000 mL) to isolate the polymer, and the

precipitate was rinsed several times with *iso*-propyl alcohol. The obtained off-white powder was dried at 60 ℃ in a vacuum oven for 24 h. Final yield of SPAES-60 in the potassium form was larger than 92%. SPAES-70 (Yield > 90%) and SPAES-80 (Yield > 85%) in the potassium form were synthesized using the same procedure except for the molar ratios of SDFDPS to DFDPS.

Preparation of porous poly[(3-Phenyl-3,4-dihydro-6-tert-butyl-2*H*-1,3-benzoxazine-*co*-(2,2'-(*m*-phenylene)-5,5'-(bibenzimidazole)] (P(*p*BUa-*co*-BI)-#) substrates

3-Phenyl-3,4-dihydro-6-*tert*-butyl-2*H*-1,3-benzoxazine (*p*BUa) and poly[2,2'-(*m*-phenylene)-5,5'-(bibenzimidazole)] (*p*BUa) were synthesized as reported previously [20]. The yields of *p*BUa and PBI are 94% and 95%, respectively, and the inherent viscosity of the PBI (0.91 dL g^{-1}) is sufficient to produce free-standing films with reasonable physical properties for fuel cell application [26]. The mixture of *p*BUa, PBI, and DBP as a porogen was used to prepare the porous substrate, where *p*BUa and PBI in the weight ratio of 50: 50 was used because this ratio was found to produce a cross-linked copolymer membrane with high mechanical strength [20]. The content of DBP was changed from 70 to 90 wt% compared with the total weight of the *p*BUa and PBI mixture, and when the

content of DBP is 70, 80, and 90 wt%, they are abbreviated as P(*p*BUa-*co*-BI)-70, P(*p*BUa-*co*-BI)-80, and P(*p*BUa-*co*-BI)-90, respectively. The following procedure was used for the preparation of P(*p*BUa-*co*-BI)-90. A solution mixture consisting of 0.68 g of PBI, 0.68 g of *p*BUa, and 1.23 g of DBP in 5.83 g of DMAc was cast onto a clean flat glass plate. The thickness of the blended solution was controlled using a doctor blade film applicator. The cast solution was heated from 60 to 220 ℃ for 4 h and then maintained at 220 ℃ for 1 h in a convection oven. After cooling to room temperature, the obtained brown-colored membrane was soaked in distilled water and peeled from the glass plate. DBP was then extracted from the membrane by immersing in methanol for 4 h. The porous substrate, P(*p*BUa-*co*-BI)-90, was obtained after washing with distilled water several times and drying in a vacuum oven overnight. The P(*p*BUa-*co*-BI)-50, -70, and -80 substrates were fabricated using the same procedure except for the weight ratios of DBP to *p*BUa and PBI. The thicknesses of all P(*p*BUa-*co*-BI)-# substrates were in the range of 15 to 20 μm.

Preparation of pore-filling and pristine SPAES membranes

Pore-filling membranes were fabricated by the polymer impregnation method. P(*p*BUa-*co*-BI)-90 was selected as a porous substrate for the preparation of the

reinforced pore-filling membranes because it has a reasonable mechanical strength with the largest porosity, which can give the largest proton conductivity, as discussed in the Results and Discussion part. P(*p*BUa-*co*-BI)-90 were submerged in each dilute SPAES-X solution (mass fraction less than 10 wt% in DMF) at 60 ℃ for 2 h. The substrates were then unfolded on the glass plate and dried at 100 ℃ for 2 h. The impregnation and drying processes were repeated two times in order to eliminate or minimize voids and pin-holes in the pore-filling membrane. Then, the membranes were vacuum dried at 80 ℃ for 24 h to remove any further residual solvent. After cooling to room temperature, the obtained membranes were soaked in distilled water and then dried in a vacuum oven for 24 h. The obtained pore-filling membranes were denoted as PF-X membranes. X indicates the DS of SPAES-X estimated using the feed monomer ratio of the SDFDPS. Therefore, PF-60, PF-70, and PF-80 membranes are the pore-filling membranes which were prepared with the SPAES-60, -70, and -80 solutions, respectively. The thicknesses of all the PF-X membranes were found to be in the range of 15 to 20 μm.

Pristine SPAES-60 and -70 membranes were prepared as the control samples by casting 15 wt% of each solution onto the glass plate followed by drying at 100 ℃ for 24 h. The film thicknesses of the SPAES-60 and -70 membranes were controlled using a doctor blade film applicator and membranes with a thickness of

about 50 μm were prepared. SPAES-80 could not be prepared as a pristine membrane because its free standing state is not maintained during the protonation process due to the high DS. Therefore, SPAES-80 was only used as a filling polymer electrolyte for the preparation of the PF-80 membrane, not for the free standing membrane. The SPAES-X and PF-X membranes in potassium form (K^+) were transformed to their acid form (H^+) by soaking in 1 M H_2SO_4 aqueous solution at 40 ^oC for 24 h. The membranes in acid form were then rinsed with distilled water several times and then dried in a vacuum oven for 24 h.

Preparation of membrane electrode assemblies (MEAs)

Membrane electrode assemblies (MEAs) were fabricated by a decal method [3]. The catalyst inks were prepared by mixing catalyst powder (50 wt. % Pt/C, Tanaka Kikinzoku Kogyo), Aquivion^{TM} ionomer dispersion (EW750, Solvay) and solvent mixture comprising water and ethanol. The ink was mixed using an ultrasonic vibrator (Sonic, Vibra-cell) to obtain a uniformly dispersed ink mixture. The catalyst layer was prepared by coating the ink mixture on a PTFE sheet and drying it at 60 ℃. The catalyst layer was then placed onto the membrane, and the two layers were hot pressed together at 120 ℃ to transfer catalyst layer onto the

membrane and prepare the MEA. The Pt loading of the MEA was 0.4 mg/cm^2, and the ionomer content in the catalyst layer was 30%.

Characterization

The ^{1}H-NMR spectra were collected on Avance 400 (Bruker, Germany) with a proton frequency of 400 MHz using deuterated dimethylsulfoxide as the solvent and tetramethylsilane as the internal standard. Ion-exchange capacity (IEC) of the samples was estimated by back-titration method [27]. The membranes were soaked in 1 M NaCl aqueous solution for 24 h, and then the solution was titrated with 0.01 M NaOH aqueous solution. The value of IEC was calculated using the following equation:

$$IEC\ [mequiv.g^{-1}] = (C_{NaOH} \cdot \Delta V_{NaOH} / W_s) \times 1000 \quad (1)$$

where C_{NaOH}, ΔV_{NaOH}, and W_s are the concentration of NaOH (aq), the consumed volume of NaOH (aq), and the weight of the dry membrane, respectively.

Molecular weights (M_n and M_w) were measured at 35 ℃ by gel permeation chromatography consisting of a Waters 510 HPLC pump, three columns PLgel 5 μm guard, MIXED-C, MIXED-D, and a Viscoter T60A dual detector. HPLC grade DMF was used as the eluent and the flow rate was 1.0 mL min^{-1}. Calibration was performed with poly(methyl methacrylate) standards. Average pore-size and

porosity of the P(*p*BUa-*co*-BI)-# substrates were measured by mercury porosimeter (Autopore Ⅳ 9500, Micromeritics, USA). In order to minimize experimental error, three samples of each substrate were tested and the average value was taken. Density of the porous substrate was calculated from membrane dimension and weight after drying at 100 ℃ for 24 h. The porosity ($\oint$ p, %) of the porous substrates was also calculated using the following equation [19,28,29].

$$\oint \mathrm{p}(\%) = \left\{1 - \frac{\mathrm{w_{sub}}/\rho_{\mathrm{sub}}}{\mathrm{V_{sub}}}\right\} \times 100 \quad (2)$$

where W_{sub} and ρ_{sub} are the dry substrate weight and density of substrate material, and V_{sub} is the dry membrane volume, estimated from membrane area and thickness.

The cross-sectional morphology of the porous P(*p*BUa-*co*-BI) substrates and pore-filling membrane was analyzed using a field-emission scanning electron microscopy (FE-SEM, Carl Zeiss SUPRA 55VP, Germany) equipped with energy-dispersive spectrometer (EDS). All the samples were coated with platinum under vacuum prior to the test. The cross-sectional specimens of the membranes were prepared by breaking the membrane manually after cooling using liquid nitrogen [30]. Distribution of carbon, nitrogen, sulfur, and sodium atoms along with the cross-sectional surface of the pore-filling membrane was determined by an EDS

mapping method [31]. To confirm the distribution of the sulfonic acid group of the SPAES in the pore-filling membrane, the pore-filling membrane in acid form (H^+) was converted to sodium form (Na^+) by immersing it in 1M NaOH solution for 24 h to produce sodium SPAES (Na-SPAES-X) and sodium pore-filling membranes (Na-PF-X). Through this treatment, the sodium element was used as a signal of the sulfonic acid group in the SPAES. FT-IR spectra of samples were recorded in the attenuated total reflectance (ATR) mode in the frequency range of 4000 to 650 cm^{-1} on a Nicolet 6700 instrument (Thermo Scientific, USA). The spectra were recorded as an average of 32 scans with the resolution of 8 cm^{-1}. The samples were put in equal physical contact with the sampling plate of the spectrometer accessory to avoid differences caused by pressure and penetration depth. The water uptake and dimensional change of the membranes were determined by measuring their change in weight, area, and thickness between the dry and swollen membranes. The dry membranes were cut into 2 cm × 2 cm, and then their weight and thickness were measured. Then, the membranes were immersed in deionized water at a given temperature for 2 h. After the membranes were taken out and wiped with tissue paper, their weight, area, and thickness were measured as soon as possible. The water uptake and change in area and thickness of the membranes were calculated by the following equations:

$$\text{Water uptake [\%]} = [(W_{wet}-W_{dry})/W_{dry}] \times 100 \quad (3)$$

Change in area [%] = $[(A_{wet} - A_{dry})/A_{dry}] \times 100$ (4)

Change in thickness [%] = $[(T_{wet} - T_{dry})/T_{dry}] \times 100$ (5)

where W_{dry} and W_{wet} are the weight of the dry and wet membranes. A_{dry} and A_{wet} are the area of the dry and wet membranes, and T_{dry} and T_{wet} are the thickness of the dry and wet membranes, respectively.

The mechanical properties were measured using a universal testing machine (Lloyd LR-10K, UK). Dumbbell specimens were prepared using the ASTM standard D638 (Type V specimens). The tensile properties of the membrane samples were measured in air at 25 ℃ under a 40% RH with a gauge length and cross head speed of 15 mm and 5 mm min^{-1}, respectively. For each measurement, at least seven samples were used and their average value was calculated. Proton conductivity of the membranes was estimated over the relative humidity (RH) of 20-90% at 120 ℃. The membrane was fixed to a four-point conductivity cell and connected to the test equipment (BekkTech BT-552MX, USA) for the continuous control of cell temperatures and RH. The RH in the cell was controlled by feeding with hydrogen gas humidified by passing the gas flow through a humidification column using hydrogen at 120 ℃ and 230 kPa under an input flow rate of 500 cm^3 min^{-1}. The membrane was pre-equilibrated at 120 ℃ and 70% RH for 2 h, the conductivity measurement was then started from 70% RH. The test was continued

by lowering the humidity to 20% RH and then by raising to 90% RH at 10% intervals with a 15 min equilibration time for each measurement. Thermo-gravimetric analyzer (TGA, Q5000IR, TA instruments, USA) was used to measure the thermal stability and water bound state [32,33]. The samples were heated from 35 to 800 ℃ with a heating rate of 10 ℃ min^{-1} under air atmosphere. Before the TGA measurement, the samples were soaked in water at 40 ℃ for 4 h, and then pre-equilibrated in a temperature and humidity controllable chamber (Espec, SH-241) at 80 ℃ and 40% RH for 2 h, in order to ensure the membranes are exposed to the identical pre-treatment. The fraction of physically-bound water was quantified by measuring the weight loss below 100 ℃. The content of chemically-bound water was calculated by subtracting the physically-bound water content from the total water content [33]. The total water content could be estimated by the weight difference of the samples before and after the vacuum drying step.

To test performance of the MEAs prepared from the membranes, the cells were assembled by placing two gas diffusion layers (TGP-H-060, Toray) on both sides of the MEA. The PTFE gaskets of 130 μm thickness were used to provide adequate compression and seal the cell. The assembled the cell was connected to a fuel cell test station (Scribner Associates Inc., 850e Fuel Cell Test Station), and the temperature was raised to 120 ℃. The flow rates of hydrogen and air were 52 cm^3 min^{-1} and 200 cm^3 min^{-1}, respectively, and both inlet gases were humidified to

the level of 40% RH. The cells were operated at the ambient pressure and the voltage values at each current density were taken after one minute of current application.

4.3. Results and Discussion

Synthesis of Sulfonated Poly(arylene ether sulfone)s (SPAESs)

A series of sulfonated poly(arylene ether sulfone)s (SPAESs) with different degree of sulfonation (DS, mol%) were successfully synthesized *via* the K_2CO_3 catalyzed nucleophilic aromatic substitution reaction of 4,4'-dihydroxybiphenyl (BP) with different molar ratio of 4,4'-diflourodiphenylsulfone (DFDPS) and 3,3'-disulfonate-4,4'-difluorodiphenylsulfone (SDFDPS) from 20: 80 to 40: 60, as shown in **Figure 4.1(a)** [34]. The chemical structures and compositions of the obtained SPAESs in the potassium form (K^+) were confirmed by ^{1}H NMR spectroscopy (**Figure 4.1(b)**). The DS values of SPAES-60, SPAES-70, and SPAES-80 calculated from the integral ratio of proton peaks were 57, 67, and 76, respectively (**Table 4.1**). The difference between the feed molar content of SDFDPS and DS should be caused by the different reactivity of DFDPS and SDFDPS because they have different chemical structures [25,35]. The experimental IEC values of SPAESs, calculated from the equation (1), were found to also be close to the calculated values obtained from ^{1}H NMR results and the molecular weights of SPAESs, which are larger than 75000 g mol^{-1}, could be confirmed by the GPC results (**Table 4.1**).

Preparation of porous P(*p*BUa-*co*-BI) substrates

A series of porous substrates, P(*p*BUa-*co*-BI)-# (where # is the wt% of DBP to *p*BUa and PBI), were prepared by mixing, casting, and stepwise heating the mixture of 3-phenyl-3,4-dihydro-6-*tert*-butyl-2*H*-1,3-benzoxazine (*p*BUa) and poly[2,2'-(*m*-phenylene)-5,5'-(bibenzimidazole)] (PBI) with dibutyl phthalate (DBP) as a porogen in DMAc followed by extraction of the porogen from the casted film as shown in **Figure 4.2**. The cross-linked copolymer structure of P(*p*BUa-*co*-BI) was formed by the spontaneous polymerization and cross-linking process of *p*BUa with PBI upon stepwise heating [20].

Table 4.2 shows the properties of the porous P(*p*BUa-*co*-BI) substrates, prepared using 0 to 120 wt% of DBP to the total weight of *p*BUa and PBI. The P(*p*BUa-*co*-BI)-# substrates were also prepared using DBP larger than 90 wt%, such as P(*p*BUa-*co*-BI)-100, 120, and 150, while they were found to be physically weak because their pore content is too large and these films could not maintain their free-standing film state (**Table 4.2** and **Figure. 4.3**). Therefore, the maximum content of DBP required to form the physically stable porous substrate was 90 wt%. The average pore diameter (Å) and porosity (Vol. %) of the porous P(*p*BUa-*co*-BI) substrates were measured by the mercury intrusion method [36,37]. With increasing the DBP contents from 70% to 90%, the average pore diameter increased from 426 to 523 Å, while the porosity values did not increase

significantly, only increasing from 63.6% to 66.3%. However, the porosity values calculated from equation (2) obviously increased more and almost linearly with the increase of the porogen (DBP) content. It was also found that the calculated porosity values are smaller than the experimental porosity values. The mismatch between the calculated and experimental values was previously reported [38]. Therefore, the porosity values in Table 2 only provide the outline of the porous substrate structure rather than the exact information of the pore content. The mechanical properties such as Young's modulus, tensile strength, and elongation at break of the P(*p*BUa-*co*-BI)-# substrates are shown in **Table 4.2**. The modulus and tensile strength decrease with increasing DBP contents. For example, the Young's modulus and tensile strength values of P(*p*BUa-*co*-BI)-0 are 4091 and 97.5 MPa, respectively, and those of P(*p*BUa-*co*-BI)-90 are 968 and 24.2 MPa, respectively. The increased porosity and pore-size with the increase of DBP content can clearly explain the decrease in the mechanical strength of the porous P(*p*BUa-*co*-BI) substrates. It is important that the porous substrate has a reasonable pore-size and mechanical strength for the pore-filling membrane in fuel cell application. As shown in **Table 4.2** and **Figure 4.3**, the porous substrates prepared using DBP larger than 90 wt% are not mechanically strong enough to maintain the free-standing state induced by the external impact because their pores and porosity are too large. Although the porous substrates prepared using

DBP smaller than 90 wt% have smaller pores and porosity values, they are mechanically stronger having reasonable mechanical strength. Therefore, P(*p*BUa-*co*-BI)-90 was chosen as the porous substrates for the pore-filling membranes because it has the largest pore-size and porosity among the substrates that are mechanically strong enough to be used as a reinforcing framework of pore-filling membranes for application in fuel cells operating at high temperature and low RH conditions [14,16,33,39].

Preparation and morphology of pore-filling membranes

Pore-filling membranes (PF-X membranes; X denotes the DS of SPAES) were prepared by impregnating the P(*p*BUa-*co*-BI)-90 substrate with the SPAES-X solutions in DMF at 60 ℃ for 2 h (**Figure 4.2**). The pore-filling process is possible because of the capillary action of the pores in the substrate. Transparent, ultrathin (15-20 μm), and highly-flexible pore-filling membranes were able to be prepared after the process was repeated two times. **Figure 4.4** shows the cross-sectional SEM images of the porous P(*p*BUa-*co*-BI)-90 substrate and the pore-filling PF-60 membrane. The porous substrate shows irregular large pores with a diameter of 1-2 μm interconnected through narrow orifices with a diameter of 20-100 nm, as shown in **Figure 4.4(a)**. Most of the pores and orifices in the substrate

were found to be filled with SPAES, as shown in **Figure 4.4(b)**. The transparency of the pore-filling membrane is another strong indication that most of the pores are filled with SPAES, as shown in **Figure 4.2**. **Figure 4.4(c)** shows the EDS elementary mapping images of carbon, nitrogen, sulfur, and sodium in the cross-section of the sodium PF-60 membrane (Na-PF-60), where the bright dots corresponded to a high content of elements. The sulfur (S) from the sulfone ($-SO_2-$) and sulfonate ($-SO_3$) group in SPAES is not shown in the substrate prepared by *p*BUa and PBI. To confirm the existence of the sulfonate group, proton of the sulfonic acid group in the PF-60 membrane was converted to sodium by immersing in NaOH solution and the sodium signal was observed. The bright red sodium signal in the membrane is further evidence that SPAES-60 is sufficiently filled in the pores of P(*p*BUa-*co*-BI)-90. Although the thickness of the pore-filling membrane shown in **Figure 4.4(b)** is 20 μm, the thickness could be easily adjusted by changing the thickness of the substrate and the concentration of the filling SPAES solutions. In this study, the pore-filling membranes having the thicknesses of 15-20 μm showed very small hydrogen cross-over values in the range of 0.15 to 0.16 mA cm^{-2} at 300 mV of constant voltage and reproducible fuel cell performances at high temperature and low humidity conditions. Such thin SPAES membranes could also be prepared by simply adjusting the thickness of the doctor blade and polymer concentrations, while the MEAs from these thin

SPAES membranes showed excessive gas cross-over and membrane failures due to the poor physical and mechanical properties of the thin membranes at the operating condition. Reproducible fuel cell performance results of MEA from the SPAES membrane could only be obtained when the thickness is larger than 50 μm. For example, the hydrogen cross-over value of the MEA from the SPAES membrane having the thickness of 50 μm is about 0.20 mA cm^{-2} at 300 mV, which is close to that of the MEAs from the pore-filling membranes having a thickness in the range of 15 to 20 μm. The detailed discussions on the cell performance of the membranes related to the membrane thickness are shown in cell performance section.

FT-IR spectroscopy

Since the acid-base interaction and/or hydrogen bonding between the basic imidazole groups in the porous substrate and acidic sulfonic acid groups in SPAES filling the pores are possible, they can increase the physicochemical stability and mechanical strength of the pore-filling membrane [6,7,40,41]. **Figure 4.5(a)** shows the FT-IR spectra of the porous P(*p*BUa-*co*-BI)-90 substrate, the SPAES-60 membrane, the PF-60 membrane, and the sodium substituted membranes such as Na-SPAES-60 and Na-PF-60. The symmetric stretching peak

of the -SO_2- was observed at the same position at 1146 cm^{-1} in both SPAES-60 and PF-60, while the symmetric and asymmetric stretching vibration of the -SO_3 were observed at different positions indicating that there is the interactions between the acid group in SPAES and the substrate (**Figure 4.5(b)**). It is very possible that the interactions between the sulfonic acid and imidazole group shift the -SO_3 peak positions at 1021 and 1093 cm^{-1} for SPAES-60 to 1024 and 1095 cm^{-1} for PF-60, respectively[34,42]. Such shift was not observed for Na-SPAES-60 and Na-PF-60 because such interactions are not possible [43].

Water absorption behavior and dimensional stability

The water absorption behavior and dimensional stability of the membranes were evaluated by measuring the water uptake and the dimensional change, respectively. **Figure 4.6** show the water uptake and dimensional change of the membranes after being soaked in deionized water at given temperatures for 2 h. The water uptake of SPAES-70 is always larger than that of SPAES-60 and it increase with temperature. Such increase with the DS and temperature has been reported previously in other studies [44,45]. Especially, the water uptake values of the SPAES-70 membrane could not be obtained at 60-80 ℃ because it swells excessively to form a coagulated gel. In contrast, the water uptake values of the

pore-filling membranes do not change considerably with temperature. Even at a high temperature of 80 ℃, the water uptake values are about 30-35%, which are close to those at room temperature. The dimensional change behavior of the membranes is close to the water uptake behavior because it is strongly associated with the water contents of the membranes [8]; a smaller dimensional change is observed from the pore-filling membranes. The rigid P(*p*BUa-*co*-BI)-90 substrate can effectively prevent the membranes from absorbing excessive water and suppress the dimensional change of the membranes. Furthermore the acid-base interaction between the sulfonic acid groups of SPAES and the imidazole units of the P(*p*BUa-*co*-BI)-90 substrate is found to decrease the water absorption and dimensional change of the pore-filling membrane [6,46,47]. **Figure 4.7** shows the water uptake and area based dimensional change behavior of the membranes after immersed in deionized water at 40 ℃ for 4 h. It is found that the pore-filling membranes such as the PF-60 and Na-PF-60 membranes filled with SPAES in the proton form and the Na-SPAES in the sodium form exhibit larger water uptake values and dimensional changes than the porous P(*p*BUa-*co*-BI)-90 substrate because the pore-filling materials such as SPAES and Na-SPAES have larger water uptake values and dimensional changes. Interestingly, the PF-60 membrane filled with SPAES in the proton form shows smaller water uptake values and dimensional change than the Na-PF-60 membrane filled with Na-SPAES in the

sodium form, although the difference is not significant. We believe this result is due to the strong acid-base interaction between the sulfonic acid group in SPAES and the basic imidazole group in P(*p*BUa-*co*-BI)-90. The mechanical property results shown in the following section supports this result.

Mechanical properties

Figure 4.8 shows the mechanical properties of the membranes and the values are listed in **Table 4.3**. As the DS of the SPAES increases, Young's modulus and tensile strength values both of the SPAES and pore-filling membranes decrease, possibly because the membranes can absorb water at the mechanical property measurement condition and the polymers with high DS can absorb more water [48]. Then, water can act as the plasticizer to decrease the mechanical property of the membranes [49]. Nevertheless, the pore-filling membranes from PF-60 to PF-80 exhibit significantly larger Young's modulus and tensile strength values than the SPAES membranes due to the reinforcement effect of the mechanically robust P(*p*BUa-*co*-BI)-90 substrate. Furthermore the PF-60 membrane filled with SPAES-60 in the proton form shows higher mechanical strength (*i.e*. tensile strength) than the Na-PF-60 membrane filled with Na-SPAES-60 in the sodium form. Although the mechanical strength of SPAES is lower than that of Na-SPAES

because the ionic interactions in the Na-SPAES membrane is stronger than the possible hydrogen bonding in the SPAES membrane, the PF-60 membrane containing SPAES has higher mechanical strength due to the acid-base interaction between the sulfonic acid in SPAES and basic imidazole group in P(*p*BUa-*co*-BI)-90, while such interaction does not exist in the Na-PF-60 membrane containing Na-SPAES. The physical cross-linking between the sulfonate/imidazole ion pairs induced by the acid-base interaction should act as a hardening unit to increase the mechanical strength of the PF-60 membrane, as shown in **Figure 4.9** [50,51]. The elongation at break values of the pore-filling membranes are comparable to that of the P(*p*BUa-*co*-BI)-90 substrate because the chain cleavage by the elongation should be determined from the substrate of the membranes. Although, the elongation at break values of the pore-filling membranes is smaller than that of the SPAES membranes, these values are large enough for the PEMFC application.

Proton conductivity

Figure 4.10 shows the proton conductivity behavior of the SPAES and pore-filling membranes at 120 ℃ by changing the RH from 20 to 90%. The proton conductivity values of the SPAES-70 and SPAES-80 membranes could not be obtained due to their poor dimensional stability at the given conditions. The

proton conductivity values of the pore-filling membranes are smaller than those of the SPAES-60 membrane over the RH ranges because the ionic insulating P(*p*BUa-*co*-BI)-90 substrate is included in the membrane system. Generally, proton conductivity of pore-filling membranes is strongly dependent upon the porosity and the pore-size of the porous substrates, because proton transport occurs exclusively in the impregnating proton conducting electrolytes [5,52]. The experimental porosity value of the P(*p*BUa-*co*-BI)-90 substrate is 66.3%, implying that 33.7% of volume is an inactive volume for proton transport in the membranes, leading to the decrease of proton conductivity. The acid-base interaction between the P(*p*BUa-*co*-BI)-90 and SPAES can also cause the conductivity drop of the pore-filling membranes as it can decrease the concentration of the sulfonic acid group in the membrane [44,53,54]. The conductivity value of the pore-filling membrane with SPAES having larger DS is larger than that with SPAES having smaller DS. It is obvious that sulfonated PEMs with larger DS have higher proton conductivity because they have larger ion exchange capacity (IEC) and water content. As a result, the proton conductivity values of PF-60, -70 and -80 at 120 ^{o}C and 40% RH are 3.1, 5.3, and 6.5 mS cm^{-1}, respectively.

Cell Performance

The fuel cell performances of the MEAs prepared using the SPAES-60 and pore-filling membranes were evaluated at 120 ℃ and 40% RH condition. **Figure 4.11** shows current-voltage curves for the H_2/air cells of the MEAs employing the SPAES-60 and pore-filling membranes. The thickness values of the SPAES-60 and the pore-filling membranes are 50 and 15-20 μm, respectively. If the PEMs can maintain their physicochemical and mechanical stability during the fuel cell operation, it is very desirable to use the thinnest membranes because they can have the minimum resistance and the shortest proton pathway within the membrane system [14,17,55-57]. Therefore, we did our best to prepare the membrane having a minimum thickness showing durable and reproducible open circuit potential and cell voltage values of the MEAs from the fuel cell performance measurement at 120 ℃ and 40% RH condition. The open circuit potential values of the four MEAs are close to 0.9 V, and the voltage decreases with the increase in the applied current. The voltage drop of the MEAs with the PF-70 and PF-80 membranes is smaller than that with the SPAES-60 membrane over the entire range of current density, although the proton conductivity values of PF-70 and PF-80 are smaller than those of the SPAES-60 membrane. The better performance of the PF-70 and PF-80 membranes than that of the SPAES-60 membrane is due to the difference in the thickness of the membranes as explained

above. Although the PF-60 membrane is also very thin, about 15-20 μm, MEA from the PF-60 membrane shows poorer performance than that from the thicker SPAES-60 membrane, possibly because the proton conductivity of the PF-60 membrane is too small to overcome the membrane performance by the thickness effect. To further explain the better cell performance of the MEAs from the pore-filling membranes at harsh operating conditions, the water-binding conditions in the membranes were investigated. The water-binding conditions in sulfonated PEMs have been classified into two types based on the analysis of TGA thermograms: physically-bound water (*i.e.* free and weakly-bound water) and chemically-bound water (*i.e.* strongly-bound water) [33,58]. More specifically, the weight loss below 100 ℃ is attributed to the vaporization of physically-bound water in the membranes and the weight loss above 100 ℃ is attributed to the desorption of chemically-bound water *via* hydrogen bonding and desorption of hydroxyl group [59-61]. The physically-bound water is known to be the proton transport medium for the vehicle mechanism, while chemically-bound water for the Grotthus mechanism due to the formation of ionic bonds [61,62]. Under the harsh operating conditions of high temperature and low RH, the proton transport of the MEAs is predominantly governed by the Grotthus mechanism rather than the vehicle mechanism [7]. Therefore, an in-depth investigation of the water-binding condition will provide a better understanding of the cell performance of

the pore-filling membranes operating at high temperature and low RH conditions. **Figure 4.12(a)** shows the weight loss profiles of water molecules for the SPAES-60 and pore-filling membranes measured by TGA. Based on the weight loss profiles of the membranes, the physically and chemically-bound water fraction in the total water content were quantitatively calculated (**Figure 4.12(b)**). The total water contents of SPAES-60, PF-60, PF-70, and PF-80 membranes are 12.3, 7.9, 9.8, and 10.7 wt%, respectively. More specifically, for the SPAES-60 membrane, the weight loss corresponding to the physically bound water is 76.4% and the weight loss attributed to the chemically-bound water is 23.6%. In comparison, for the PF-70 and PF-80 membranes, the weight loss of the physically-bound water is 59.2 and 60.7%, respectively, and the weight loss of the chemically-bound water is 40.8 and 39.3%, respectively. The relative fraction of chemically-bound water in the PF-70 and PF-80 membranes is quite larger than that in the SPAES-60 membrane due to the effectiveness of the acid-base interactions between the basic reinforcing porous substrate and acidic filling SPAES. Accordingly, the increase of the chemically-bound water content in the PF-70 and PF-80 membranes can also explain the increased cell performance of the pore-filling membranes at high temperature and low humidity conditions. Although the chemically-bound water content of the PF-60 membrane is comparable to that of the SPAES-60 membrane, the poorer performance of the MEA from the PF-60 membrane could be explained

by the very small total water content in the PF-60 membrane and its smallest proton conductivity.

In this study, the most substantial improvements in the cell performance of the pore-filling membranes were found to be realized by the preparation of very thin polymeric substrate using well-known engineering plastic materials such as polybenzimidazole and polybenzoxazine [63]. In the limited experiments performed in this study, the minimum thicknesses of the pore-filling membranes showing reasonable open circuit voltages of at least 0.92 V without membrane failures when MEA was fabricated was in the range of 15 to 20 μm. Although thinner membrane (thickness is less than 10 μm) could be prepared, reproducible cell performance data could not be obtained from the MEA made using these thinner membranes. The thickness of the commercialized reinforced membrane such as GORE-SELECT® (W. L. Gore & Associates, Inc.) also ranged from 10-20 μm [64]. We strongly believe that further improvement of the cell performance of reinforced pore-filling membranes might be possible using other engineering plastic materials having higher mechanical stability with other functionality such as the proton conductive groups with highly proton conductive polymeric filling materials. Such works are under progress.

4.4. Conclusions

Porous cross-linked benzoxazine-benzimidazole copolymer P(*p*BUa-*co*-BI) substrates were prepared by the reaction of PBI with benzoxazine using dibutyl phthalate as a porogen. The substrates were then filled with sulfonated poly(arylene ether sulfone)s (SPAESs) to make pore-filling membranes for the polymer electrolyte membrane fuel cell applications. Since the pore-filling membranes are composed of robust P(*p*BUa-*co*-BI) substrates and the acid-base interaction between the sulfonic acid groups of SPAES and the basic imidazole groups in the substrate is possible, their dimensional stability and mechanical strength was found to be much better than those of the pristine SPAES membrane. The fuel cell performance of the MEAs with the pore-filling membrane is superior to that prepared with the SPAES membrane at 120 ℃ and 40% RH conditions although the proton conductivity of the pore-filling membrane is slightly smaller than that of pristine SPAES membrane because physicochemically stable ultrathin pore-filling membranes having a thickness in the range of 15 to 20 μm could be used for the MEA fabrication, while the minimum thickness of the SPAES membrane having reasonable physiochemical property is about 50 μm. We believe this study provides an attractive route toward the development of conventional

hydrocarbon based reinforced membranes with desirable properties for practical application in PEMFCs operating at high temperatures and low humidity conditions.

4.5. References

[1] H. Zhang, P.K. Shen, Chem. Rev. 112 (2012) 2780-2832.

[2] K.D. Kreuer, J. Membr. Sci. 185 (2001) 29-39.

[3] K. Kim, P. Heo, T. Ko, J.-C. Lee, Electrochem. Commun. 48 (2014) 44-48.

[4] Y. Shao, G. Yin, Z. Wang, Y. Gao, J. Power Sources 167 (2007) 235-242.

[5] J.R. Lee, J.H. Won, N.Y. Kim, M.S. Lee, S.Y. Lee, J. Colloid Interf. Sci. 362 (2011) 607-614.

[6] T. Ko, K. Kim, M.Y. Lim, S.Y. Nam, T.H. Kim, S.K. Kim, J.C. Lee, J. Mater. Chem. A 3 (2015) 20595-20606.

[7] T. Ko, K. Kim, S.K. Kim, J.C. Lee, Polymer 71 (2015) 70-81.

[8] T. Ko, K. Kim, B.K. Jung, S.H. Cha, S.K. Kim, J.C. Lee, Macromolecules, 48 (2015) 1104-1114.

[9] K. Kim, P. Heo, T. Ko, K.H. Kim, S.K. Kim, C. Pak, J.C. Lee, J. Power Sources 293 (2015) 539-547.

[10] M.P. Rodgers, J. Berring, S. Holdcroft, Z. Shi, J. Membr. Sci. 321 (2008) 100-113.

[11] L. Wang, B.L. Yi, H.M. Zhang, Y.H. Liu, D.M. Xing, Z.G. Shao, Y.H. Cai, J. Power Sources 167 (2007) 47-52.

[12] H. Munakata, D. Yamamoto, K. Kanamura, Chem. Commun. (2005) 3986-3988.

[13] N. Hara, H. Ohashi, T. Ito, T. Yamaguchi, J. Phys. Chem. B 113 (2009) 4656-4663.

[14] D.M. Yu, S. Yoon, T.H. Kim, J.Y. Lee, J. Lee, Y.T. Hong, J. Memb. Sci. 446 (2013) 212-219.

[15] T.H. Nguyen, X. Wang, Sep. Purif. Technol. 67 (2009) 208-212.

[16] S. Alwin, S.D. Bhat, A.K. Sahu, A. Jalajakshi, P. Sridhar, S. Pitchumani, A.K. Shukla, J. Electrochem. Soc. 158 (2011) B91-B98.

[17] X. Zhu, H. Zhang, Y. Liang, Y. Zhang, Q. Luo, C. Bi, B. Yi, J. Mater. Chem. 17 (2007) 386-397.

[18] J.R. Lee, N.Y. Kim, M.S. Lee, S.Y. Lee, J. Membr. Sci. 367 (2011) 265-272.

[19] T. Nguyen, X. Wang, J. Power Sources. 195 (2010) 1024-1030.

[20] S.K. Kim, S.W. Choi, W.S. Jeon, J.O. Park, T. Ko, H. Chang, J.C. Lee, Macromolecules, 45 (2012) 1438-1446.

[21] S.K. Kim, T. Ko, S.W. Choi, J.O. Park, K.H. Kim, C. Pak, H. Chang, J.C. Lee, J. Mater. Chem. 22 (2012) 7194-7205.

[22] S.K. Kim, K.H. Kim, J.O. Park, K. Kim, T. Ko, S.W. Choi, C. Pak, H. Chang, J.C. Lee, J. Power Sources 226 (2013) 346-353.

[23] F. Wang, M. Hickner, Y.S. Kim, T.A. Zawodzinski, J.E. McGrath, J.Membr. Sci. 197 (2002) 231-242.

[24] Y.S. Kim, F. Wang, M. Hickner, S. McCartney, Y.T. Hong, W. Harrison, T.A. Zawodzinski, J.E. McGrath, J. Polym. Sci. Part B: Polym. Phys. 41 (2003) 2816-2828.

[25] W.L. Harrison, F. Wang, J.B. Mecham, V.A. Bhanu, M. Hill, Y.S. Kim, J.E. McGrath, J. Polym. Sci. Part A: Polym. Chem. 41 (2003) 2264-2276.

[26] J.S. Wainright, J.T. Wang, D. Weng, R.F. Savinell, M. Litt, J. Electrochem. Soc. 142 (1995) L121-L123.

[27] E.A. Weiber, S. Takamuku, P. Jannasch, Macromolecules, 46 (2013) 3476-3485.

[28] T. Yamaguchi, F. Miyata, S.-i. Nakao, J. Membr. Sci. 214 (2003) 283-292.

[29] T. Yamaguchi, H. Kuroki, F. Miyata, Electrochem. Commun. 7 (2005) 730-734.

[30] T.H. Kim, T.W. Lim, Y.S. Park, K. Shin, J.C. Lee, Macromol. Chem. Physic. 208 (2007) 2293-2302.

[31] M. Schulze, M. von Bradke, R. Reissner, M. Lorenz, E. Gulzow, Fresen J. Anal. Chem. 365 (1999) 123-132.

[32] S.-P. Tung, B.-J. Hwang, J. Membr. Sci. 241 (2004) 315-323.

[33] J.-H. Seol, J.-H. Won, K.-S. Yoon, Y.T. Hong, S.-Y. Lee, Solid State Ionics 190 (2011) 30-37.

[34] H. Kang, K. Kim, D. Kang, J.C. Lee, Rsc Adv. 5 (2015) 64031-64036.

[35] W.L. Harrison, M.A. Hickner, Y.S. Kim, J.E. McGrath, Fuel Cells 5 (2005) 201-212.

[36] W.-H. Seol, Y.M. Lee, J.-K. Park, J. Power Sources 170 (2007) 191-195.

[37] C.-G. Lee, D.-H. Kim, H.-C. Lim, J. Electrochem. Soc. 154 (2007) B396-B404.

[38] H. Fashandi, M. Karimi, Thermochim. Acta 547 (2012) 38-46.

[39] C.-H. Shen, L.-c. Jheng, S.L.-c. Hsu, J.T.-W. Wang, J. Mater. Chem. 21 (2011) 15660-15665.

[40] H. Bai, H. Zhang, Y. He, J. Liu, B. Zhang, J. Wang, J. Membr. Sci. 454 (2014) 220-232.

[41] T. Yamaguchi, H. Zhou, S. Nakazawa, N. Hara, Adv. Mater. 19 (2007) 592-596.

[42] M. Ueda, H. Toyota, T. Ouchi, J.-I. Sugiyama, K. Yonetake, T. Masuko, T. Teramoto, J. Polym. Sci. Part A: Polym. Chem. 31 (1993) 853-858.

[43] J. Jouanneau, R. Mercier, L. Gonon, G. Gebel, Macromolecules. 40 (2007) 983-990.

[44] L.C. Fu, G.Y. Xiao, D.Y. Yan, J. Mater. Chem. 22 (2012) 13714-13722.

[45] S. Zhou, S.D. Hai, D. Kim, Fuel Cells, 12 (2012) 589-598.

[46] Y. Qi, Y. Gao, S. Tian, A.R. Hlil, J. Gaudet, D. Guay, A.S. Hay, J. Polym. Sci. Part A: Polym. Chem. 47 (2009) 1920-1929.

[47] J. Wang, H. Bai, H. Zhang, L. Zhao, H. Chen, Y. Li, Electrochim. Acta, 152 (2015) 443-455.

[48] M.-S. Kang, Y.-J. Choi, I.-J. Choi, T.-H. Yoon, S.-H. Moon, J. Membr. Sci. 216 (2003) 39-53.

[49] K. Si, R. Wycisk, D. Dong, K. Cooper, M. Rodgers, P. Brooker, D. Slattery, M. Litt, Macromolecules, 46 (2013) 422-433.

[50] R. Jin, Y. Li, W. Xing, X. Qiu, X. Ji, L. Gao, Polym. Adv. Technol. 23 (2012) 31-37.

[51] J.L. Wang, J.B. Liao, L. Yang, S.G. Zhang, X.L. Huang, J.B. Ji, J. Membr. Sci. 415 (2012) 644-653.

[52] J.-H. Seol, J.-H. Won, M.-S. Lee, K.-S. Yoon, Y.T. Hong, S.-Y. Lee, J. Mater. Chem. 22 (2012) 1634-1642.

[53] H. Zhang, X. Li, C. Zhao, T. Fu, Y. Shi, H. Na, J. Membr. Sci. 308 (2008) 66-74.

[54] M. Han, G. Zhang, M. Li, S. Wang, Z. Liu, H. Li, Y. Zhang, D. Xu, J. Wang, J. Ni, H. Na, J. Power Sources 196 (2011) 9916-9923.

[55] C. Wieser, Fuel Cells 4 (2004) 245-250.

[56] D.M. Xing, B.L. Yi, F.Q. Liu, Y.Z. Fu, H.M. Zhang, Fuel Cells 5 (2005) 406-411.

[57] J.Y. Lee, D.M. Yu, T.-H. Kim, S.J. Yoon, Y.T. Hong, J. Membr. Sci. 492 (2015) 209-219.

[58] S.P. Tung, B.J. Hwang, J. Membr. Sci. 241 (2004) 315-323.

[59] M.A. Hickner, H. Ghassemi, Y.S. Kim, B.R. Einsla, J.E. McGrath, Chem. Rev. 104 (2004) 4587-4612.

[60] J.M. Lim, J.H. Won, H.J. Lee, Y.T. Hong, M.S. Lee, C.H. Ko, S.Y. Lee, J. Mater. Chem. 22 (2012) 18550-18557.

[61] D.W.M. Hofmann, L. Kuleshova, B. D'Aguanno, V. Di Noto, E. Negro, F. Conti, M. Vittadello, J. Phys. Chem. B 113 (2009) 632-639.

[62] K.-D. Kreuer, S.J. Paddison, E. Spohr, M. Schuster, Chem. Rev. 104 (2004) 4637-4678.

[63] V. Mittal, Manufacturing of Nanocomposites with Engineering Plastics, Elsevier, Amsterdam, Netherlands 2015.

[64] J.R. Grohs, Y. Li, D.A. Dillard, S.W. Case, M.W. Ellis, Y.-H. Lai, C.S. Gittleman, J. Power Sources 195 (2010) 527-531.

Table 4.1 Synthesis and properties of SPAES with different degree of sulfonation.

Polymer	Degree of sulfonation x (%)		IEC$_w$ (mequiv./g)		M_w[e] (-)	M_n[e] (-)	M_w/M_n (-)
	Monomer[a]	^{1}H NMR[b]	Calc.[c]	Expt.[d]			
SPAES-60	60	57	2.12	2.08	90,600	48,200	2.5
SPAES-70	70	67	2.51	2.47	82,000	35,000	2.3
SPAES-80	80	76	2.70	2.68	75,000	38,000	2.0

[a] Degree of sulfonation obtained from feed monomer ratio.

[b] Degree of sulfonation obtained from peak integration in ^{1}H NMR spectra.

[c] Calculated from ^{1}H NMR spectra.

[d] Determined experimentally by acid-base titration method.

[e] Weight-average molecular weight (M_w) and number average molecular weight (M_n) calculated from the GPC measurement using poly(methyl methacrylate) standards.

Table 4.2 Properties of the porous P(*p*BUa-*co*-BI) substrates prepared with different amount of dibutyl phthalate (DBP).

P(*p*BUa-*co*-BI)-#[a]	Average pore diameter[b] (4V/A, Å)	Porosity[b] (Vol. %)	Density[c] (g cm^{-3})	Porosity[d] (Vol. %)	Young's Modulus (MPa)	Tensile strength (MPa)	Elongation at break (%)
P(*p*BUa-*co*-BI)-0	(-)	(-)	1.11	(-)	4091 ± 68	97.5 ± 11.4	3.2 ± 0.7
P(*p*BUa-*co*-BI)-70	426	63.6	0.58	53.0	1072 ± 54	30.3 ± 2.0	5.7 ± 1.4
P(*p*BUa-*co*-BI)-80	473	65.6	0.55	56.4	1009 ± 58	28.9 ± 4.3	6.3 ± 0.8
P(*p*BUa-*co*-BI)-90	523	66.3	0.51	59.6	968 ± 45	24.2 ± 3.1	9.1 ± 0.9
P(*p*BUa-*co*-BI)-120	751	73.3	(-)	(-)	(-)	(-)	(-)

[a] # is the wt.% of DBP to the total weight of *p*BUa and PBI.

[b] Determined experimentally by mercury porosimeter.

[c] Calculated from membrane dimension and weight after drying.

[d] Calculated from equation (2).

Table 4.3 Mechanical properties of P(*p*BUa-*co*-BI)-90, pristine SPAES (SPAES-60 and -70) and pore-filling (PF-60, -70, and -80) membranes.

Sample	Young's modulus (MPa)	Tensile strength (MPa)	Elongation at break (%)
P(*p*BUa-*co*-BI)-90	968 ± 45	24.2 ± 3.1	9.1 ± 0.9
SPAES-60	2077 ± 168	50.4 ± 0.9	34.0 ± 3.6
SPAES-70	1512 ± 391	41.6 ± 5.0	24.9 ± 5.5
PF-60	4874 ± 284	93.8 ± 10.1	9.5 ± 1.6
PF-70	4621 ± 335	88.9 ± 16.6	8.6 ± 0.6
PF-80	4231 ± 369	80.6 ± 11.9	8.5 ± 1.4

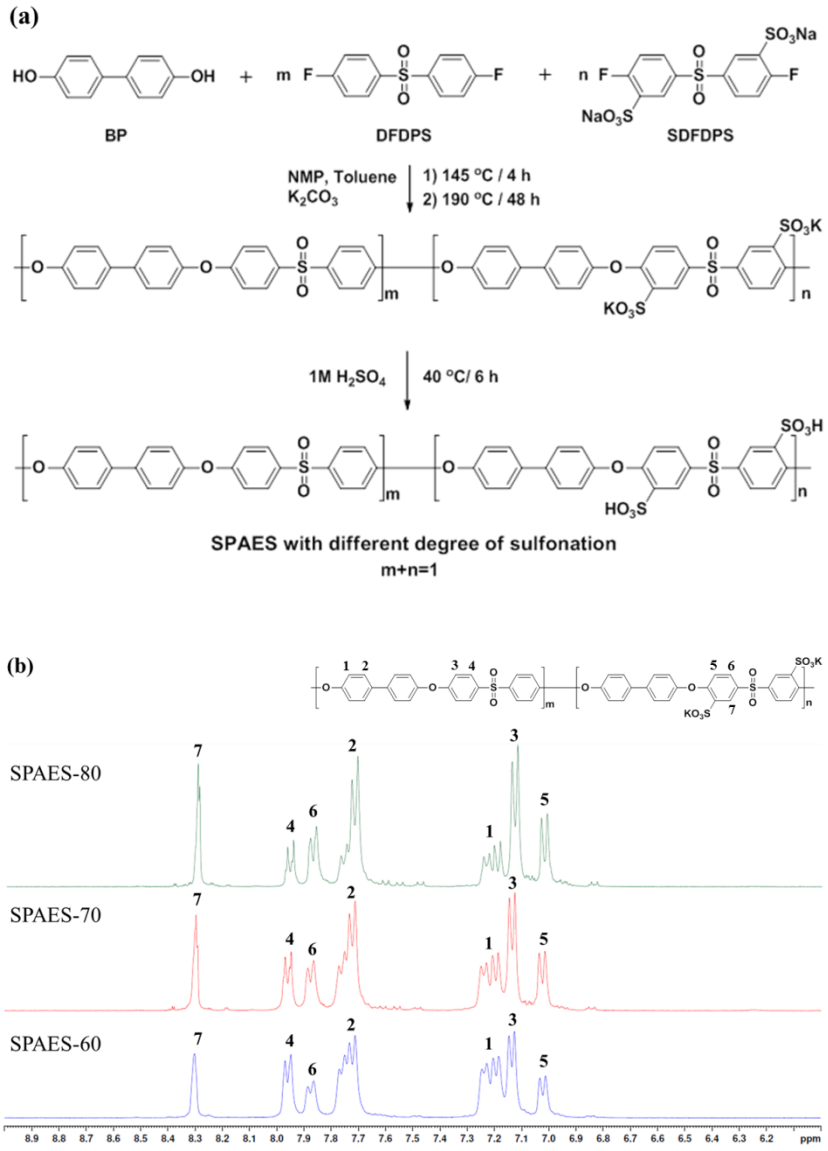

Figure 4.1 (a) Synthetic scheme of sulfonated poly(arylene ether sulfone)s (SPAESs). (b) ^{1}H- NMR spectra of SPAESs with different degree of sulfonation from 60 to 80.

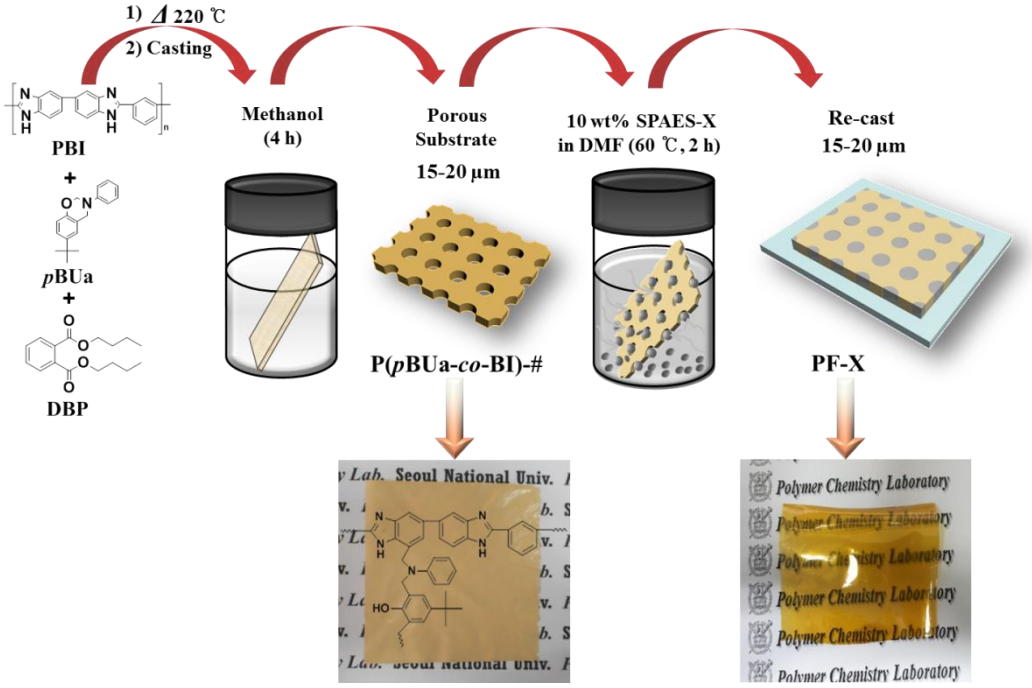

Figure 4.2 Schematic illustration for the preparation of pore-filling membranes and photo images of porous P(*p*BUa-*co*-BI) substrate and pore-filling membrane, wherein the chemical structures of PBI, *p*BUa, DBP, and P(*p*BUa-*co*-BI) are also illustrated.

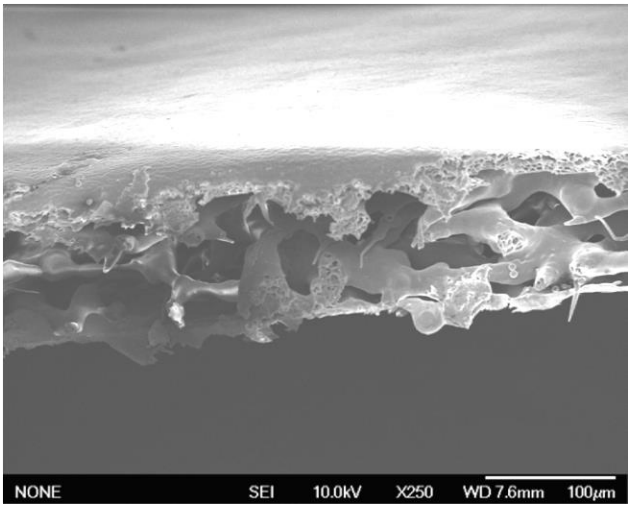

Figure 4.3 Cross-section SEM image of P(*p*BUa-*co*-BI)-150.

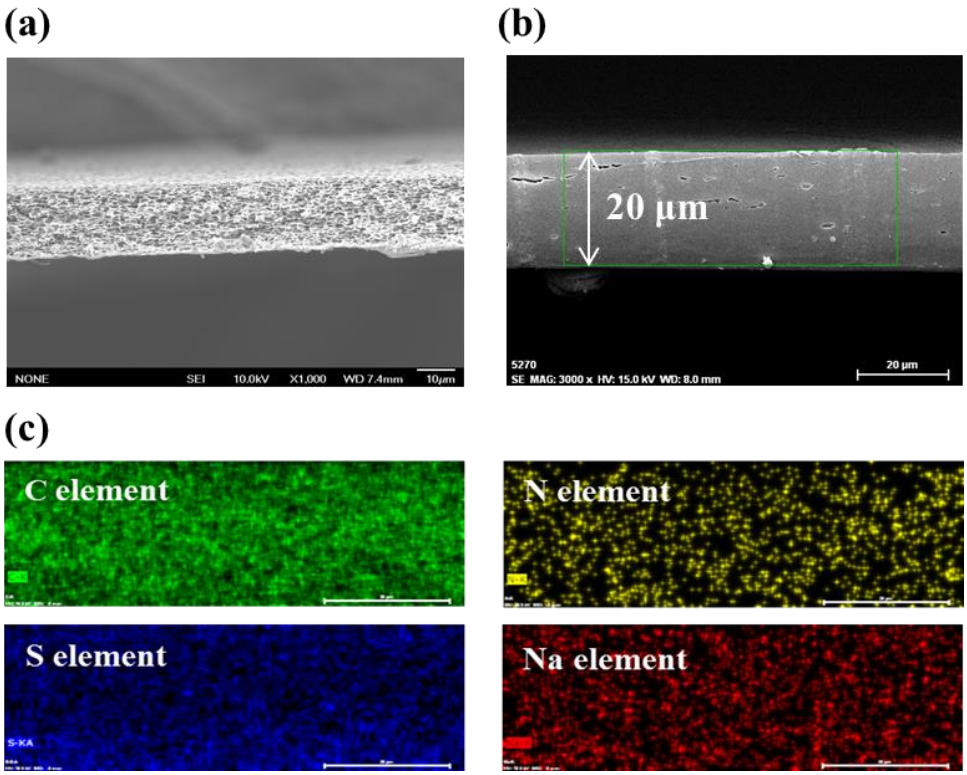

Figure 4.4 Cross-section SEM images of (a) P(*p*BUa-*co*-BI)-90, (b) Na-PF-60 membrane, and (c) EDS mapping for carbon, nitrogen, sulfur and sodium elements in Na-PF-60 membrane.

(a)

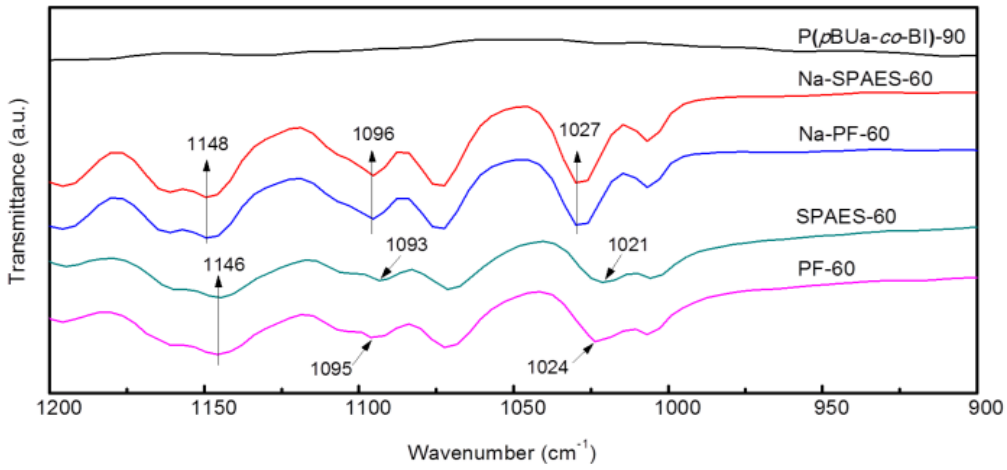

(b)

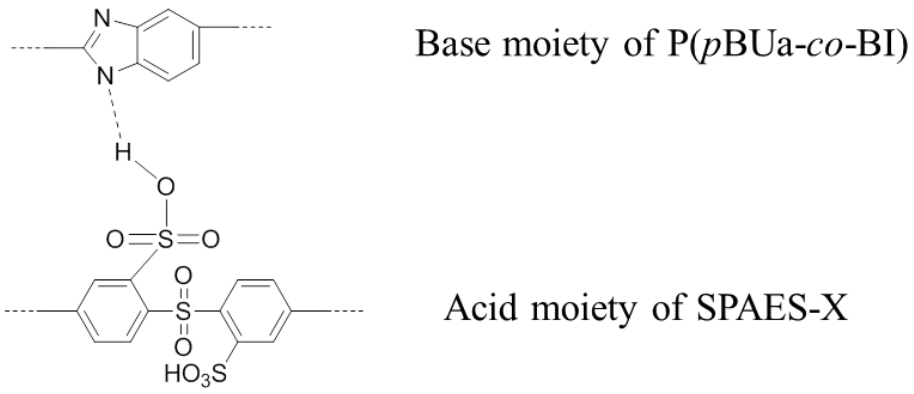

Figure 4.5 Infrared spectra of P(*p*BUa-*co*-BI)-90, SPAES-60, Na-SPAES-60, PF-60 and Na-PF-60 membranes and (b) schematic diagram of the acid-base interaction between P(*p*BUa-*co*-BI) and SPAES.

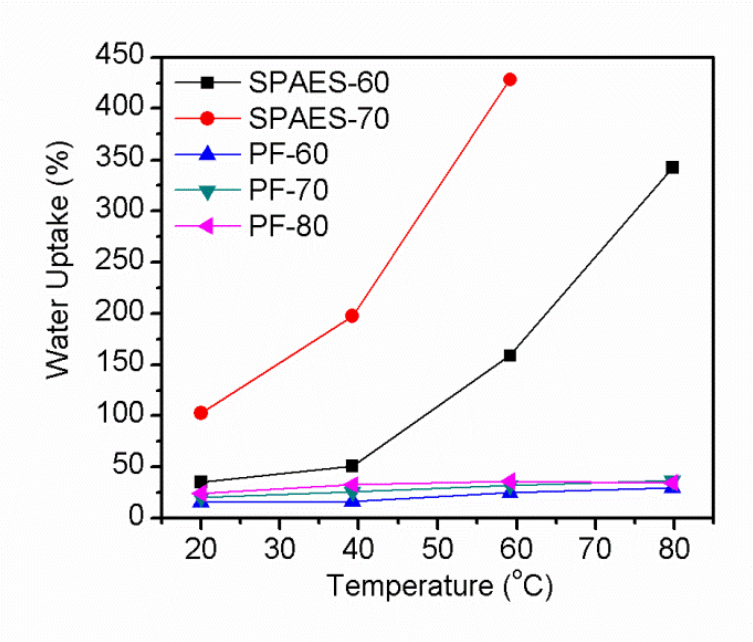
Water Uptake (%)
Temperature (°C)
SPAES-60
SPAES-70
PF-60
PF-70
PF-80
0
50
100
150
200
250
300
350
400
450
20
30
40
50
60
70
80

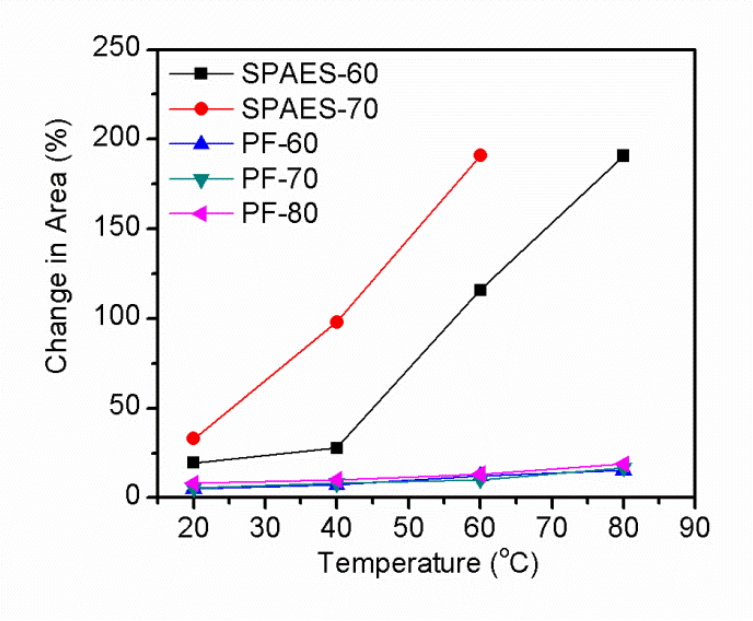
Change in Area (%)
Temperature (°C)
SPAES-60
SPAES-70
PF-60
PF-70
PF-80
0
50
100
150
200
250
20
30
40
50
60
70
80
90

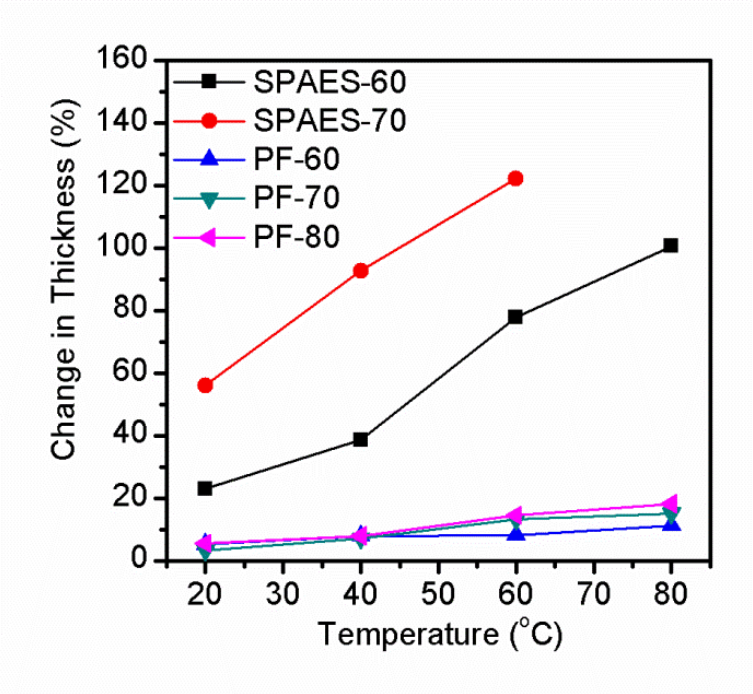

Figure 4.6 Water uptake, and dimensional change in area and thickness of pristine SPAES and pore-filling membranes at various temperatures.

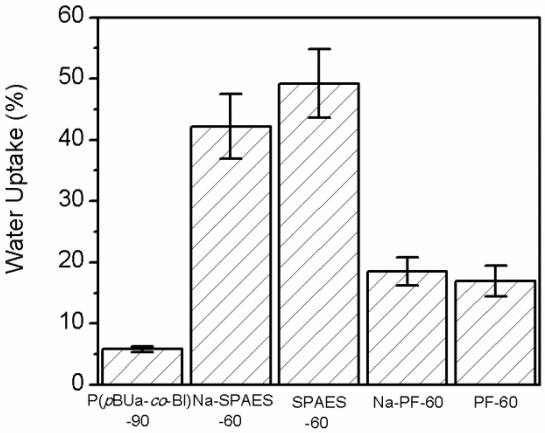

Sample	Dry State	Wet State
P(*p*BUa-*co*-BI)-90		ΔA 1.6 %
Na-SPAES-60		ΔA 34.4 %
SPAES-60		ΔA 34.8 %
Na-PF-60		ΔA 7.0 %
PF-60		ΔA 4.0 %

Figure 4.7 Water uptake and photo images of change in area of P(*p*BUa-*co*-BI)-90, Na-SPAES-60, SPAES-60, Na-PF-60, and PF-60 membranes.

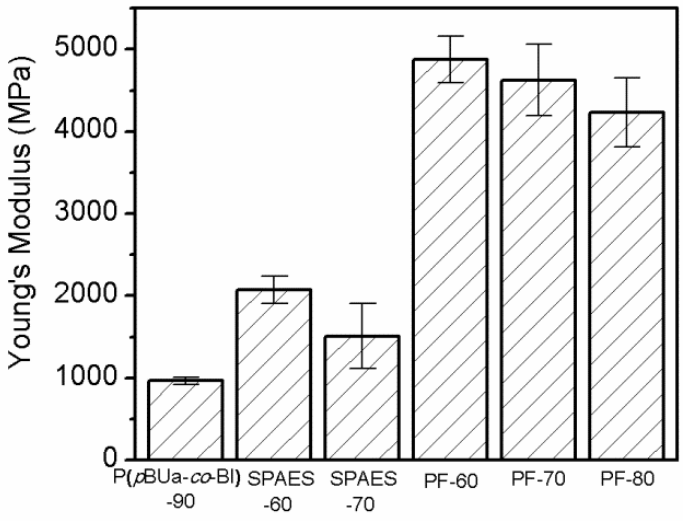
Young's Modulus (MPa)
0
1000
2000
3000
4000
5000
P(pBUa-co-BI) -90
SPAES -60
SPAES -70
PF-60
PF-70
PF-80

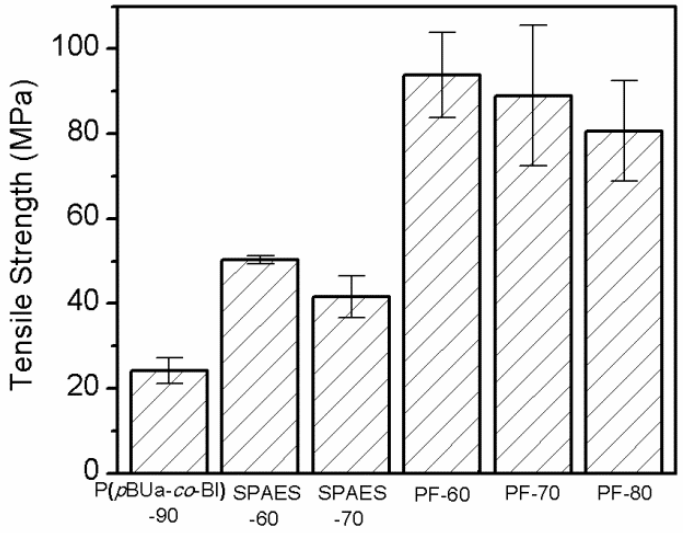
Tensile Strength (MPa)
0
20
40
60
80
100
P(pBUa-co-BI) -90
SPAES -60
SPAES -70
PF-60
PF-70
PF-80

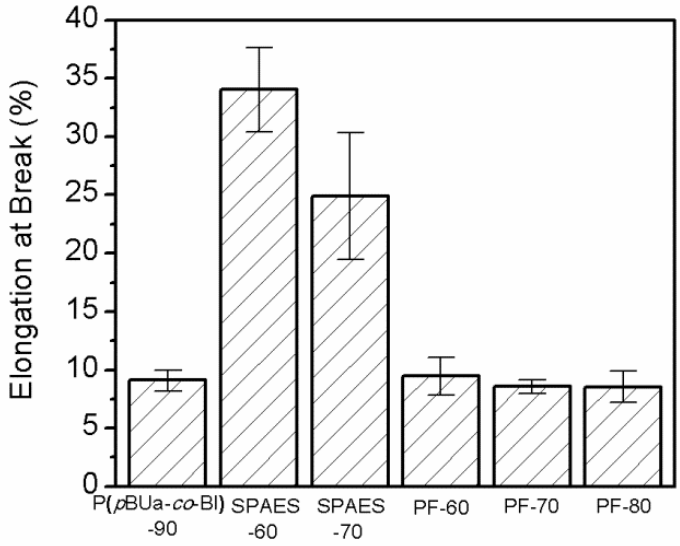

Figure 4.8 Mechanical properties of porous P(*p*BUa-*co*-BI)-90 substrate, pristine SPAES and pore-filling membranes: Young's modulus, tensile strength and elongation at break.

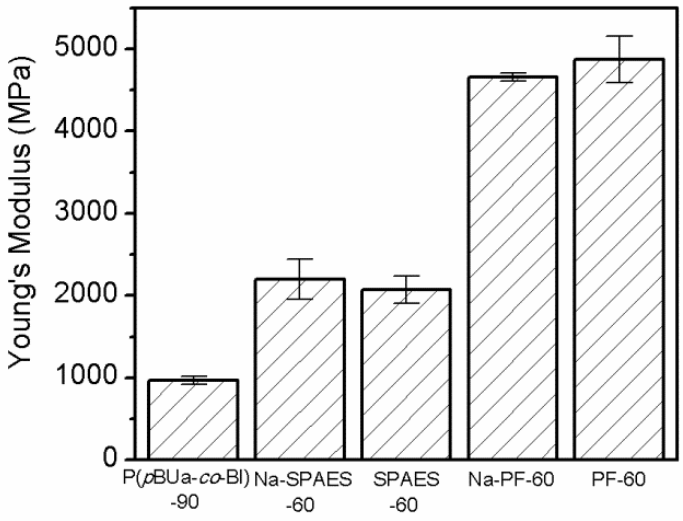
Young's Modulus (MPa)
5000
4000
3000
2000
1000
0
P(pBUa-co-Bl) -90
Na-SPAES -60
SPAES -60
Na-PF-60
PF-60

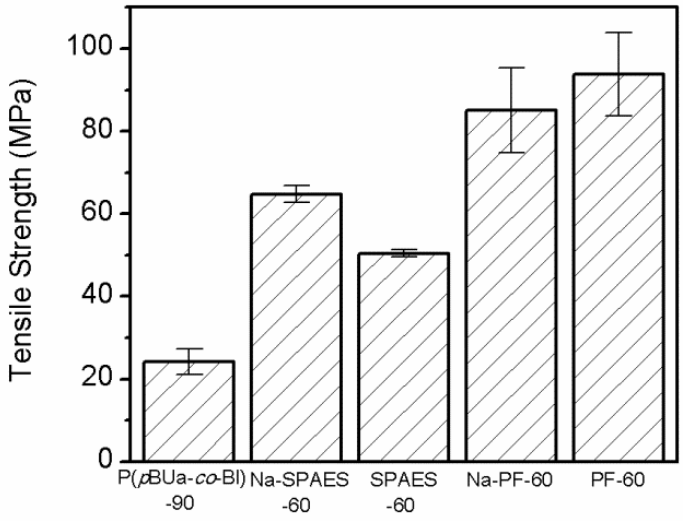
Tensile Strength (MPa)
100
80
60
40
20
0
P(pBUa-co-Bl) -90
Na-SPAES -60
SPAES -60
Na-PF-60
PF-60

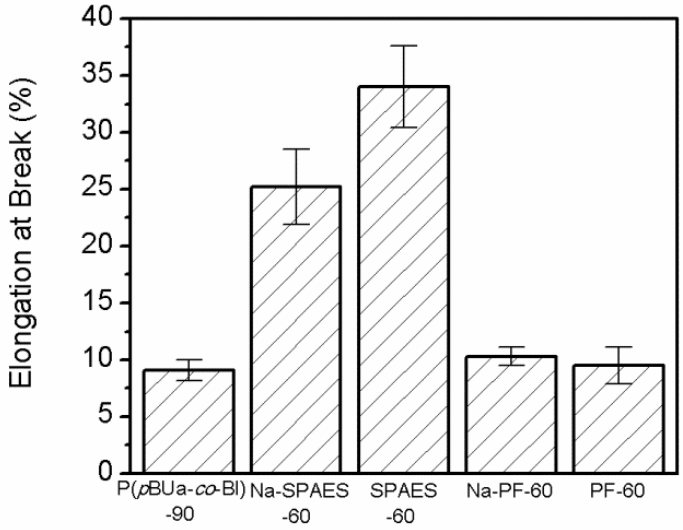

Figure 4.9 Mechanical properties of P(*p*BUa-*co*-BI)-90, Na-SPAES-60, SPAES-60, Na-PF-60, and PF-60 membranes: Young's modulus, tensile strength, and elongation at break.

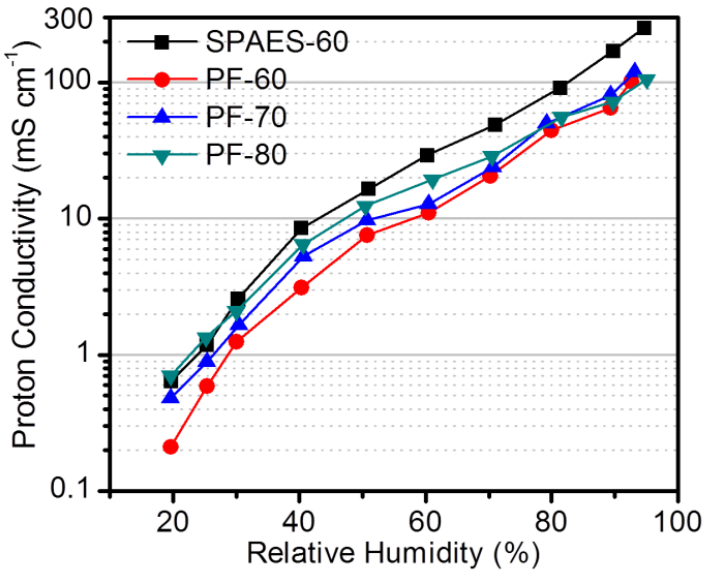

Figure 4.10 Proton conductivities of SPAES-60, PF-60, PF-70, and PF-80 membranes having thickness of 50, 19, 18, and 18 μm, respectively, at 120 °C as a function of relative humidity.

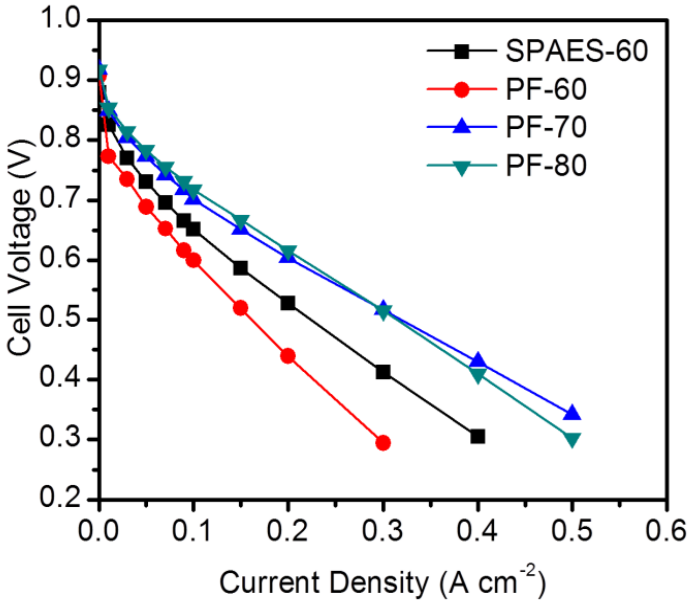

Figure 4.11 Cell performance of MEAs prepared using SPAES-60, PF-60, PF-70, and PF-80 membranes having thickness of 50, 19, 18, and 18 µm, respectively, at 120 °C and 40% RH conditions. Active area of the MEAs is 10 cm^2.

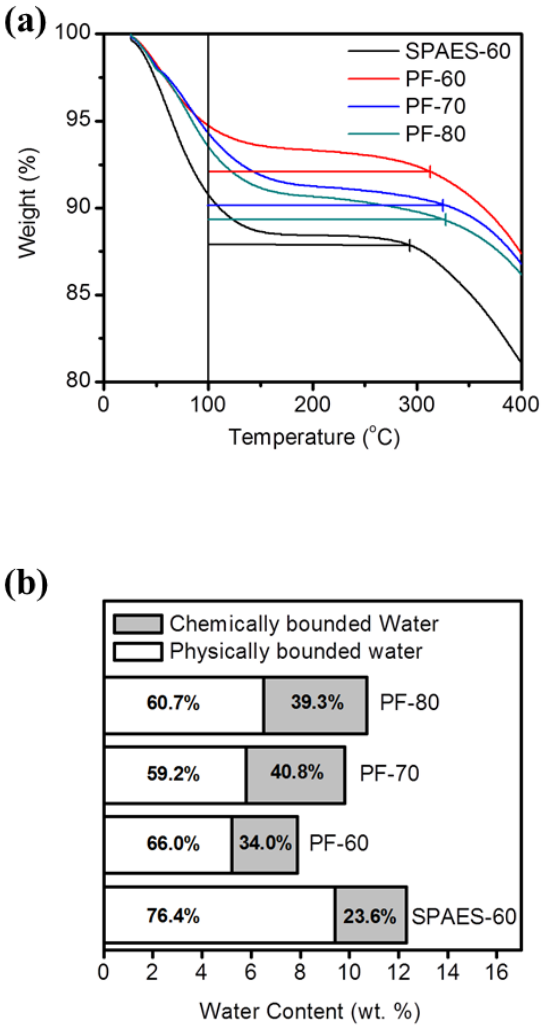

Figure 4.12 Analysis of state of water for SPAES-60, PF-60, PF-70, and PF-80 membranes with thickness of 50, 19, 18, and 18 µm, respectively: (a) TGA thermgrams at a heating rate of 10 °C min^{-1}; (b) relative fractions of physically-bound water and chemically-bound water in total water content of the membranes.

Chapter 5

Proton Conductive Porous Substrate Supported Sulfonated Poly(Arylene Ether Sulfone) Pore-Filling Membrane for High-Temperature Fuel Cell Applications

5.1. Introduction

The development of thin polymer electrolyte membranes (PEMs) operating at high temperatures (> 100 ℃) and low relative humidity (< 50% RH) conditions has received much attention for practical application of polymer electrolyte membrane fuel cells (PEMFCs) in automobile transportation [1,4]. Since the automotive applications necessitate high-power density, thin and high-conductive PEMs are strongly required [5-7]. However, thin membranes mostly have poor physical stability and low mechanical strength that prevents their practical application for PEMFCs [8,9]. Among various approaches to overcome these limitations, the development of reinforced pore-filling membranes has attracted considerable attentions because thin PEMs with outstanding physical properties could be prepared from the reinforcing porous substrates filled with proton conducting ionomers [10]. Representative examples of the reinforcing porous substrates showing the dimensional and physical stabilities are poly(tetrafluoroethylene) (PTFE) [11,12], polyimide (PI) [13,14], polypropylene [15], polyacrylonitrile [16], and polycarbonate [17], wherein the proton conductivity of the pore-filling membranes from these substrates are much lower than that of the proton conductive pore-filling polymers because the substrate is

non-proton conductive materials [7-13]. Therefore, it would be possible to increase the proton conductivity of the pore-filling membranes by introducing the proton conductive porous substrates having the dimensional stability, while such approach has not reported from our best knowledge, although the proton conductive silicate and inorganic encapsulated polymer composite substrates are reported [18,19].

In this study, we tried to prepare novel proton conductive porous substrates consisting of cross-linked benzoxazine-benzimidazole copolymers to develop a dimensionally stable pore-filling membrane system with increased proton conductivity and fuel cell performance. A sulfonated poly(arylene) ether sulfone having the degree of sulfonation of 70 mol% was used as the filling materials because of its high proton conductivity [20]. Although SPAES-70 has very high proton conductivity, it could not be used as a free standing film for high temperature PEMFCs due to its poor physical stability in the hydrated condition [21]. However, it can be used as the proton conducting ionomer in the pore-filling membrane system because the porous cross-linked benzoxazine-benzimidazole copolymer substrates used in this study have outstanding physicochemical stabilities.

The detailed synthetic procedures and properties such as morphology, chemical stability, hydrophilicity, mechanical properties and proton conductivity of the

proton conducting porous substrates and the pore-filling membranes are discussed in this paper.

5.2. Experimental

Materials

4,4’-Dihydroxybiphenyl (BP, 97.0%, Aldrich), 4,4’-difluorodiphenylsulfone (DFDPS, 99.0%, Aldrich) and isophthalic acid (99%, Aldrich), were recrystallized from methanol, toluene, and ethanol, respectively. 3,3’-Disulfonate-4,4’-difluorodiphenylsulfone (SDFDPS) was obtained from DFDPS as described by Harrison *et al* [22]. The yield of SDFDPS after recrystallization using a mixture of *iso*-propylalcohol and deionized water (7/3, v/v) was 86%. *N*,*N*-Dimethylacetamide (DMAc, 99.0%, Junsei), *N*-methyl-2-pyrrolidone (NMP, 99.0%, Junsei) were stored over molecular sieves under nitrogen and toluene (99.5%, Junsei) was refluxed over calcium hydride and distilled. *N*,*N*-Dimethylformamide (DMF, 99.8%, Aldrich) as an anhydrous grade, and triethylamine (TEA, 99.0%, TCI) were used as received. Potassium carbonate (K_2CO_3, 99.0+%, Aldrich) was dried under vacuum at 80 ℃ for 48 h, prior to use. 3,3’–Diaminobenzidine (97%, Tokyo Kasei, TCI), polyphosphoric acid (PPA, 116% H_3PO_4, Junsei), phosphorous pentoxide (97%, Aldrich), fuming sulfuric acid (65% SO_3, Merck), sodium chloride (NaCl, 99.5%, Daejung), sodium hydroxide (NaOH, 98.0%, Daejung), sodium 4-hydroxybenzene sulfonate (98%, TCI), *p*–

formaldehyde (95%, Aldrich), sulfanilic acid sodium salt (98%, Aldrich) and dibutyl phthalate (DBP, 99%, Aldrich) were used without further purification. All other solvents and reagents were used as received from standard vendors.

Synthesis of sodium 3-(4-sulfonatophenyl)-3,4-dihydro-2*H*-1,3 benzoxazine-6-sulfonate (*p*S), poly(2,2‘–(*m*–phenylene)–5,5‘–(bibenzimidazole)) (PBI) and sulfonated poly(arylene ether sulfone) with the degree of sulfonation of 70 mol%.

Stoichiometric amounts of sodium 4-hydroxybenzenesulfonate (15.00 g, 0.08 mol), *p*–formaldehyde (4.81 g, 0.16 mol), and sulfanilic acid sodium salt (15.22 g, 0.08 mol) were used for the preparation of the benzoxazine monomer, *p*S (**Figure 5.1(a)**). To a 250 mL three-neck round bottom flask equipped with a condenser and a nitrogen inlet was charged with sulfanilic acid sodium salt, formaldehyde and 21.3 mL of TEA in 150.0 mL of DMF. The reaction mixture was heated at 60 ℃ until the solution became transparent. Then, sodium 4-hydroxybenzene sulfonate was added into the reaction mixture and the temperature was raised to 105 ℃ and refluxed for 16h. Upon cooling, the resulting mixture was poured into an excess of acetone and the precipitate was further purified by rinsing with acetone several times. After dried under vacuum, the product (benzoxazine

monomer, *p*S) was obtained with the yield of 88%. ^{1}H NMR (DMSO-*d6*, 400 MHz, ppm): δ 6.64- 7.51 (br, 7H, Ar-H), 5.45 (s, 2H, -O-CH_2-N-), 4.66 (s, 2H, Ar-CH_2-N). ATR-IR (cm^{-1}): 1499 (Ph), 1248 (stretch, C-O-C), 930 (benzoxazine), 1098 (stretch, O=S=O), 1030 (stretch, O=S=O).

PBI was synthesized by the condensation polymerization of 3,3'–diaminobenzidine with isophthalic acid in a reaction medium of poly(phosphoric acid) (PPA) using the synthetic procedure reported previously (**Figure 5.1(b)**) [23]. The polymerization yield is 95% and inherent viscosity of the product PBI (0.91 dL g^{-1}) is sufficiently high to fabricate linear membranes showing reasonable physical properties for PEMFC applications [24]. PBI: ^{1}H-NMR (DMSO-d_6, 400 MHz, ppm): δ 9.14 (s, 1H, Ar-H), 8.32 (d, 4H, Ar-H), 8.00 (s, 2H, Ar-H), 7.81 (d, 2H, Ar-H), 7.62 (br, 3H, Ar-H).

SPAES-70 in potassium form (K^{+}) was synthesized *via* nucleophilic step-growth polymerization using the monomer mixture of BP, DFDPS and SDFDPS (**Figure 5.1(c)**). The detailed synthesis procedure and properties of SPAES-70 in potassium form including ^{1}H-NMR spectrum, degree of sulfonation, ion-exchange capacity, and molecular weights are described (**Figure 5.2** and **Table 1**). SPAES-70: ^{1}H-NMR (DMSO-d_6, 400 MHz): δ 8.30 (br, 2H, Ar-H), 7.96 (br, 4H, Ar-H), 7.87 (br, 2H, Ar-H), 7.73 (br, 8H, Ar-H), 7.21 (br, 8H, Ar-H), 7.13 (br, 4H, Ar-H), 7.02 (br, 2H, Ar-H).

Preparation of porous substrates based on benzoxazine-benzimidazole copolymers and PBI

The proton conducting porous substrate were prepared using the solution mixture of *p*S, PBI, and DBP as a porogen where the weight ratio of *p*S and PBI is 50: 50 and the content of DBP was changed from 20 to 90 wt% compared with the total weight of *p*S and PBI. The resulting porous substrates were named as P(*p*S-*co*-BI)-20, P(*p*S-*co*-BI)-50, P(*p*S-*co*-BI)-70 and P(*p*S-*co*-BI)-90, when the content of DBP is 20, 50, 70, and 90 wt%, respectively. The weight ratio of *p*S and PBI was fixed as 50: 50 because this composition was found to produce the cross-linked copolymer membrane showing reasonable mechanical strength and hydrophilicity as discussed in the Results and Discussion part. The following procedure was used for the preparation of the porous P(*p*S-*co*-BI)-90 substrate. A solution mixture consisting of 0.68 g of PBI, 0.68 g of *p*S and 1.23 g of DBP in 5.83 g of DMAc was cast onto clean flat glass plate. The thickness of the blended solution on the glass plate could be controlled using a doctor blade film applicator and subsequently stepwise heat treatment of the blended solution was applied: The casted solution was heated from 60 to 220 ℃ for 4 h and then the temperature was kept at 220 ℃ for 1 h in a convection oven. After cooling to room temperature, the obtained membrane was immersed in distilled water and peeled from the glass plate. DBP was then extracted from the membrane by soaking in methanol for 4 h.

The porous substrate, P(*p*S-*co*-BI)-90, was obtained after rinsing with distilled water several times and then drying in a vacuum oven overnight. The other porous substrates such as P(*p*S-*co*-BI)-20, -50 and -70 were prepared using the same procedure except for the weight ratios of DBP to *p*S and PBI (**Table 2**). The thicknesses of the porous substrates were found to be in the range of 14 to 20 μm.

Two types of porous substrates composed of PBI, named as PBI-90 (**Figure 3(a)**), and cross-linked benzoxazine-benzimidazole copolymer such as 3-phenyl-3,4-dihydro-6-*tert*-butyl-2*H*-1,3-benzoxazine (*p*BUa), which is a widely used mono-functional benzoxazine as a precursor of phenolic resins or cross-linking agent in academic researches and industry applications [23-27], and PBI, named as P(*p*BUa-*co*-BI)-90 (**Figure 3(b**)), were also prepared, respectively, as control samples for comparing the polarity and proton conductivity behavior of the porous substrates as well as the fuel cell performance of the reinforced pore-filling membrane prepared from each porous substrate. The cross-linked copolymeric structure of P(*p*BUa-*co*-BI) was studied in our previous report [23]. The PBI-90 and P(*p*BUa-*co*-BI)-90 were fabricated using the same film preparation method as that used for P(*p*S-*co*-BI)-90 including the porogen (DBP) content, the stepwise thermal treatment, and the extraction process. The contents of each components, average pore-size and porosity of the PBI-90 and P(*p*BUa-*co*-BI)-90 were

provided in **Table 2**. The thicknesses of PBI-90 and P(*p*BUa-*co*-BI)-90 were 20 μm and 18 μm, respectively.

Preparation of pore-filling and linear SPAES-70 membranes

Pore-filling membrane was prepared by polymer impregnation method as reported previously [28]. P(*p*S-*co*-BI)-90 was chosen as a reinforcing porous substrate for the pore-filling membrane fabrication because it has largest pore-size and porosity with reasonable mechanical properties as discussed in the Results and Discussion part. P(*p*S-*co*-BI)-90 was immersed in the dilute SPAES-70 solution (less than 10 wt% in DMF) at 60 ℃ for 2 h, and then the substrate was unfolded on a glass plate and dried at 100 ℃ for 24 h in a convection oven. After cooling to room temperature, the membrane was immersed in distilled water and dried in a vacuum oven for 24 h to remove any residual solvent completely. The resulting pore-filling membrane was referred to as SPF-70. The thicknesses of the SPF-70 membranes were about 15-20 μm.

A linear SPAES-70 membrane was fabricated as a control sample by casting the 15 wt% solution in DMAc onto a clean glass followed by vacuum drying at 80 ℃ for 24 h. The thickness of the SPAES-70 membrane could be also controlled using the doctor blade film applicator and it was about 50 μm. Additionally, a pore-

filling membrane composed of P(*p*BUa-*co*-BI)-90 and SPAES-70, referred to as PF-70, was also prepared as a control sample in proton conductivity and cell performance tests. The PF-70 membrane was prepared using the same film fabrication method as that used for the SPF-70 membrane except for the repeated polymer (SPAES-70) impregnation and drying processes to minimize the voids and pin-holes in the PF-70 membrane because the pores in P(*p*BUa-*co*-BI)-90 were not completely filled with the SPAES-70 solution without the repeated polymer impregnation process. The thickness of the PF-70 membrane was in the range of 15-20 μm. The pore-filling membrane from PBI-90 could not be prepared because PBI-90 dissolved during the polymer impregnation progress. The SPF-70, SPAES-70, and PF-70 membranes in potassium form (K^+) were exchanged to their acid form (H^+) by soaking in 1 M H_2SO_4 aqueous solution at 30 ℃ for 24 h. After that, the membranes in acid form were washed with distilled water and then dried in a vacuum oven for 24 h.

Preparation of membrane electrode assemblies (MEAs)

Membrane electrode assemblies (MEAs) were prepared by a decal method [4]. The catalyst inks were prepared by mixing catalyst powder (50 wt. % Pt/C, Tanaka Kikinzoku Kogyo), Aquivion^{TM} ionomer dispersion (EW750, Solvay) and solvent mixture comprising water and ethanol. The catalyst ink was mixed using

an ultrasonic vibrator (Sonic, Vibra-cell) to obtain a uniformly dispersed ink mixture. The catalyst layer was fabricated by coating the ink mixture on a PTFE sheet and drying it at 60 ℃. The MEA was then prepared by hot pressing the catalyst layer and the membrane together and transferring the catalyst layer onto the membrane at 120 ℃. The Pt loading of the MEA was 0.4 mg/cm^2, and the ionomer content in the catalyst layer was 30%.

Characterization

The ^{1}H NMR spectra were recorded on an Avance 400 (Bruker, Germany) with a frequency of 400 MHz using deuterated dimethylsulfoxide (DMSO-d_6) as the solvent. Number average molecular weight (M_n) and weight average molecular weight (M_w) were measured at 35 ℃ by gel permeation chromatography consisting of a Waters 510 HPLC pump, three columns PLgel 5 μm guard, MIXED-C, MIXED-D, and a Viscoter T60A dual detector. HPLC grade DMF was used as the eluent and the flow rate was 1.0 mL min^{-1}. Calibration was performed with poly(methyl methacrylate) standards. Ion-exchange capacity (IEC) of the polymer (SPAES-70) was measured by back-titration method. Inherent viscosity of PBI was measured using an Ubbelode viscometer in a water bath at 30 ℃. PBI powder, dried under vacuum at 70 ℃ for 48 h, was dissolved in 96% H_2SO_4

solution at 0.3 g dL^{-1} for the viscosity tests. FT-IR spectra were obtained in an attenuated total reflectance (ATR) mode in the frequency range of 4000 to 650 cm^{-1} on a Nicolet 6700 instrument (Thermo Scientific, USA). The samples were put in equal physical contact with the sampling plate of the spectrometer accessory to avoid differences caused by pressure and penetration depth. The element contents were calculated for carbon, hydrogen, nitrogen and sulfur by an element analyzer TruSpec® Micro (Leco, USA). Differential scanning calorimetry (DSC) was measured on a TA Instruments DSC Q20 modulated calorimeter at a heating rate of 10 ℃ min^{-1}. The glass transition temperature (T_g) was taken as the point of inflection of the plot of the change in heat capacity with temperature in the DSC thermograms. Solubility test of the membranes was carried out by immersing the sample in an excess of DMF at 80 ℃ for 1 h. Average pore size and porosity of the porous P(*p*S-*co*-BI) substrates were obtained by mercury porosimeter (Autopore Ⅳ 9500, Micromeritics, USA) using more than three samples and the average value was taken. The mechanical properties of the membranes were measured using a universal testing machine (UTM, Lloyd LR-10K, UK). Dumbbell specimens were prepared by a pressing with the ASTM standard D638 (Type V specimens). The tensile properties of the membranes were measured at 25 ℃ under 40% RH conditions with a gauge length and cross head speed of 15 mm and 5 mm min^{-1}, respectively. For each measurement, at least

seven samples were used and their average value was taken. The surface and cross-sectional morphology of the membranes were analyzed using a field-emission scanning electron microscopy (FE-SEM, Carl Zeiss SUPRA 55VP, Germany) equipped with energy-dispersive spectrometer (EDS). All the samples were coated with platinum under vacuum prior to the measurement. The cross-sectional specimens of the membranes were prepared by breaking the membrane manually after cooling using liquid nitrogen. The water wettability (*i.e.*, hydrophilicity) of the porous substrates was examined by observing the membrane surfaces after dropping water onto the membrane surface immediately [18]. The water contact angles of the membranes were measured at room temperature and ambient RH conditions using a Krüss DAS10 contact angle analyzer connected to drop shape analysis software. Contact angles for the samples were measured more than three times on three independently prepared membranes. The dimensional stability of the membranes was determined by measuring their change in area between the dry and swollen state. The membranes were immersed in deionized water at 25 ℃ for 24 h and then they were taken out. A rectangular punch (1 cm × 5 cm) was used to ensure that the swollen state of the membranes had the same dimension and then the membranes were dried in a vacuum oven at 80 ℃ for 24 h. The area of the membranes was recorded before (A_{wet}) and after (A_{dry}) the drying process. The area based dimensional change (ΔA) of the membranes was

calculated by the following equations:

$$\Delta A\ (\%) = [(A_{wet} - A_{dry})/A_{dry}] \times 100 \qquad (1)$$

Proton conductivities of the membranes were measured at 120 ℃ under different RH conditions using a conductivity measurement system (BekkTech BT-552MX, USA) with a H_2 flow rate of 500 $cm^3\ min^{-1}$. The samples were pre-equilibrated at 120 ℃ and 70% RH for 2 h, and then the conductivity measurements were performed. The proton conductivity measurement was continued by lowering the humidity to 20% RH and then by raising to 90% RH at 10% intervals with a 15 min equilibration time for each measurement.

For the measurement of the MEA performance, the cells were assembled by placing two gas diffusion layers (TGP-H-060, Toray) on both sides of the MEA. The performance of the cell which had the active area of 10 cm^2 was measured with a fuel cell test station (Scribner Associates Inc., 850e Fuel Cell Test Station) at the temperature of 120 ℃. The flow rates of H_2 and air were 52 $cm^3\ min^{-1}$ and 200 $cm^3\ min^{-1}$, respectively, and both inlet gases were humidified to the level of 40% RH. The cells were operated at the ambient pressure, and the voltage values at each current density were taken after one minute of current application.

5.3. Results and Discussion

Preparation and characterization of *p*S, P*p*S and P(*p*S-*co*-BI)-#

The chemical structure of the benzoxazine monomer, sodium 3-(4-sulfonatophenyl)-3,4-dihydro-2*H*-1,3 benzoxazine-6-sulfonate (*p*S) was confirmed by ^{1}H NMR spectroscopy (**Figure 5.4(a)**). The characteristic signals at 5.45 and 4.67 ppm having the intensity ratio of 1 to 1, the theoretical ratio, attributed to the methylene protons of –O-CH_2-N- and Ar-CH_2-N- in the oxazine ring, respectively, were observed. Elemental analysis of *p*S was conducted and the result is shown in **Table 3**. The contents of each element obtained from the elemental analysis are close to the theoretical values calculated from the chemical structure of *p*S. It is well known that poly(benzoxazine)s can be obtained *via* a ring-opening polymerization of benzoxazine monomers initiated by thermal treatments [25,29,30]. The benzoxazine monomer, *p*S, was found to be polymerized by stepwise heating to 220 ℃ and the formation of the polymer, P*p*S, was confirmed by ^{1}H NMR spectroscopy (**Figure 5.4(a)**). The disappearance of the signals at 5.45 and 4.67 ppm and the appearance of the new signals at around 5.16 and 5.03 ppm indicate the complete formation of symmetric Mannich bridges by the thermal treatment at 220 ℃ [23,31-33]. The chemical structure and

polymerization of *p*S were further confirmed by FT-IR spectroscopy (**Figure 5.4(b)**). The symmetric and asymmetric stretching peaks of the -SO_3 were observed at 1030 and 1098 cm^{-1} in both *p*S and P*p*S, respectively [34]. Ring-opening polymerization of *p*S was confirmed by the disappearance of the oxazine ring peaks at around 1499 cm^{-1} (tri-substituted benzene ring), 1248 cm^{-1} (C-O-C asymmetric stretching mode), and 930 cm^{-1} (-C-O-C- cyclic acetal vibrational mode or a C-H out-of-plane deformation) [23,33]. The polymerization can be further supported by the appearance of tetra-substituted benzene ring peak at 1490 cm^{-1}, and broad absorption bands assigned to -OH stretching vibrations at 3700 ~ 3000 cm^{-1}. Based on the ^{1}H NMR, elemental analysis, and FT-IR measurements, it could be concluded that *p*S was synthesized successfully and it can be polymerized by the thermal treatment.

A series of porous substrate, P(*p*S-*co*-BI)-# (where # is the wt% of DBP to *p*S and PBI), were fabricated by mixing, casting, and heating the solution mixtures of *p*S and PBI with DBP as a porogen in DMAc followed by the extraction of DBP from the casted membranes, as shown in **Figure 5.5(a)**. The formation of the cross-linked copolymeric structure of P(*p*S-*co*-BI) could be confirmed by comparing the DMF solubility behavior with the mixed membrane prepared by the thermal treatment of the solution mixture of *p*S: PBI: DBP in weight ratio of 50: 50: 90, the same ratio used for P(*p*S-*co*-BI)-90 preparation. **Figure 5.5(b)** shows the

porous substrate, P(*p*S-*co*-BI)-90, and the mixed membrane after being immersed in DMF at 60 ℃ for 24 h. P(*p*S-*co*-BI)-90 was not dissolved in DMF, although some degree of swelling was observed, while the mixed membrane was completely dissolved in DMF indicating that P(*p*S-*co*-BI)-90 has the covalently bended cross-linked structure. **Figure 5.5(c)** shows the DSC thermograms of P(*p*S-*co*-BI)-90 and P*p*S obtained by second heating DSC ranging up to 250 ℃ under a nitrogen atmosphere; glass transition temperature (T_g) of P*p*S was observed at 165 ℃, while that of P(*p*S-*co*-BI)-90 could not be easily detectable. It is well known that T_g of the cross-linked polymers having rigid ring structures could not be easily detected by DSC [23,35,36]. This result combined with the DMF solubility test result indicates that the porous substrates based on P(*p*S-*co*-BI) are not simple mixture of *p*S and PBI, but the covalently bonded cross-linked products. The chemical structure of P(*p*S-*co*-BI) postulated by the polymerization mechanism of benzoxazine illustrated by our and other studies [23,30,31,33,35], is shown in **Figure 5.5(a)**.

The average pore diameter (Å) and porosity (Vol. %) of the porous substrates, prepared using 20 to 90 wt% of DBP to the total weight of *p*S and PBI, were measured by the mercury intrusion method [37,38] (**Table 2**). Since the porous substrates were prepared by the extraction of DBP, the pore-size and porosity of the porous substrates should be affected by the initial composition ratio of DBP to

*p*S and PBI. With increasing the DBP contents from 20% to 90%, the average pore diameter and porosity were found to increase from 239 Å to 530 Å and from 43.9% to 67.1%, respectively. The cumulative and incremental pore areas of the porous substrates are also shown in **Figure 5.6**.

Based on the pore-size and porosity of the porous substrates prepared in this study, P(*p*S-*co*-BI)-90 was selected as a porous substrate for the pore-filling membrane because it can contain largest amount of proton conducting ionomer (SPAES-70) and has the largest pore-size and porosity values. It is highly desirable for the porous substrate used in the pore-filling membrane in fuel cell application to have the largest porosity with reasonable pore-size and mechanical strength. Compared with the other porous substrates reported previously, the mechanical strength of P(*p*S-*co*-BI)-90 is strong enough to be used as the reinforcing framework of pore-filling membranes in PEMFC applications (**Figure 5.11(d)**) [16,28,39,40]. **Figure 5.7** shows the surface and cross-sectional SEM images of P(*p*S-*co*-BI)-90. The porous substrate with a 15 μm thickness shows irregular large pores with a diameter of 1-3 μm interconnected through narrow orifices with a diameter of 50-100 nm.

It is very desirable for the reinforcing porous substrates and impregnated proton conducting electrolytes to have the interfacial compatibility (similar polarity) to fabricate the pore-filling membrane effectively [5,8,41]. For example, it was

found to be very difficult to fill the very polar proton conducting electrolytes, such as Nafion® and SPAES into the relatively hydrophobic porous substrates such as poly(tetrafluoroethylene) (PTFE) or polyimide (PI) due to their large polarity difference [9,12]. However, when proton conductive polar porous substrates such as silicate encapsulated polyimide nonwoven fabrics were used, the polar electrolyte could be easily impregnated into the pores [5,18]. Therefore, we intentionally prepared the porous substrate, P(*p*S-*co*-BI)-90, having the sulfonic acid groups to match the polarity with the polar polymer electrolyte used as the filling materials. For the study of the polarity behavior of P(*p*S-*co*-BI)-90, other porous substrates such as PBI-90 and P(*p*BUa-*co*-BI)-90 were intentionally fabricated using the same film preparation method. As shown in **Figure 5.8**, PBI-90 and P(*p*BUa-*co*-BI)-90 do not readily absorbed water due to the hydrophobic nature of PBI and P(*p*BUa-*co*-BI), while P(*p*S-*co*-BI)-90 could be easily wetted due to the presence of hydrophilic P*p*S moiety. Additionally, the hydrophilicity of the porous substrates based on P(*p*S-*co*-BI) was systematically controlled by changing the composition ratio of *p*S to PBI, as shown in **Figure 5.9**.

The proton conductivity behavior of P(*p*S-*co*-BI)-90 was investigated at 120 ℃ as a function of RH (**Figure 5.10**). The proton conductivity of P(*p*S-*co*-BI)-90 increases as RH is increased from 20% to 95% as observed from other sulfonated hydrocarbon PEMs. Although the proton conductivity values of the P(*p*S-*co*-BI)-

90 itself (0.1 to 8 mS cm^{-1} from 20% to 95% RH) are not high enough to be used in practical fuel cell applications, it is very notable that our porous substrate, P(*p*S-*co*-BI)-90, prepared for the mechanically reinforcing framework for the proton conductive polymer electrolytes has the proton conductivity behavior. Meanwhile, we also tried to measure the proton conductivity of the PBI-90 and P(*p*BUa-*co*-BI)-90, while the proton conductivity values of these porous substrates could not be obtained under the our experimental conditions.

Preparation and characterization of pore-filling membrane

Pore-filling membrane, SPF-70, was fabricated by impregnating P(*p*S-*co*-BI)-90 with the SPAES-70 solution in DMF at 60 ℃. As shown in **Figure 5.11(a)**, transparent, ultrathin (15-20 μm), and highly-flexible SPF-70 membrane could be obtained by the facile pore-filling process because of both the hydrophilic nature of P(*p*S-*co*-BI) and capillary action of the pores in the substrate. The cross-sectional SEM image of the SPF-70 membrane without voids and pin-holes also indicates the successful impregnation of SPAES-70 into the pores of P(*p*S-*co*-BI)-90 (**Figure 5.11(b)**).

It is desirable to have the polymer membranes in MEAs with minimum dimensional changes by humidity to maintain the cycling durability because the

volume change of the polymer can damage the MEA [42-45]. **Figure 5.11(c)** shows the area based dimensional change of the SPAES-70 and SPF-70 membrane after being soaked in deionized water at 25 ℃ for 4 h. The dimensional change values of the SPAES-70 and SPF-70 membranes are 33% and 9%, respectively. Therefore, the incorporation of the rigid P(*p*S-*co*-BI)-90 into the pore-filling membrane system improve the dimensional stability of the impregnated SPAES-70. The improvement of the dimensional stability by the reinforced porous substrate was also reported by others [12,13,16,18,39,44].

The mechanical properties of the membranes such as Young's modulus and tensile strength were measured using a UTM at room temperature under 40% RH (**Figure 5.11(d)**). The Young's modulus and tensile strength values of the SPAES-70 membrane are 1512 and 41.6 MPa, respectively, while those of the SPF-70 membrane are 4940 and 89.1 MPa, respectively. The SPF-70 membrane shows significantly larger Young's modulus and tensile strength values than the SPAES-70 membrane due to the reinforcement effect of the mechanically robust P(*p*S-*co*-BI)-90.

The proton conductivity of the SPF-70 membrane was measured at 120 ℃ under various RH conditions from 20 to 90% and compared with that of the PF-70 membrane consisting of SPAES-70, the same pore-filling polymer used for SPF-70 and P(*p*BUa-*co*-BI)-90 as the porous substrate without any proton conductive

moiety. The proton conductivity values of the linear SPAES-70 membrane could not be obtained due to its poor physical stability at the given measurement conditions. As shown in **Figure. 5.12**, the proton conductivity values of the SPF-70 membrane are larger than those of the PF-70 membrane over the entire RH ranges, although the pore-size and porosity of P(*p*S-*co*-BI)-90 are much similar to those of P(*p*BUa-*co*-BI)-90 (**Table 3**) and pore-filling ratio of the SPF-70 membrane is comparable to that of the PF-70 membrane (**Figure 5.13**). This result demonstrates that, in addition to the pore-impregnating SPAES-70, P(*p*S-*co*-BI)-90 itself also contributes to the proton conductivity behavior of the pore-filling membrane. **Figure 5.10** shows that P(*p*S-*co*-BI)-90 can provide a proton conducting pathway over a wide range of RH. Therefore, it can be reasonably speculated that the incorporation of the proton conductive porous substrate enhances the proton conductivity of the resulting pore-filling membrane under various RH conditions.

The fuel cell performance of the MEAs prepared from the SPF-70 and PF-70 membranes was evaluated at 120 ℃ and 40% RH conditions. The operating conditions of 120 ℃ and 40% RH were intentionally used because an operating temperature up to 120 ℃ is the technical target temperature for fuel cell vehicles suggested by the U.S. Department of Energy (DOE) [46,47] and 40% RH is the maximum humidity for practical control at 120 ℃ under atmospheric pressure

without any back-pressure supplying system using only humidified reactant gases [48]. **Figure 5.14** shows the current-voltage (*I-V*) and power density curves for the H_2/air cells of the two MEAs based on the SPF-70 and PF-70 membranes. The open circuit voltages of the two cells were found to be larger than 0.9 V. The cell voltage decreases when the increase of applied current as expected. The cell voltage and power density values of the two cells show no significant difference in the low current density region (0-100 mA cm^{-2}) where the cell voltage is mainly determined by the reaction kinetics of the electrode [49-51]. The differences in the cell performance of the two cells become visible when the current density is larger than 100 mA cm^{-2} because membrane resistance cause the ohmic potential loss especially at larger current density [48]. Therefore SPF-70 membrane having larger proton conductivity than PF-70 membrane shows larger cell voltages when the current density is larger than 100 mA cm^{-2}, as shown in **Figure 5.14**. The maximum power density values of the MEAs from the SPF-70 and PF-70 membranes were found at current density value about 400 mA cm^{-2} and they are 171 and 186 mW cm^{-2}, respectively. The performances of the two cells indicate that the larger proton conductivity of the SPF-70 membrane led to the better cell performance, thus a larger power density could be obtained at the harsh operating conditions of 120 ℃ and 40% RH [52].

We believe that further improvement of the fuel cell performance of pore-filling membrane might be achieved by using the different types of benzoxazine that can further improve the proton conductivity, compatibility with the electrolytes, the mechanical stability and such works are under progress. Additionally, the improvement in the fuel cell performance of the pore-filling membranes is also possible by effectively thinning the membranes based on mechanically robust porous substrate and filling the pores using highly proton conductive polymeric filling materials such as block and comb-like copolymers [53,54].

5.4. Conclusions

Proton conductive porous substrates consisting of cross-linked benzoxazine-benzimidazole copolymers were developed by the reaction of PBI with sulfonated benzoxazine using dibutyl phthalate as a porogen. The proton conductive sulfonic acid groups in the porous substrate imparting the improved hydrophilicity and proton conductivity can increase the affinity of the substrate with the proton conductive polymers such as sulfonated poly(arylene ether sulfone) having degree of sulfonation of 70 mol% (SPAES-70). These advantages features of the porous substrates enabled the facile impregnation of SPAES-70 and the resulting pore-filling membrane showed much enhanced both physical stability and mechanical strength than the linear SPAES-70 membrane and also exhibited improved proton conductivity and cell performance than the pore-filling membrane based on the cross-linked benzoxazine-benzimidazole copolymers without any proton conductive acid groups. We strongly believe that this study will provide a new perspective for the fabrication of a proton conductive porous substrate, which contributes to improving the proton conductivity of a reinforced pore-filling membrane while acting as a mechanically reinforcing framework.

5.5. References

[1] H. Zhang, P.K. Shen, Chem. Rev. 112 (2012) 2780-2832.

[2] C.H. Park, C.H. Lee, M.D. Guiver, Y.M. Lee, Prog. Polym. Sci. 36 (2011) 1443-1498.

[3] S. Bose, T. Kuila, X.L.N. Thi, N.H. Kim, K.T. Lau, J.H. Lee, Prog. Polym. Sci. 36 (2011) 813-843.

[4] K. Kim, P. Heo, T. Ko, J.-C. Lee, Electrochem. Commun. 48 (2014) 44-48.

[5] J.R. Lee, N.Y. Kim, M.S. Lee, S.Y. Lee, J. Membri. Sci. 367 (2011) 265-272.

[6] J.A. Kolde, B. Bahar, M.S. Wilson, T.A. Zawodzinski, S. Gottesfeld, Proceedings of the First International Symposium on Proton Conducting Membrane Fuel Cells 1995, pp. 95-23.

[7] B. Kienitz, J. Kolde, S. Priester, C. Baczkowski, M. Crum, ECS Trans. 41 (2011) 1521-1530.

[8] T. Yamaguchi, Polymer Membranes for Fuel Cells, Springer, 2009, pp. 385-399.

[9] J.R. Lee, J.H. Won, N.Y. Kim, M.S. Lee, S.Y. Lee, J. Colloid. Interf. Sci. 362 (2011) 607-614.

[10] M.P. Rodgers, J. Berring, S. Holdcroft, Z.Q. Shi, J. Membri. Sci. 321 (2008) 100-113.

[11] J. Shim, H.Y. Ha, S.A. Hong, I.H. Oh, J. Power Sources 109 (2002) 412-417.

[12] X.B. Zhu, H.M. Zhang, Y.M. Liang, Y. Zhang, Q.T. Luo, C. Bi, B.L. Yi, J. Mater. Chem. 17 (2007) 386-397.

[13] T. Yamaguchi, H. Zhou, S. Nakazawa, N. Hara, Adv. Mater. 19 (2007) 592-596.

[14] N. Hara, H. Ohashi, T. Ito, T. Yamaguchi, J. Phys. Chem. B 113 (2009) 4656-4663.

[15] K.M. Nouel, P.S. Fedkiw, Electrochim. Acta 43 (1998) 2381-2387.

[16] D.M. Yu, S. Yoon, T.H. Kim, J.Y. Lee, J. Lee, Y.T. Hong, J. Membri. Sci. 446 (2013) 212-219.

[17] K.H. Kim, S.Y. Ahn, I.H. Oh, H.Y. Ha, S.A. Hong, M.S. Kim, Y. Lee, Y.C. Lee, Electrochim. Acta 50 (2004) 577-581.

[18] J.-H. Seol, J.-H. Won, M.-S. Lee, K.-S. Yoon, Y.T. Hong, S.-Y. Lee, J. Mater. Chem. 22 (2012) 1634-1642.

[19] Y. Yao, Z. Lin, Y. Li, M. Alcoutlabi, H. Hamouda, X. Zhang, Adv. Energy Mater. 1 (2011) 1133-1140.

[20] F. Wang, M. Hickner, Y.S. Kim, T.A. Zawodzinski, J.E. McGrath, J. Membri. Sci. 197 (2002) 231-242.

[21] Y.S. Kim, F. Wang, M. Hickner, S. McCartney, Y.T. Hong, W. Harrison, T.A. Zawodzinski, J.E. McGrath, J. Polym. Sci., Part B: Polym. Phys. 41 (2003) 2816-

2828.

[22] W.L. Harrison, F. Wang, J.B. Mecham, V.A. Bhanu, M. Hill, Y.S. Kim, J.E. McGrath, J. Polym. Sci., Part A: Polm. Chem. 41 (2003) 2264-2276.

[23] S.K. Kim, S.W. Choi, W.S. Jeon, J.O. Park, T. Ko, H. Chang, J.C. Lee, Macromolecules, 45 (2012) 1438-1446.

[24] J.S. Wainright, J.T. Wang, D. Weng, R.F. Savinell, M. Litt, J. Electrochem. Soc. 142 (1995) L121-L123.

[25] S.W. Choi, J.O. Park, C. Pak, K.H. Choi, J.C. Lee, H. Chang, Polymers 5 (2013) 77-111.

[26] Y.H. Jeong, J.H. Jung, E. Choi, S. Han, A.I. Begley, S.J. Yoo, J.H. Jang, H.-J. Kim, S.W. Nam, K.-Y. Lee, J. Power Sources 299 (2015) 480-484.

[27] J.K. Fink, Reactive polymers fundamentals and applications: a concise guide to industrial polymers, William Andrew, 2013.

[28] S. Alwin, S.D. Bhat, A.K. Sahu, A. Jalajakshi, P. Sridhar, S. Pitchumani, A.K. Shukla, J. Electrochem. Soc. 158 (2011) B91-B98.

[29] N.N. Ghosh, B. Kiskan, Y. Yagci, Prog. Polym. Sci. 32 (2007) 1344-1391.

[30] Y.X. Wang, H. Ishida, Macromolecules, 33 (2000) 2839-2847.

[31] S.K. Kim, T. Ko, S.W. Choi, J.O. Park, K.H. Kim, C. Pak, H. Chang, J.C. Lee, J. Mater. Chem. 22 (2012) 7194-7205.

[32] B.J. Yao, X.L. Yan, Y. Ding, Z.J. Lu, D.X. Dong, H. Ishida, M. Litt, L. Zhu,

Macromolecules 47 (2014) 1039-1045.

[33] S.K. Kim, T. Ko, K. Kim, S.W. Choi, J.O. Park, K.H. Kim, C. Pak, H. Chang, J.C. Lee, Macromol. Res. 20 (2012) 1181-1190.

[34] H. Kang, K. Kim, D. Kang, J.C. Lee, Rsc Adv. 5 (2015) 64031-64036.

[35] S.K. Kim, K.H. Kim, J.O. Park, K. Kim, T. Ko, S.W. Choi, C. Pak, H. Chang, J.C. Lee, J. Power Sources 226 (2013) 346-353.

[36] T.-H. Kim, S.-K. Kim, T.-W. Lim, J.-C. Lee, J. Membri. Sci. 323 (2008) 362-370.

[37] W.-H. Seol, Y.M. Lee, J.-K. Park, J. Power Sources 170 (2007) 191-195.

[38] C.-G. Lee, D.-H. Kim, H.-C. Lim, J. Electrochem.l Soc. 154 (2007) B396-B404.

[39] J.-H. Seol, J.-H. Won, K.-S. Yoon, Y.T. Hong, S.-Y. Lee, Solid State Ionics 190 (2011) 30-37.

[40] C.-H. Shen, L.-c. Jheng, S.L.-c. Hsu, J.T.-W. Wang, J. Mater. Chem. 21 (2011) 15660-15665.

[41] H.J. Lee, J.H. Kim, J.H. Won, J.M. Lim, Y.T. Hong, S.Y. Lee, Acs Appl. Mater. Inter. 5 (2013) 5034-5043.

[42] T. Ko, K. Kim, B.K. Jung, S.H. Cha, S.K. Kim, J.C. Lee, Macromolecules, 48 (2015) 1104-1114.

[43] T. Ko, K. Kim, M.Y. Lim, S.Y. Nam, T.H. Kim, S.K. Kim, J.C. Lee, J. Mater.

Chem. A 3 (2015) 20595-20606.

[44] T. Nguyen, X. Wang, J. Power Sources 195 (2010) 1024-1030.

[45] M.S. Jung, T.H. Kim, Y.J. Yoon, C.G. Kang, D.M. Yu, J.Y. Lee, H.J. Kim, Y.T. Hong, J. Membri. Sci. 459 (2014) 72-85.

[46] M.A. Hickner, H. Ghassemi, Y.S. Kim, B.R. Einsla, J.E. McGrath, Chem. Rev. 104 (2004) 4587-4612.

[47] C. Houchins, G. Kleen, J. Spendelow, J. Kopasz, D. Peterson, N. Garland, D. Ho, J. Marcinkoski, K. Martin, R. Tyler, D. Papageorgopoulos, Membranes 2 (2012) 855-878.

[48] K. Kim, P. Heo, T. Ko, K.H. Kim, S.K. Kim, C. Pak, J.C. Lee, J. Power Sources 293 (2015) 539-547.

[49] Y. Shao, G. Yin, Z. Wang, Y. Gao, J. Power Sources 167 (2007) 235-242.

[50] B. Yao, X. Yan, Y. Ding, Z. Lu, D. Dong, H. Ishida, M. Litt, L. Zhu, Macromolecules 47 (2014) 1039-1045.

[51] J. Zhang, Z. Xie, J. Zhang, Y. Tang, C. Song, T. Navessin, Z. Shi, D. Song, H. Wang, D.P. Wilkinson, J. Power Sources 160 (2006) 872-891.

[52] K. Si, R. Wycisk, D. Dong, K. Cooper, M. Rodgers, P. Brooker, D. Slattery, M. Litt, Macromolecules 46 (2013) 422-433.

[53] S. Lee, J. Ann, H. Lee, J.H. Kim, C.S. Kim, T.H. Yang, B. Bae, J. Mater. Chem. A 3 (2015) 1833-1836.

[54] N. Li, C. Wang, S.Y. Lee, C.H. Park, Y.M. Lee, M.D. Guiver, Angew. Chem. Int. Edit. 50 (2011) 9158-9161.

Table 5.1 Properties of SPAES-70.

Polymer	Degree of sulfonation x (%)		IEC_w (mequiv./g)		M_w[e] (-)	M_n[e] (-)	M_w/M_n (-)
	Monomer[a]	^{1}H NMR[b]	Calc.[c]	Expt.[d]			
SPAES-70	70	67	2.51	2.47	82,000	35,000	2.3

[a] Degree of sulfonation obtained from feed monomer ratio.

[b] Degree of sulfonation obtained from peak integration in ^{1}H NMR spectra.

[c] Calculated from ^{1}H NMR spectra.

[d] Determined experimentally by acid-base titration method.

[e] Weight-average molecular weight (M_w) and number average molecular weight (M_n) calculated from GPC measurement using poly(methyl methacrylate) standard.

Table 5.2 Preparation conditions, average pore-size and porosity of porous substrates.

Porous substrate	Benzoxazine		PBI (g)	DBP (g)	Average pore diameter[d] (4V/A, Å)	Porosity[d] (Vol. %)
	*p*S[b] (g)	*p*BUa[c] (g)				
PBI-90[a]	-	-	1.36	1.23	546	68.2
P(*p*S-*co*-BI)-20[a]	0.681	-	0.681	0.273	239	43.9
P(*p*S-*co*-BI)-50[a]	0.681	-	0.681	0.681	307	63.5
P(*p*S-*co*-BI)-70[a]	0.681	-	0.681	0.954	421	65.7
P(*p*S-*co*-BI)-90[a]	0.681	-	0.681	1.23	530	67.1
P(*p*BUa-*co*-BI)-90[a]	-	0.681	0.681	1.23	523	66.3

[a] Number means weight % of DBP to total weight of benzoxazine *(p*S or *p*BUa*)* and PBI.

[b] *p*S is used for P(*p*S-*co*-BI)-#

[c] *p*BUa is used for P(*p*BUa-*co*-BI)-90

[d] Determined experimentally by mercury porosimeter.

Table 5.3 Elemental analysis of *p*S.

Element	*p*S	
	Theoretical (%)	Experimental (%)
C	40.48	39.01
N	3.37	3.31
S	15.44	15.16
H	2.64	3.43

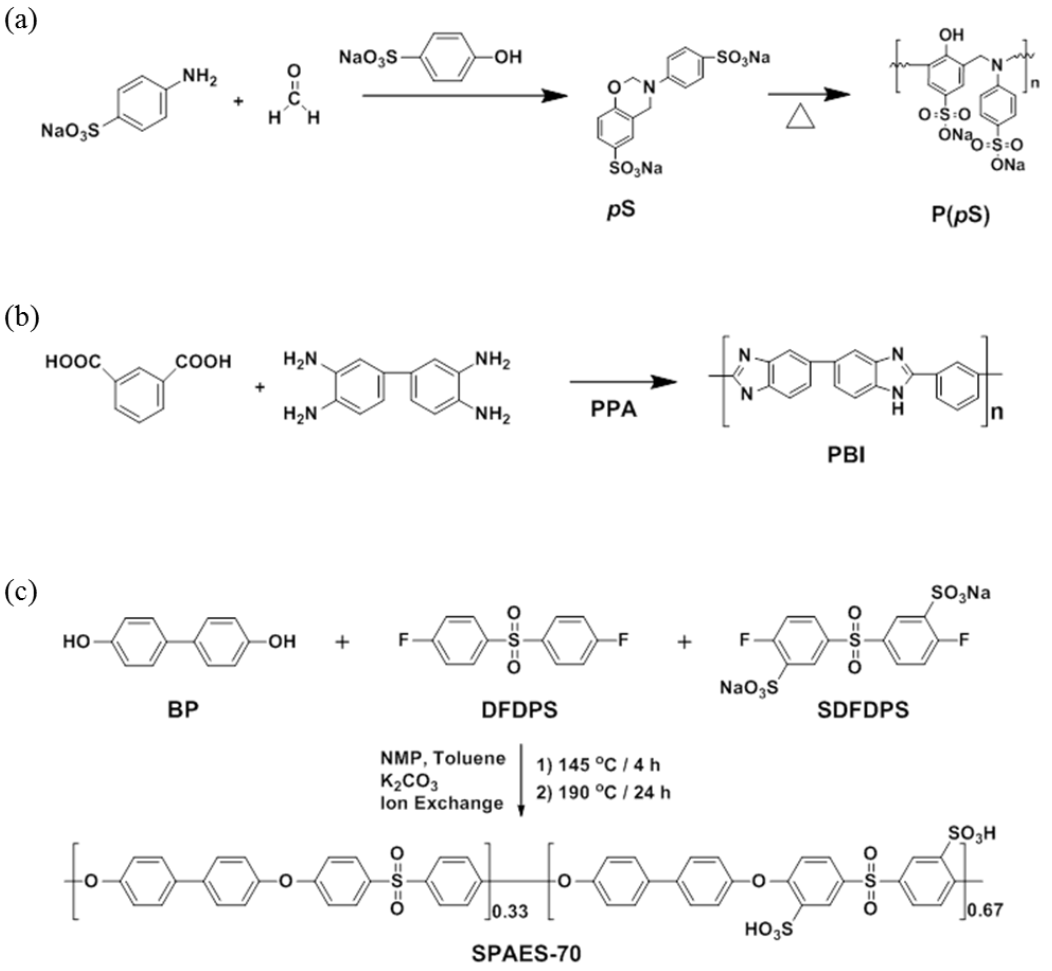

Figure 5.1 Synthesis of (a) *p*S and P(*p*S), (b) PBI and (c) SPAES-70.

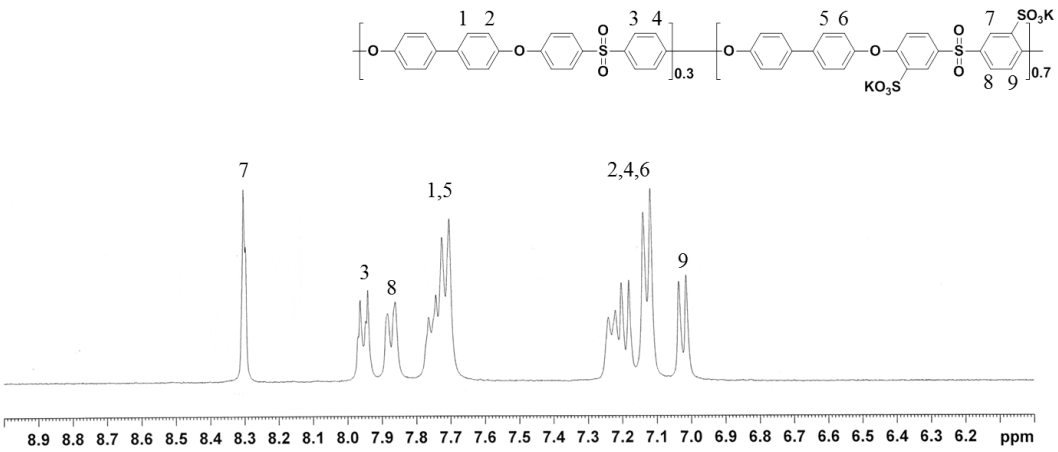

Figure 5.2 ^{1}H NMR spectrum of SPAES-70.

(a)

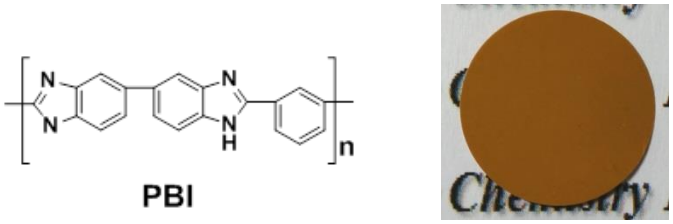

(b)

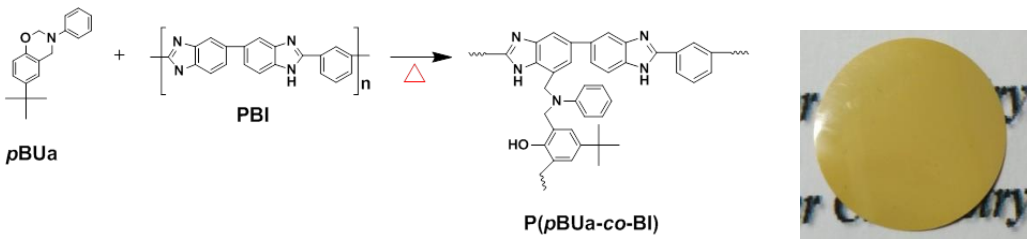

Figure 5.3 Chemical structure of (a) PBI and (d) P(*p*BUa-*co*-BI), wherein photo images are (a) PBI-90 and (b) P(*p*BUa-*co*-BI)-90.

(a)

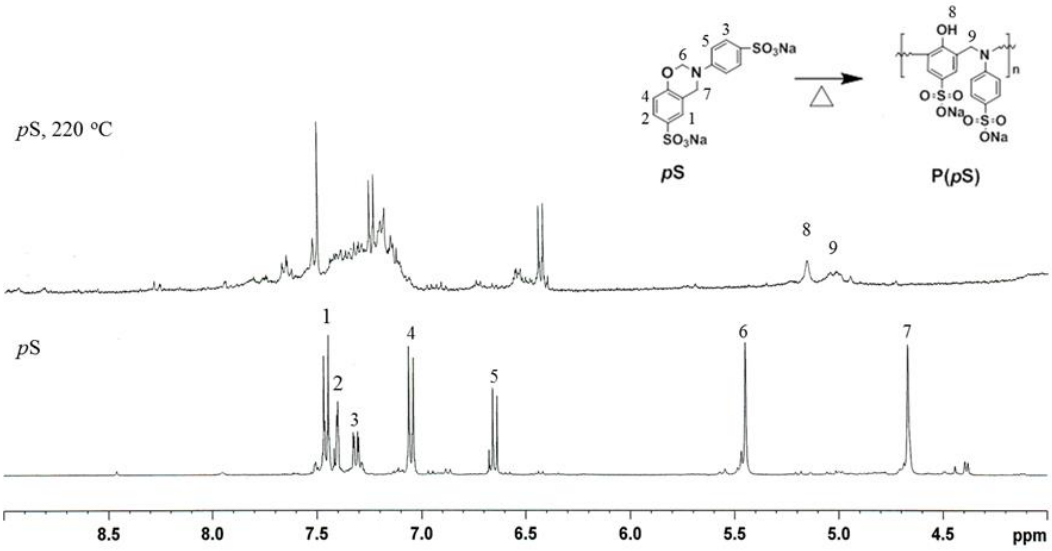

(b)

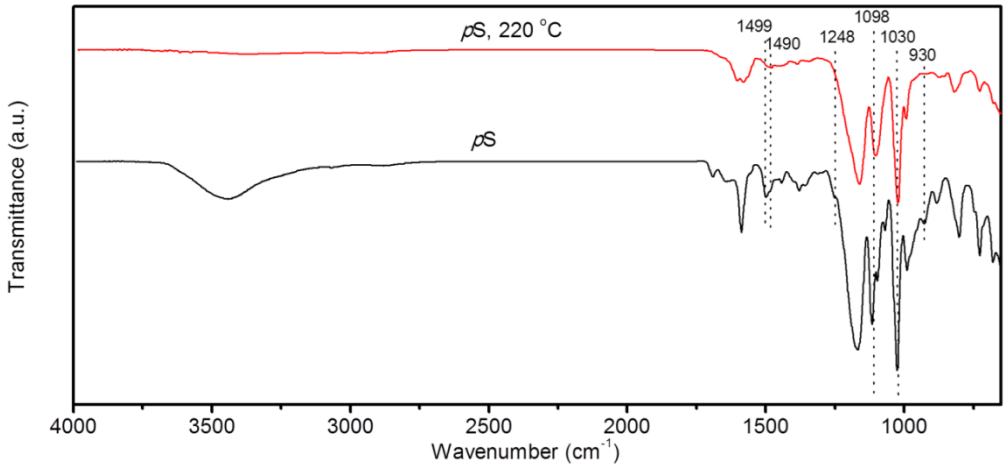

Figure 5.4 (a) ^{1}H NMR spectra and (b) infrared spectra of *p*S after thermal treatment at 220 °C.

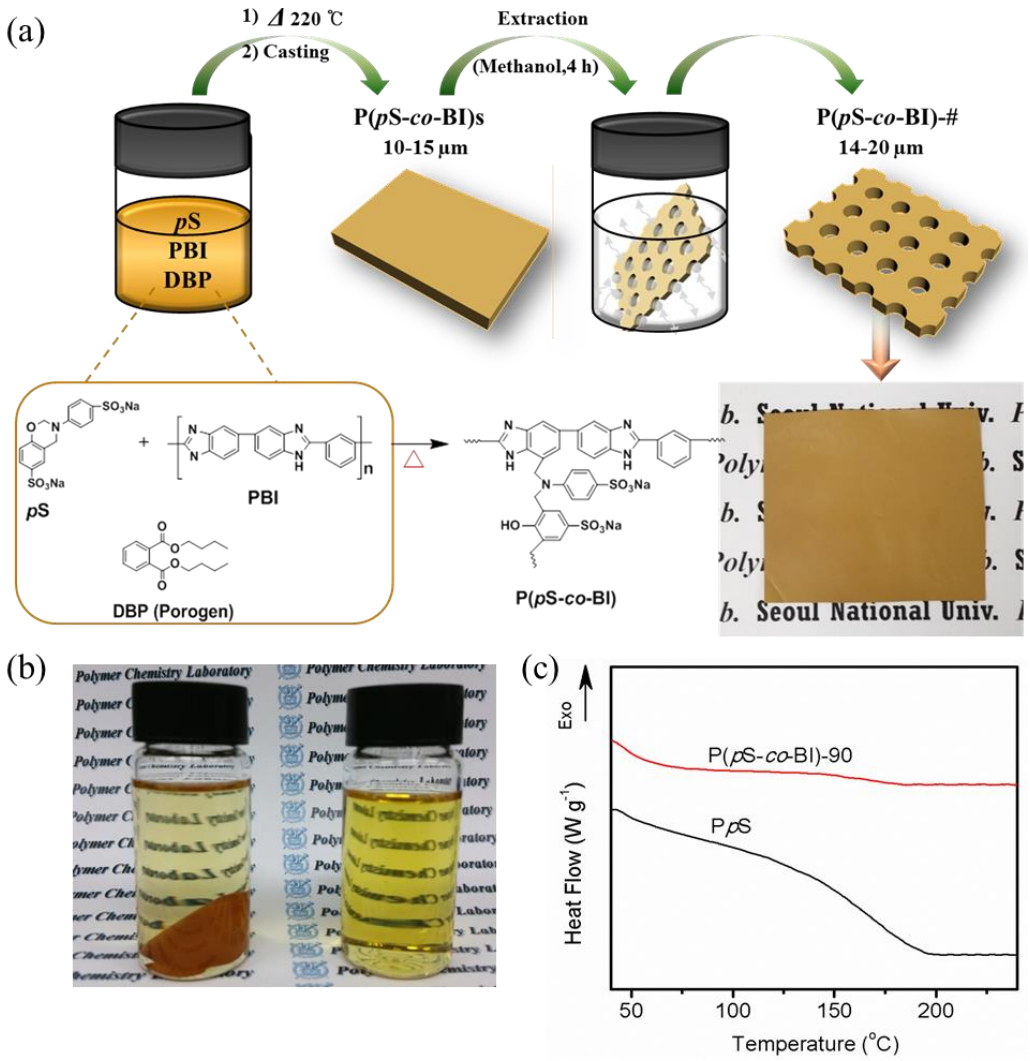

Figure 5.5 (a) Schematic illustration for the preparation of porous substrate, wherein the possible covalent bonded cross-linked structure of P(*p*S-*co*-BI) and photograph of P(*p*S-*co*-BI)-90 substrate is included. (b) Solubility test of P(*p*S-*co*-BI)-90 (left) and mixed membrane (*p*S: PBI: DBP= 50: 50: 90 (wt%), right) after being immersed in DMF at 60 ^{o}C for 24 h and (c) DSC second heating curves of P*p*S and P(*p*S-*co*-BI)-90.

(a)

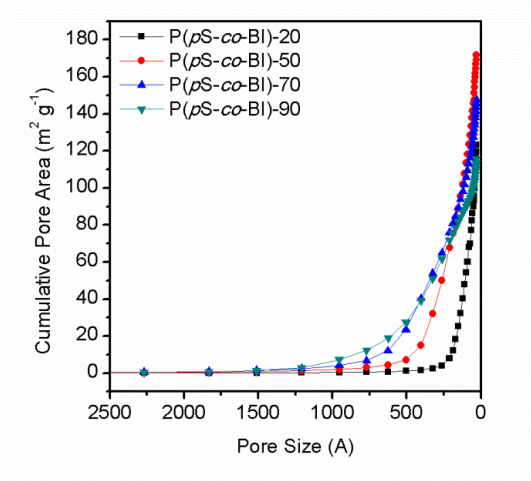

(b)

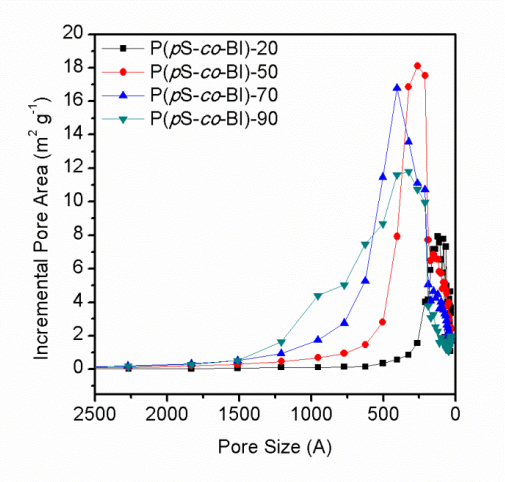

Figure 5.6 (a) Cumulative and (b) incremental pore area of porous P(*p*S-*co*-BI) substrates prepared with different amount of dibutyl phthalate (DBP).

(a)

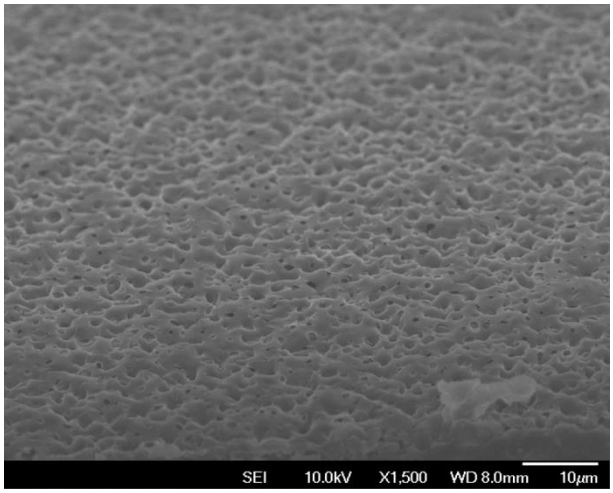

(b)

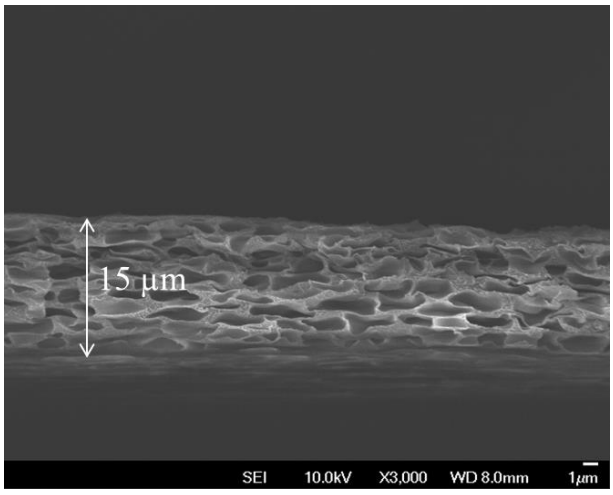

Figure 5.7 (a) surface and (b) cross-sectional SEM images of P(*p*S-*co*-BI)-90.

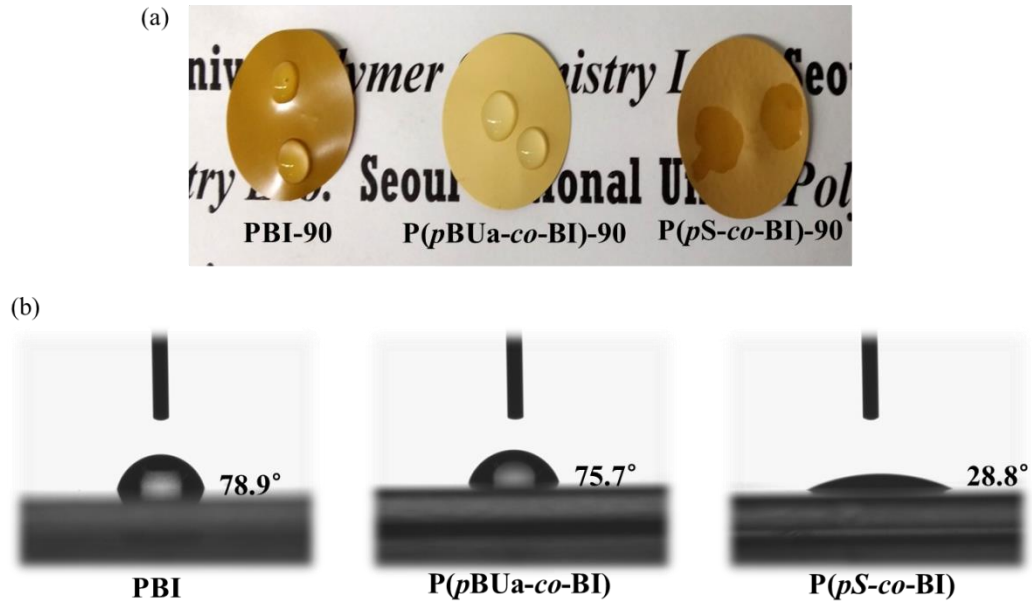

Figure 5.8 (a) Water wettability of PBI-90, P(*p*BUa-*co*-BI)-90 and P(*p*S-*co*-BI)-90 and (b) contact angles of PBI, P(*p*BUa-*co*-BI) and P(*p*S-*co*-BI) membranes. During the contact angle measurement, the non-porous films were intentionally used to exclude the capillary action of pores in porous substrate.

(a)

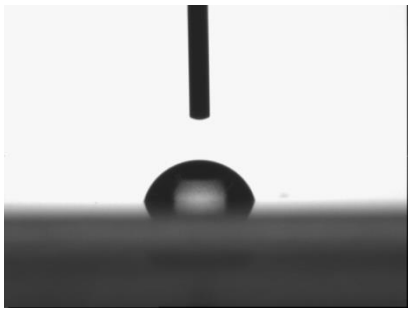

(b)

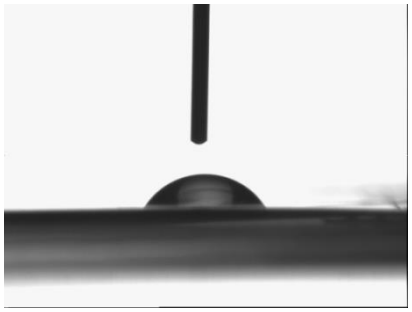

(c)

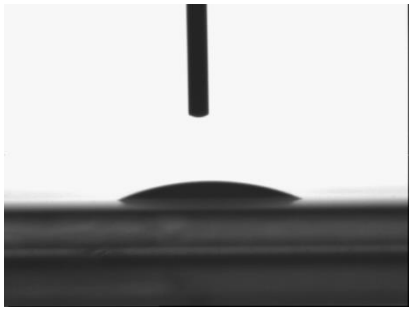

Figure 5.9 contact angle of P(*p*S-*co*-BI) based membranes with three different composition ratios: (a) *p*S: PBI = 0: 1 (b) *p*S: PBI = 0.25: 0.75 and (c) *p*S: PBI = 0.5: 0.5. The measurements were performed with non-porous type membranes.

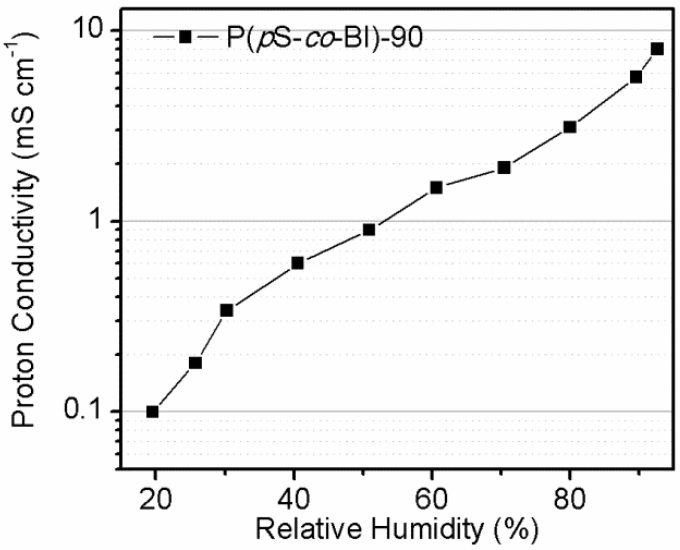

Figure 5.10 Proton conductivities of porous P(*p*S-*co*-BI)-90 substrate at 120 °C as a function of relative humidity.

(a)

(b)

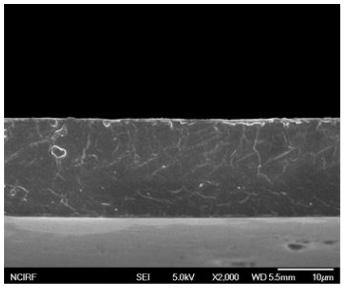

(c)

Sample	Wet State	Dry State
SPAES-70	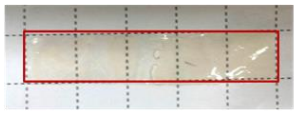	 ΔA ~ 35%
SPF-70	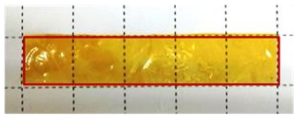	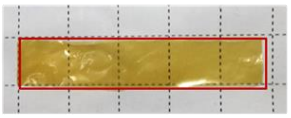 ΔA ~ 6%

(d)

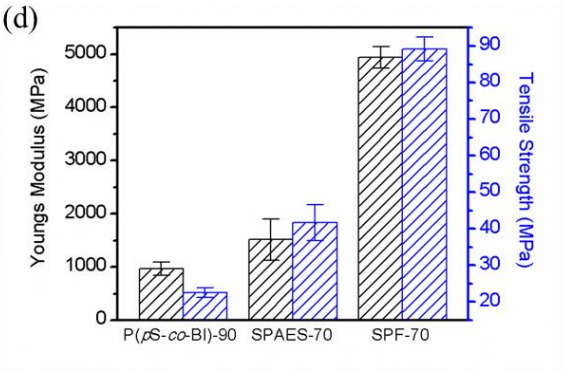

Figure 5.11 (a) photograph and (b) cross-sectional SEM image of SPF-70 membrane. (c) Area based dimensional change of SPAES-70 and SPF-70 membranes and (d) mechanical properties of P(*p*S-*co*-BI)-90, SPAES-70 membrane and SPF-70 membrane.

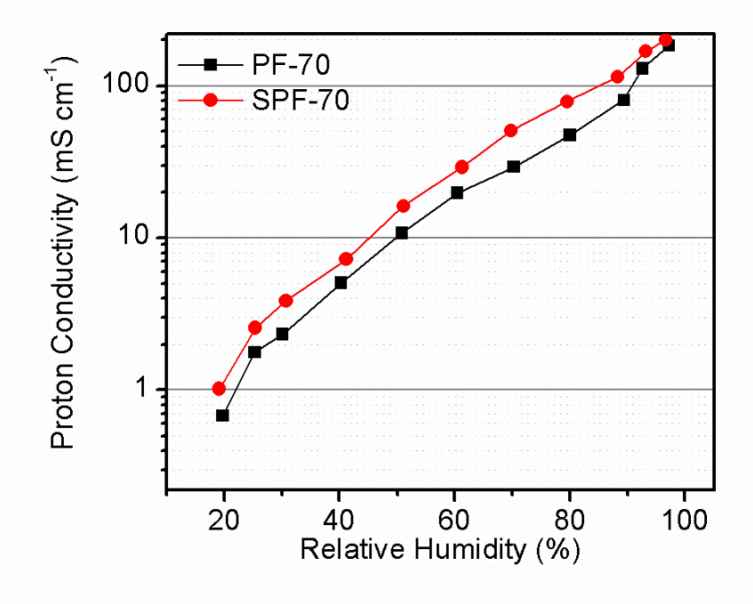

Figure 5.12 Proton conductivity of SPF-70 membrane based on P(*p*S-*co*-BI) having proton conductive moiety and PF-70 membrane based on P(*p*BUa-*co*-BI) without any proton conductive moiety at 120 °C as a function of relative humidity.

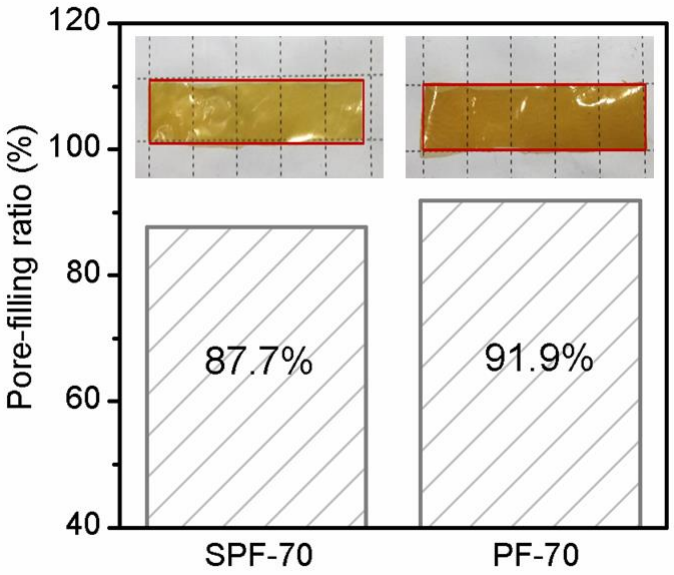

Figure 5.13 Pore-filling ratio and (inset) photo images of SPF-70 and PF-70 membranes.

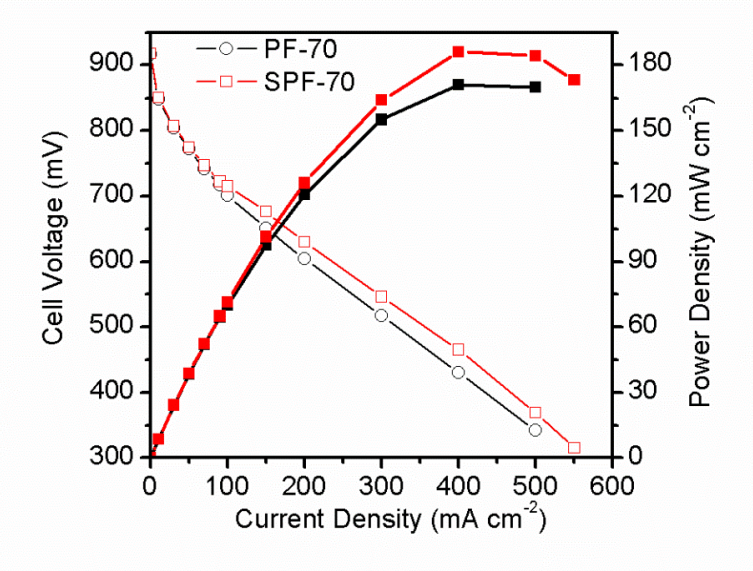

Figure 5.14 Fuel cell performances of MEAs prepared using SPF-70 and PF-70 membranes having thickness of 18 µm at 120 °C and 40% RH conditions.

Chapter 6

A Simple and Effective Cross-Linking Technology for the Design of a High-Performance Proton Exchange Membrane for Automotive Fuel Cell Applications

6.1. Introduction

Polymer electrolyte membranes (PEMs) operating at mid temperatures (90-120 ℃) and low relative humidity conditions have been intensively studied for the practical application of polymer electrolyte membrane fuel cells (PEMFCs) in automobile transportation [1, 2]. Since the currently used radiators in automobiles are designed to be operated at mid temperatures, it is highly desirable for PEMs to be applicable to the same temperature ranges. However, the optimum operating temperature for the commonly used perfluorinated PEMs such as Nafion® is lower such as 60 to 80 ℃ [3, 4]. There have been a series of studies on the development of alternative PEMs based on sulfonated aromatic polymers (SAPs) for possible application at mid temperatures due to their high thermal stability, low cost and structural diversity [5, 6]. However, high electrochemical performances such as proton conductivity and cell performance of SAP-membranes can only achieved when SAPs have a sufficiently high degree of sulfonation (DS), while the SAP membranes with high DS do not have high enough physicochemical stability to exhibit desirable cell performance during operation. Some literature reported that the physicochemical stability of SAPs having high DS could be improved by cross-linking technology without the deterioration of proton conductivity [7, 8].

Although cross-liked SAP membranes were found to have proton conductivity that was comparable with or even higher than that of their liner membranes, the cell performance of the membrane electrode assemblies (MEAs) with cross-linked membranes exhibited smaller than those with their linear membranes due to the 1) brittleness problems from the rigid cross-liked structures with high cross-linking density [9] and 2) interfacial incompatibility issues between the cross-linked membranes and electrode surfaces [7].

In this study, we propose a simple but effective cross-linking technology for the design of better performing cross-linked sulfonated poly(arylene ether sulfone) (C-SPAES) membrane showing both highly improved physicochemical stability and electrochemical performance than the linear SPAES membrane. The C-SPAES membrane is prepared by simple one-step process using a mixture of modified SPAES having chloromethyl side groups and perfluoropolyether (PFPE) consisting of a fluorinated backbone and two chain-ends bearing hydroxyl groups as a cross-linker. The newly selected flexible oligomeric cross-linker, PFPE, can increase the flexibility of the rigid cross-linked SPAES polymer networks, while the high fluorine concentration in the PFPE structure can effectively enhance the interfacial compatibility between the C-SPAES membrane and electrode surfaces, resulting in much improved cell performance of the MEA with the C-SPAES membrane compared with that of the SPAES membrane. The details for the

synthesis of cross-linkable SPAES and the properties of the C-SPAES membrane, including its cell performance, are described.

6.2. Experimental

Materials

4,4'-Difluorodiphenyl sulfone (DFDPS, 99%, Aldrich) and dihydroxybiphenyl (BP, 97.0%, Aldrich) were purified by recrystallization from toluene and methanol, respectively. 3,3'-Disulfonated-4,4'-difluorodiphenyl sulfone (SDFDPS) was synthesized from DFDPS according to the previous report [10]. The yield of SDFDPS after recrystallization from a mixture of *iso*-propylalcohol and deionized water (7/3, v/v) was 85%. Perfluoropolyether (PFPE, Solvay-Solexis Fluorolink E10H) and potassium carbonate (K_2CO_3, 99.0%, Aldrich) was dried under vacuum at 60 ^{o}C for 48 h, prior to use. Average molecular weight (M_n) of PFPE is about 1,600 g mol^{-1}, and the p/q ratio and n, shown in PFPE structure in Fig. 1, is $1.5<p/q<2$ and $1.5<n<2.5$, respectively [11]. Chloromethyl methyl ether (95.0%, Kanto Chemical), tin (IV) chloride (99%, Aldrich), sodium chloride (NaCl, 99.5%, Daejung), sodium hydroxide (NaOH, 98.0%, Daejung), triethylamine (TEA, 99.0%, TCI) were used as received. *N*,*N*-Dimethylacetamide (DMAc, 99%, Junsei) and dimethyl sulfoxide (DMSO, 99%, Junsei) were stored over molecular sieves under nitrogen and toluene (99.5%, Junsei) was refluxed over calcium hydride and distilled. All other solvents and reagents were used as received from standard

vendors.

Synthesis of sulfonated poly(arylene ether sulfone) (SPAES)

To a 500 ml four-neck reactor equipped with a nitrogen inlet and outlet, a Dean-Stark trap, a condenser, a thermometer, and an overhead mechanical stirrer was charged with 5.009 g (26.90 mmol) of BP, 2.393 g (9.415 mmol) of DFDPS, 8.014 g (17.48 mmol) of SDFDPS, and 4.461 g (32.28 mmol) of K_2CO_3 in 79.39 mL of DMSO, and 39.69 mL of toluene. The reaction mixture was refluxed at 140 ℃ for 5 h to complete dehydration as an azeotrope with toluene and then temperature was raised to 185 ℃ for the complete removal of toluene. The reaction was continued for 24 h until the solution became very viscous. The viscous solution was cooled down to room temperature and 10.00 mL of DMSO was added to dilute the solution. The diluted solution was filtered to remove the salts and poured into *iso*-propyl alcohol (5000 mL) to precipitate the polymer, and the precipitate was washed several times with *iso*-propyl alcohol. Then, the product was purified by Soxhlet extraction with *iso*-propyl alcohol. The product polymer was obtained in 78% of yield after dried in a vacuum oven at 60 ℃ for 24.

Modification of SPAES to SPAES with chloromethyl side group (SPAES-Cl)

The solution containing 6.653 g (12.58 mmol of repeat units) of SPAES in 110.9 mL of DMAc was added into a dried 250.0 mL two-neck round bottom flask equipped with a condenser. 1.616 g (18.86 mmol) of chloromethyl methyl ether and 3.448 g (12.58 mmol) of tin(IV) chloride were added into the reactor at room temperature, and the solution mixture was heated at 50 ℃ and stirred for 24 h. The mixture solution was then poured into *iso*-propanol. The precipitate was washed several times with methanol and deionized water. The SPAES-Cl was obtained in 84% of yield after dried in a vacuum oven at 60 ℃ for 24. The successful introduction and the content of the chloromethyl groups were confirmed by ^{1}H-NMR. The content of chloromethyl group in SPAES-Cl was found to be 8 mol%, indicating that there are 0.08 equivalents of chloromethyl groups per repeating unit.

Preparation of Cross-linked SPAES (C-SPAES) and linear SPAES membranes

The C-SPAES membrane was prepared by *in-situ* casting and heating the SPAES-Cl solution mixture containing PFTE as a cross-linker. 0.5000 g (0.9384 mmol of

repeat units) of SPAES-Cl, 0.05930 g (0.03706 mmol) of PFTE, and 0.09666 g (0.9384 mmol) of TEA were dissolved in 3.900 mL of DMAc. The amount of PFTE was decided to make the molar ratio between the hydroxyl group of PFTE and the chloromethyl groups of SPAES-Cl to be 1:1. The amount of TEA was decided by the molar content of the hydroxyl group of PFTE and DMAc was determined to adjust the total concentration of SPAES-Cl, PFTE, and TEA to be 12 wt%. The solution mixture was then spread onto a clean glass plate and its thickness was controlled by a doctor blade film applicator. The casted solution was heated at 120 ℃ in a vacuum oven for 12h. The obtained film was washed with distilled water several times to remove the any remaining solvent and TEA. The membrane with a thickness of about 18-20 μm was obtained after drying in a vacuum oven for 24 h.

Linear SPAES membrane was prepared as a control sample by casting the 12 wt% SPAES solution in DMAc onto a glass plate. The same film fabrication method used for the C-SPAES membrane including the solution casting, heat treatment, and drying processes was employed. The thickness of the SPAES membrane could be also controlled by the doctor blade film applicator and it was in the range of 17-22 μm. The C-SPAES and SPAES membranes in salt form (K^+) were than transformed to their acid form (H^+) by soaking in 1 M H_2SO_4 aqueous solution at 30 ℃ for 24 h. The membranes in acid form were rinsed with distilled water

several times and then dried in a vacuum oven for 24 h.

Preparation of membrane electrode assemblies (MEAs)

Membrane electrode assemblies (MEAs) were fabricated by the decal method. The catalyst ink was prepared by mixing catalyst powder (50 wt. % Pt/C, Tanaka Kikinzoku Kogyo), Aquivion^{TM} ionomer dispersion (EW750, Solvay), and solvent mixture comprising 1: 4 weight ratio of water: dipropylene glycol. The catalyst layer was prepared by coating the ink on a decal substrate and drying it at 60 ℃. The amounts of Pt catalyst and Aquivion^{TM} ionomer were 0.4 mg cm^{-2} and 0.35 mg cm^{-2} in the catalyst layers for anode and cathode, respectively. The membrane with the catalyst layers (10 cm^2 of active area) was sandwiched and hot pressed at 120 ℃, and gas diffusion layers (25BC, SGL) were placed on both sides of the catalyst layers.

Characterization

The ^{1}H-NMR spectra were measured at 400 MHz on an Avance-400 (Bruker, Germany) spectrometer using DMSO-*d6* as solvent. Molecular weights were obtained by gel permeation chromatography (GPC) consisting of a Waters 510

HPLC pump, three columns PLgel 5 μm guard, MIXED-C, MIXED-D, and a Viscoter T60A dual detector. HPLC grade DMF was used as an eluent and calibration was performed with poly(methyl methacrylate) standards. Solubility test was carried out by immersing the membranes in various solvents at 30 and 80 ℃ for 1 h, respectively. Gel fraction test was conducted by the solvent extraction method. The dry membranes with size of 2 cm × 2 cm were weighed (W_1), and then they were refluxed in excess DMAc at 80 ℃ for 12 h. The membranes were then washed with distilled water several times and dried at 100 ℃ under vacuum until the constant weight (W_2) was obtained. The gel fractions were calculated as follows:

$$\text{Gel fraction [\%]} = W_2/W_1 \times 100 \quad (1)$$

The oxidative stability of the membranes was evaluated by Fenton's test by observing the dissolution behavior of the membranes after being exposed to a Fenton's reagent (3 wt% H_2O_2 aqueous solution containing 16 ppm Fe^{2+}). After immersing the membranes in the Fenton's reagent at 80 °C, the membranes were observed periodically and the times when the membranes began to break into small pieces (τ_1) and completely dissolved (τ_2) were recorded, respectively.

Mechanical properties were tested using a universal testing machine (Lloyd-LS1, UK). The ASTM standard D638 (Type V specimens) was used for the preparation

of dumbbell specimens. The measurement was carried out at 23 ℃ and 45% RH conditions with a gauge length and a cross head speed of 15 mm and 5 mm min^{-1}, respectively.

Ion-exchange capacity (IEC) of the membranes was determined by typical back-titration method. The samples were soaked in 1 M NaCl aqueous solution for 4 h, and then the solutions were titrated with 0.01 M NaOH aqueous solution. The IEC value was calculated using the following equation:

$$IEC\ [mequiv.g^{-1}] = (C_{NaOH} \cdot \Delta V_{NaOH} / W_s) \times 1000 \quad (2)$$

where C_{NaOH}, ΔV_{NaOH}, and W_s are the concentration of NaOH (aq), the consumed volume of NaOH (aq), and the weight of the dry membrane, respectively.

The humidity dependent water absorption of the membrane was estimated by the weight change of the dry membrane (W_{dry}) at 90 ℃ with different humidity conditions from 20% to 98% RH in a humidity control chamber (Espec, SH-241). After equilibration for 4 h at given RH conditions, the membrane was removed and weighed (W_{wet}). The humidity dependent water uptake was calculated by measuring the weight changes of the membrane. The number of water molecules per sulfonic acid (hydration number, λ) at given RH can be calculated as follow:

$$\lambda = [(W_{wet}-W_{dry})/W_{dry}] \times 1000/(M_{H2O} \times IEC) \quad (3)$$

where M_{H2O} is the molecular weight of water (18 g mol^{-1}) and IEC is calculated from equation (2).

The water uptake and dimensional change of the membranes were estimated by measuring their changes in weight and volume, respectively. The dry membranes were cut into 1 cm x 5 cm, and then their weights and volumes were measured. Thereafter, the membranes were immersed in deionized water at 90 ℃ for 4 h. After the membranes were taken out and wiped, their weights and volumes were measured. The volume based dimensional change was calculated as follows:

$$\text{Volume based dimensional change [\%]} = [(1+\Delta L)(1+\Delta W)(1+\Delta T) -1]\times 100 \quad (4)$$

where, ΔL, ΔW, and ΔT are the change of the length, width, thickness of the membranes, respectively.

The atomic force microscopic (AFM) observations were conducted with an INNOVA AFM instrument (BRUCKER), using a silicon-based n-type cantilever with a force constant of 1.2-20 N m^{-1} in a tapping mode. Before measurement, the membranes were dried for more than 12 h in a vacuum oven at 60 ℃.

Proton conductivities of the membranes were tested at 90 ℃ under different RH conditions. The sample was fitted to a four-point conductivity cell and connected to the test station (BekkTech, BT-552MX) for the continuous control of the cell temperatures and RH. Hydrogen gas humidified by passing the gas flow through

a humidification column using H_2 at 90 ℃ under an input flow rate of 500 cm^3 min^{-1}. The membrane was pre-equilibrated at 90 ℃ and 70% RH for 2 h, and then the conductivity measurement was started from 70% RH. The proton conductivity measurement was continued by lowering the humidity to 20% RH and then by raising to 90% RH at 10% intervals with a 30 min of stabilization time for each measurement.

The water bound state in the membrane was measured using a Modulated TA Instruments Q20 differential scanning calorimeter (DSC) at a heating rate of 10 ℃ min^{-1}. The membrane was equilibrated in 98% RH chamber and then hermetically sealed in an aluminum pan. The cooling and heating cycle was repeated in the temperature range of −80 to 20 ℃, and the melting endotherms near 0 ℃ were averaged. The content of physically-bound water was defined as the ratio of the endothermic peak area recorded for the wet sample to the endothermic heat of melting of pure water (333.6 J/g) [9] [12], referenced to the total weight of water in the sample. The content of chemically-bound water was calculated by subtracting the physically-bound water content from the total water content in the sample. The weights of physically- and chemically-bound water in the membranes were converted to hydration number (λ).

The chemical composition and concentration of the material was determined by field-emission scanning electron microscopy (FE-SEM, JEOL JSM-7800-F) in the

National Center for Inter-university Research Facilities (NCIRF) at Seoul National University, operated at an accelerating voltage of 15 kV and equipped with energy-dispersive spectroscopy (EDS). All samples were coated with platinum under vacuum prior to microscopy. The sample distance was 8.5 mm, and the magnification was × 1000.

6.3. Results and Discussion

SPAES was synthesized *via* nucleophilic aromatic substitution reaction under a nitrogen atmosphere, as described in supporting information. The chemical structure and composition of the resulting polymer was confirmed by ^{1}H NMR spectroscopy (**Figure 6.1**). The degree of sulfonation calculated from the ^{1}H NMR spectrum was 63 mol%. The number-average molecular weight (M_n) and weight-average molecular weight (M_w) calculated from the GPC measurement were 49,700 and 212,000, respectively. SPAES with chloromethyl side group (SPAES-Cl) was prepared by Fridel-Crafts alkylation of SPAES using chloromethyl methyl ether as a reagent, and tin (IV) chloride as a catalyst. The chemical structure and degree of chloromethylation of SPAES-Cl was also confirmed by ^{1}H NMR spectroscopy (**Figure 6.1**). The appearance of a new signal at around δ4.42 originating from the methine groups adjacent to the chlorine demonstrates the successful introduction of chloromethyl groups into SPAES. The content of chloromethyl group in SPAES calculated by comparing the integrals of the signals at δ7.96 and at δ4.42 was found to be 8.0 mol% per repeating unit.

The cross-linked SPAES (C-SPAES) membrane was prepared by simultaneously casting and heating the solution mixture of SPAES-Cl, trimethylamine (TEA), and

perfluoropolyether (PFPE) as the cross-linker in *N*,*N*-dimethylacetamide (DMAc). The cross-linked structure of the C-SPAES membrane could be formed by the nucleophilic substitution reaction between the hydroxyl groups in PFPE and chloromethyl groups in SPAES-Cl upon heating, where TEA was used as a basic catalyst to increase the nucleophilicity of the hydroxide (**Figure 6.2**). To illustrate the chemistry, a model reaction of PFPE with benzyl chloride was conducted as a separate experiment, under the same conditions as that used for the membrane preparation (**Figure 6.3**). The reaction scheme, ^{1}H NMR and FT-IR spectra of the reactants and product, indicated that the S_N2-type reaction between the hydroxy groups in PFPE and the chloride functionality of the benzyl compound successfully occurred at elevated temperature.

The formation of the cross-linked polymer network in the C-SPAES membrane could also be confirmed by solubility test (**Table 6.1**). The SPAES and C-PAES membranes were soaked in various solvents and water at 30 and 80 ℃ for 1 h. The membranes were not soluble in alcohols and swelled in water although different degrees of swelling between the membranes were observed. The SPAES membrane was soluble in the polar aprotic solvents such as DMAc, dimethly sulfoxide, *N*-methly-2-pyrroidone; meanwhile, the C-SPAES membrane at 30 ℃ was found to be not soluble in these solvents, but at 80 ℃, a large portion of the membrane was dissolved. This result indicates that the C-SPAES membrane has a

cross-linked structure with low cross-liking density that does not dissolve in the good solvents for SPAES, while it also has some branched parts that can be dissolved at high temperatures. The mechanical properties described in **Figure 6.4** support the cross-liked structure of the C-SPAES membrane. The fully cross-linked portion of the C-SPAES membrane estimated by measuring the weight changes before and after the gel fraction test in DMAc at 80 ℃ for 24 h was 27.8% (**Figure 6.5(a)**). The oxidative stability of the membranes was investigated to evaluate the chemical stability of the membranes against the attack of reactive oxygen species such as oxygen radicals and hydrogen peroxide. After immersing the membranes in the Fenton's reagent (3 wt% H_2O_2 containing 16 ppm Fe^{2+}) at 80 ℃, the stability was estimated by measuring the times when the membranes broke into pieces (τ_1) and dissolved completely (τ_2) (**Figure 6.5(b)**). The C-SPAES membrane was found to be much more stable than the SPAES membrane. The remarkably increased oxidative stability of the C-SPAES membrane can be ascribed to the combined effect of cross-linked structure and extremely high chemical resistance of PFPE like Teflon [13].

Figure 6.6 and **Table 6.2** show the results of the humidity dependent water uptake and hydration number (λ) of the membranes. The water uptake of the SPAES membrane increased with the RH increase, reaching 79% at 98% RH, corresponding to a λ of 17.9. The water uptake of the C-SPAES membrane also

increased with the RH increase, but the values only reached 43% (λ=11.9), due to the cross-linked structure of the C-SPAES membrane with the hydrophobic PFPE. The dimensional stability of the membranes was also evaluated by measuring their changes in dimension after being soaked in deionized water at 90 ℃ for 4 h (**Table 6.3**). The C-SPAES membrane shows a much smaller dimensional change compared to the SPAES membrane. This result clearly indicates that the cross-linked system formed by PFPE can effectively prevent the membrane from excessive water absorption, and suppress dimensional change of the membrane.

The nanophase morphology of the membranes was measured by AFM in tapping mode (**Figure 6.7**). The phase images of the membranes were recorded under ambient conditions on 500 × 500 nm^2 size scales. The dark and bright regions were assigned to the soft structure corresponding to the hydrophilic sulfonic acid groups containing water, and the hard structure corresponding to the hydrophobic polymer moieties, respectively [14]. The C-SPAES membrane was found to have more distinct hydrophilic-hydrophobic morphologies, but slightly smaller ionic clusters than the SPAES membrane possibly due to the cross-linked structure using the strongly hydrophobic perfluorinated cross-linker. Therefore, the C-SPAES membrane revealed lower water absorption and swelling behavior than the SPAES membrane as described above.

Figure 6.8 shows the proton conductivities of the membranes as a function of RH at 90 ℃. In general, the proton conductivity values of the cross-linked membranes are smaller than those of their linear polymer membrane, due to the decrease of polymer chain mobility and size of the ionic cluster that facilitate proton transport [15]. However, the proton conductivity values of the C-SPAES membrane were found to be comparable with those of the SPAES membrane, especially at low RH conditions, because the flexible perfluoro-aliphatic chain structure of PFPE can minimize the decrease in chain mobility of SPAES in the C-SPAES membrane having low cross-linking density, thus resulting hydrophilic domains were well connected with each other, showing distinct phase separated structures (**Figure 6.7**). Such phase separated morphology allows effective proton transportation of the C-SPAES membrane, even under low RH conditions, although a smaller size of hydrophilic domains was observed [16]. **Figure 6.9(a)** shows the low temperature DSC curves of the membranes equilibrated at 98% RH. The SPAES membrane shows an exothermic freezing peak at around -25 ℃ in the cooling curves and an endothermic melting peak at around -6 ℃ in the heating curves, which indicate the presence of freezable (weakly-bound) water in the membrane [9]. The areas of these two peaks are very close and their average value is about 107.1 J g^{-1}. Since the heat of fusion of pure water is about 333.6 J g^{-1}, the freezable water content in SPAES is calculated as 0.32 g per gram of the

membrane and the absorbed water amount in the SPAES membrane at 98% RH is 0.79 g. Therefore the freezable water fraction determined by DSC was about 41% of the total water absorption. The rest, 59%, was non-freezable water fraction, strongly bound to the sulfonic acid groups in the membrane. Since λ for the SPAES membrane at 98% RH was 17.9, there were 7.4 freezable water and 10.5 non-freezable water molecules per sulfonic acid group. Meanwhile, the C-SPAES membrane equilibrated at 98% RH shows exothermic and endothermic melting peaks at around -45 and -8 ℃, respectively. Since the proton concentration (impurity) of the C-SPAES membrane is greater, the peak positions of the C-SPAES membrane also move to lower temperatures compared to those of the SPAES membrane, and both peak areas of the C-SPAES membrane (≈ 36.8 J g^{-1}) were much smaller than those of the SPAES membrane. The absorbed water in the C-SPAES membrane at 98% RH was 0.43 g and corresponding λ was 11.9. Based on the above analysis used for the SPAES membrane, there were 3.1 freezable and 8.8 non-freezable water molecules per sulfonic acid group for the C-SPAES membrane. This result indicates that the incorporation of the cross-linked structure using PFPE can decrease the content of loosely-bound water much more than that of strongly-bound water, by preventing the membrane from excessive swelling. Meanwhile, the SPAES (λ= 5.6) and C-SPAES (λ= 4.8) membranes equilibrated at 50% RH exhibited no exothermic and endothermic peaks during the DSC

measurement (**Figures 6.9(b)** and **6.9(c)**), indicating that all the absorbed water molecules at low RH were in the strongly-bound state [12]. Therefore, the C-SPAES membrane utilized absorbed water more efficiently in the hydrophilic domains.

Figure 6.10(a) shows the current-voltage and power density curves for the H_2/air cells of the MEAs based on the C-SPAES and SPAES membranes at the operating conditions of 90 ℃ and 50% RH under 150 kPa. In general, membranes having larger proton conductivity values exhibit larger cell performance values than those having smaller proton conductivity values [3]. However, the operating voltages and power densities of the cell based on the C-SPAES membrane were found to be larger than those based on SPAES over the entire range of current density: the power density values at 0.65 V of the cells based on the C-SPAES and SPAES membranes are 1.17 and 0.85 mW cm^{-2}, respectively. Since the same catalyst layers with perfluoro-ionomer binder were used for the measurements, the cell performance should be attributed to membrane associated properties, such as the membrane and interfacial resistances at the membrane-electrode interface [17]. It was reported that the interfacial compatibility between membrane and electrode was affected by the fluorine concentration at the membrane-electrode interface of the MEAs form the perfluoro-ionomer as the binder or membrane materials [17, 18]. The elemental composition and concentration of the membrane surface were

analyzed by field-emission scanning microscopy coupled with energy dispersive spectroscopy (FE-SEM/EDS, **Figure 6.11**). As expected, the EDS spectrum of the C-SPAES membrane shows the additional presence of fluorine (5.14 wt.%), compared with that of the SPAES membrane. Therefore, it can be reasonably speculated that the high concentration of fluorine on the surface of the C-SPAES membrane originating from PFPE improved its compatibility with the electrode surface, resulting in the high cell performance of the MEA with the C-SPAES membrane.

Figure 6.10(b) shows the impedance spectra of two cells that were evaluated at OCV with an H_2 feed in both the anode and cathode sides at the operating conditions. The left intercept of the semi-circle represents the membrane area resistance (R_m) of the cells, and includes the membrane resistance, contact resistance, and minor ohmic losses of the electrodes [19]. The R_m value estimated from *in-situ* electrochemical impedance spectroscopy of the cell with the C-SPAES membrane, 272 mΩ cm^2, is much smaller than that of the cell with the SPAES membrane, 310 mΩ cm^2. This result combined with the EDS result indicates that the fluorine moieties on the C-SPAES membrane surface improve its compatibility with the electrode surface and decrease contact resistance between the membrane and electrodes. In addition, the fluorine moieties in the C-SPAES membrane increase the solubility of the reactant gases and this

phenomenon can increase electrochemical reaction rate in the electrode [20, 21]. The charge transfer resistance (R_{ct}), determined by electrochemical reactions including interface reaction kinetics, ionic conductivity and diffusion limitations within the catalyst layer, was estimated by the radius of the semi-circle [22]. The smaller R_{ct} value calculated from the C-SPAES membrane (40 mΩ cm^2) than that of the SPAES-membrane (80 mΩ cm^2) demonstrates the increase in electrochemical reaction rate at the membrane-electrode interface. The higher cell voltages of the cell with the C-SPAES membrane in the kinetically controlled current density region (0.25 A cm^{-2}) can be ascribed to the increase in kinetic activity due to the increase in gas concentration, as well as the compatibility with the C-SPAES membrane and electrodes. To the best of our knowledge, the cell performance of the MEA with the C-SPAES membrane is one of the best fuel cell performances ever published of a hydrocarbon-based PEM under mid-temperature and low humidity conditions, the practical operating conditions for fuel cell vehicles. The outstanding cell performances of the MEAs with the C-SPAES membranes at various operating conditions further indicate the potential applications of the C-SPAES membrane as a polymer electrolyte for various energy conversion devices (**Figure 6.12**).

6.4. Conclusions

We have successfully designed and prepared a cross-linked sulfonated poly(arylene ether sulfone) (C-SPAES) membrane using perfluoropolyether (PFPE) as a cross-linker for the first time. Compared to the linear SPAES membrane, the C-SPAES membrane showed much better chemical stability and dimensional stability, as well as effective water utilization behavior, due to the well-defined phase-separated structure from the cross-linked polymer network using PFPE. Although the proton conductivity values of the C-SPAES membrane were smaller than those of the SPAES membrane, the cell performances of the MEAs with the C-SPAES membranes were much larger than those of the MEAs with the SPAES membranes at various operating conditions, including the practical operating conditions of automotive fuel cells. This is because high fluorine concentration on the C-SPAES membrane surface improved the interfacial compatibility and decreased the contact resistance with the electrode surface. We believe that this cross-linking technology could be applicable to various PEM materials to meet the requirements of practical fuel cell applications. In addition, the C-SPAES membrane system is versatile, because this system can be easily tuned by the cross-linking density and ion exchange capacity, which can

be further optimized to address various energy applications. Further investigations on this study of cross-linked membranes are under progress.

6.4. References

[1] C. Houchins, G.J. Kleen, J.S. Spendelow, J. Kopasz, D. Peterson, N.L. Garland, D.L. Ho, J. Marcinkoski, K.E. Martin, R. Tyler, Membranes 2 (2012) 855-878.

[2] M.-C.K. Andrew M. Herring, Mei-Chen Kuo, Andrew R. Motz, Terra Dunham, V.B.2 Advanced Hybrid Membranes for Next Generation PEMFC Automotive Applications, DOE Hydrogen and Fuel Cells Program, FY 2015 Annual Progress Report (2015) V-69-V72.

[3] K. Kim, P. Heo, T. Ko, J.-C. Lee, Electrochem. Commun. 48 (2014) 44-48.

[4] A.-C. Dupuis, Prog. Mater Sci. 56 (2011) 289-327.

[5] S. Bose, T. Kuila, T.X.H. Nguyen, N.H. Kim, K.-t. Lau, J.H. Lee, Polymer membranes for high temperature proton exchange membrane fuel cell: recent advances and challenges, Prog Polym. Sci. 36 (2011) 813-843.

[6] H. Zhang, P.K. Shen, Recent development of polymer electrolyte membranes for fuel cells, Chem. Rev. 112 (2012) 2780-2832.

[7] T. Ko, K. Kim, B.K. Jung, S.H. Cha, S.K. Kim, J.C. Lee, Cross-Linked Sulfonated Poly(arylene ether sulfone) Membranes Formed by in Situ Casting and Click Reaction for Applications in Fuel Cells, Macromolecules 48 (2015) 1104-

1114.

[8] N.R. Kang, S.Y. Lee, D.W. Shin, D.S. Hwang, K.H. Lee, D.H. Cho, J.H. Kim, Y.M. Lee, Effect of end-group cross-linking on transport properties of sulfonated poly (phenylene sulfide nitrile) s for proton exchange membranes, J. Power Sources 307 (2016) 834-843.

[9] K. Si, R. Wycisk, D.X. Dong, K. Cooper, M. Rodgers, P. Brooker, D. Slattery, M. Litt, Rigid-Rod Poly(phenylenesulfonic acid) Proton Exchange Membranes with Cross-Linkable Biphenyl Groups for Fuel Cell Applications, Macromolecules 46 (2013) 422-433.

[10] W.L. Harrison, F. Wang, J.B. Mecham, V.A. Bhanu, M. Hill, Y.S. Kim, J.E. McGrath, J. Polym. Sci., Part A: Polym. Chem. 41 (2003) 2264-2276.

[11] A. Milani, J. Zanetti, C. Castiglioni, E. Di Dedda, S. Radice, G. Canil, C. Tonelli, Eur. Polym. J. 48 (2012) 391-403.

[12] K. Si, D.X. Dong, R. Wycisk, M. Litt, J. Mater. Chem. 22 (2012) 20907-20917.

[13] J.P. Rolland, R.M. Van Dam, D.A. Schorzman, S.R. Quake, J.M. DeSimone, J. Am. Chem. Soc. 2004, 126, 2322-2323.

[14] K. Nakabayashi, K. Matsumoto, T. Higashihara, M. Ueda, J. Polym. Sci. Part A: Polym. Chem. 46 (2008) 7332-7341.

[15] K. Kim, P. Heo, T. Ko, K.-h. Kim, S.-K. Kim, C. Pak, J.-C. Lee, J. Power

Sources 293 (2015) 539-547.

[16] T. Mochizuki, M. Uchida, K. Miyatake, ACS Energy Letters 1 (2016) 348-352.

[17] C.H. Lee, S.Y. Lee, Y.M. Lee, S.Y. Lee, J.W. Rhim, O. Lane, J.E. McGrath, Acs Appl. Mater. Inter. 1 (2009) 1113-1121.

[18] Y.S. Kim, M.J. Sumner, W.L. Harrison, J.S. Riffle, J.E. McGrath, B.S. Pivovar, J. Electrochem. Soc. 151 (2004) A2150-A2156.

[19] S.-J. Seo, J.-J. Woo, S.-H. Yun, H.-J. Lee, J.-S. Park, T. Xu, T.-H. Yang, J. Lee, S.-H. Moon, Phys. Chem. Chem. Phys. 12 (2010) 15291-15300.

[20] S. Gottesfeld, I. Raistrick, S. Srinivasan, J. Electrochem. Soc. 134 (1987) 1455-1462.

[21] D.R. Lawson, L.D. Whiteley, C.R. Martin, M.N. Szentirmay, J.I. Song, J. Electrochem. Soc. 135 (1988) 2247-2253.

[22] S.K. Kim, K.H. Kim, J.O. Park, K. Kim, T. Ko, S.W. Choi, C. Pak, H. Chang, J.C. Lee, J. Power Sources 226 (2013) 346-353.

Table 6.1 Solubility test results of SPAES and C-SPAES membranes in a variety of solvents.

Membranes	DMSO	DMAc	DMF	NMP	EtOH	MeOH	Water
SPAES	++	++	++	++	Δ	Δ	Δ
C-SPAES	±	±	±	±	-	-	Δ

++, soluble at 30 °C; +, soluble at 80 °C; ± partially soluble at 80 °C; Δ swelling at 80 °C; - insoluble even at 80 °C.

Table 6.2 Ion exchange capacity (IEC) and hydration number (λ) of the membranes.

Membrane	IEC[a] (mequiv g^{-1})	λ (H_2O/SO_3H)								
		20%[b]	30%[b]	40%[b]	50%[b]	60%[b]	70%[b]	80%[b]	90%[b]	98%[b]
SPAES	2.4	2.7	3.1	4.3	5.6	7.0	7.9	9.9	13.1	17.9
C-SPAES	2.0	2.3	3.4	4.4	4.8	5.4	6.3	7.6	8.5	11.9

[a] Determined experimentally by acid-base titration.

[b] Given relative humidity conditions at 90 ℃.

Table 6.3 Water uptake (WU) and dimensional change of the membranes after being immersed in deionized water at 90 °C for 4 h.

Sample	WU (%)	Dimensional change[a] (%)				
		ΔL	ΔW	ΔT	ΔA	ΔV[b]
SPAES	243.6	33.6	28.0	154.5	71.1	335.3
C-SPAES	167.3	14.4	20.0	92.3	37.3	147.2

[a] Calculated by equation (4).

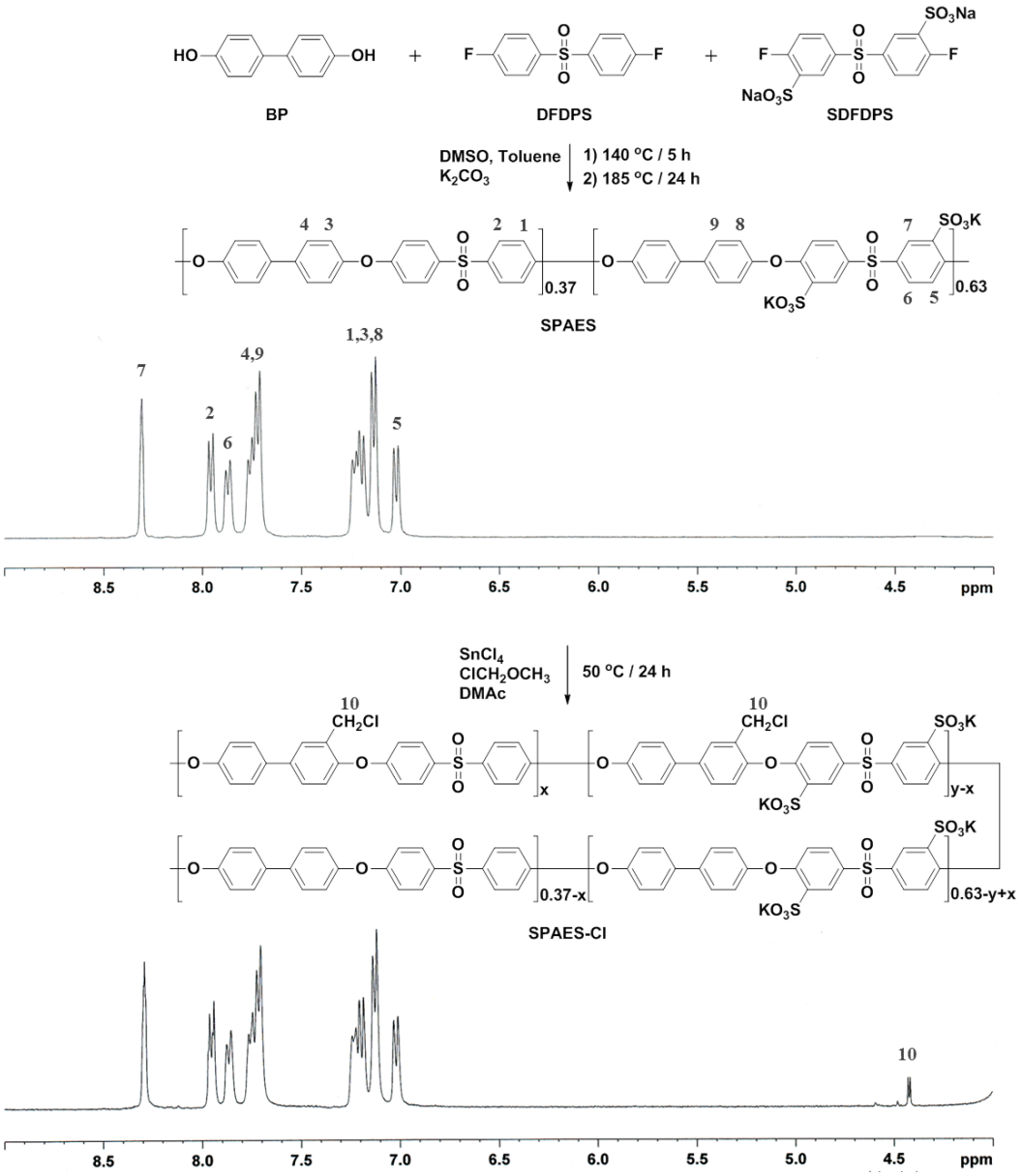

Figure 6.1 ^{1}H NMR spectra of (a) SPAES and (b) SPAES-Cl.

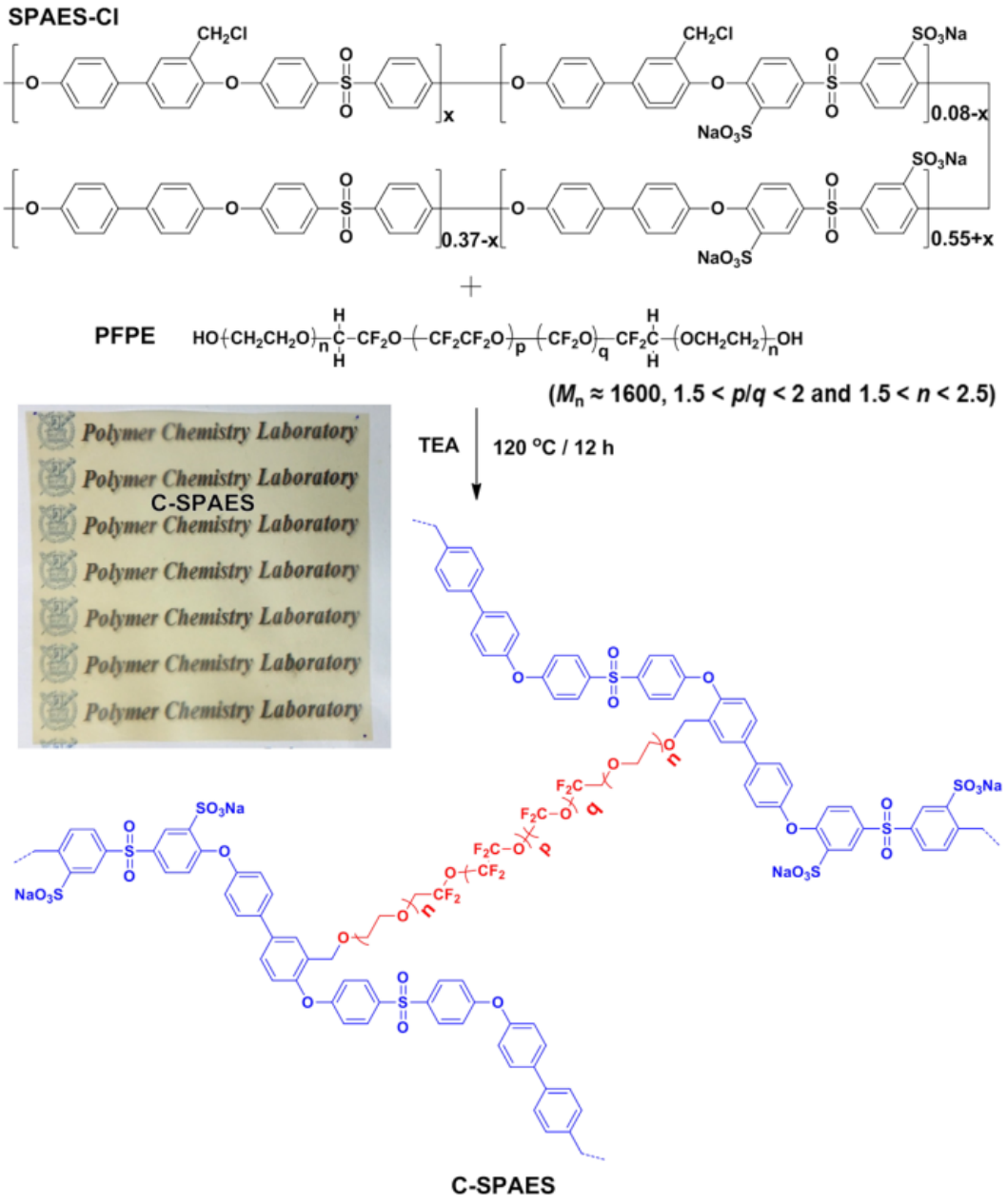

Figure 6.2 Chemical structures of SPAES-Cl, PFPE and preparation route to C-SPAES membrane, wherein the photo-image of the C-SPAES membrane is included.

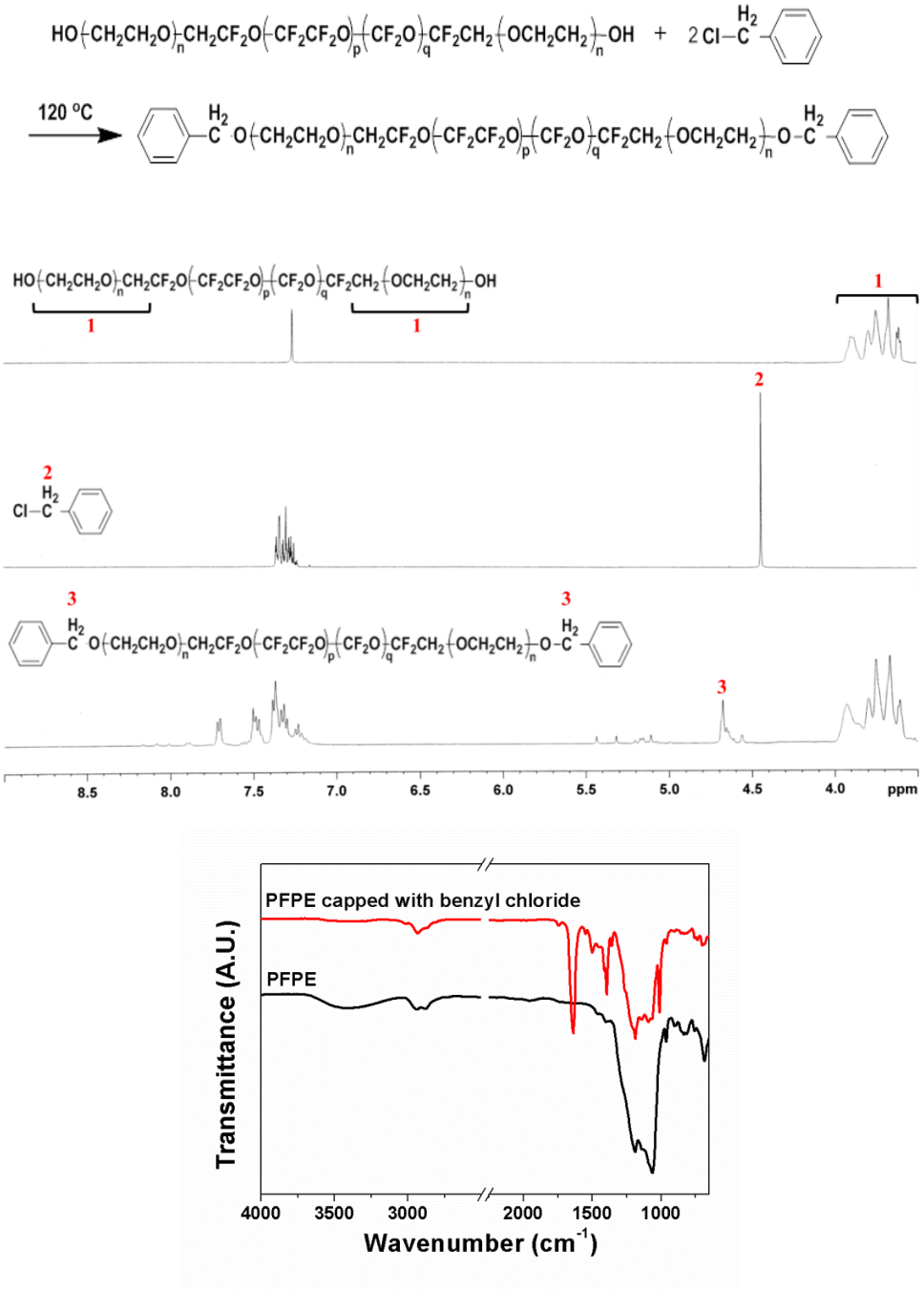

Figure 6.3 Model reaction of PFPE with benzyl chloride and their ^{1}H NMR and FT-IR spectra.

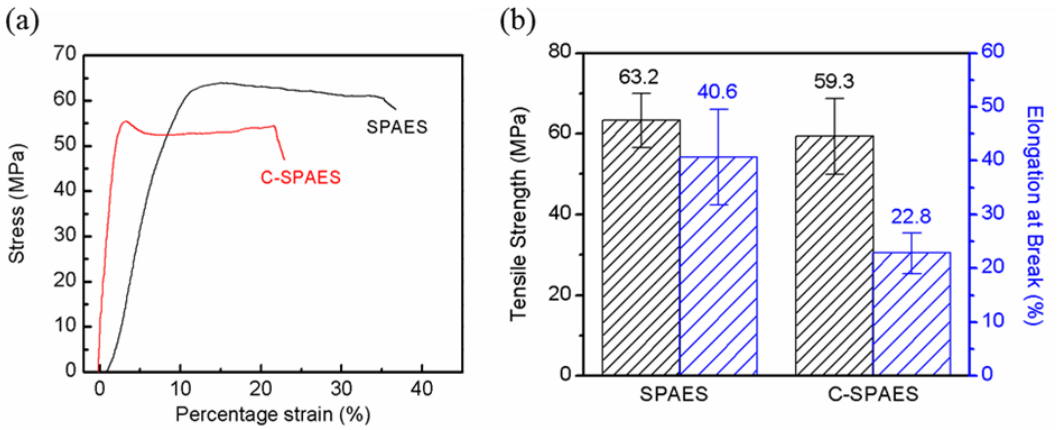

Figure 6.4 Mechanical properties of SPAES and C-SPAES membranes at 23 °C and 45% RH: (a) stress-strain curves of the membranes, and (b) average tensile strength and elongation at break values of the membranes.

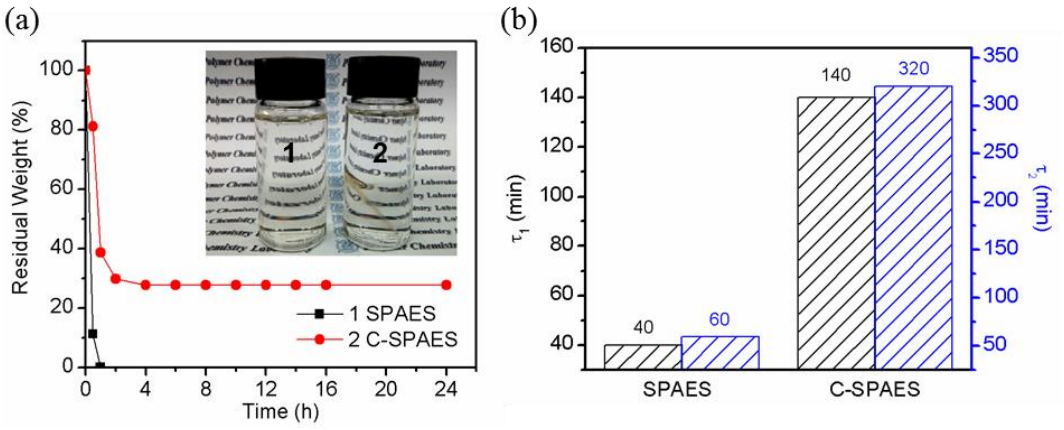

Figure 6.5 (a) Residual weights of SPAES and C-SPAES membranes after the gel fraction test in DMAC at 80 °C for 24 h. The photo image shows the DMAc solutions after the gel fraction test. (b) Chemical stability of SPAES and C-SPAES membranes using a Fenton's reagent (3 wt% H_2O_2 aqueous solution containing 16 ppm Fe^{2+}) at 80 °C.

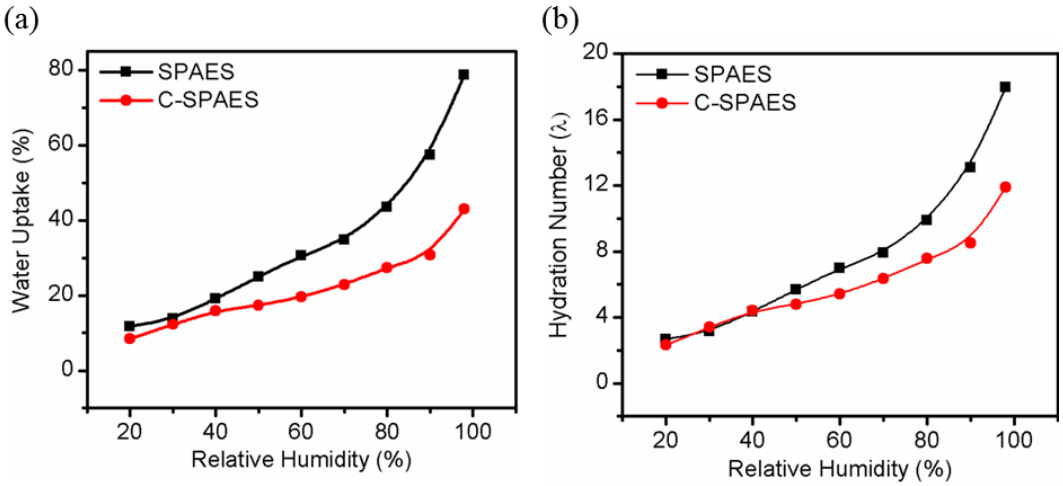

Figure 6.6 (a) Water uptake and (b) hydration number (λ) of SPAES and C-SPAES membranes as a function of relative humidity at 90 °C

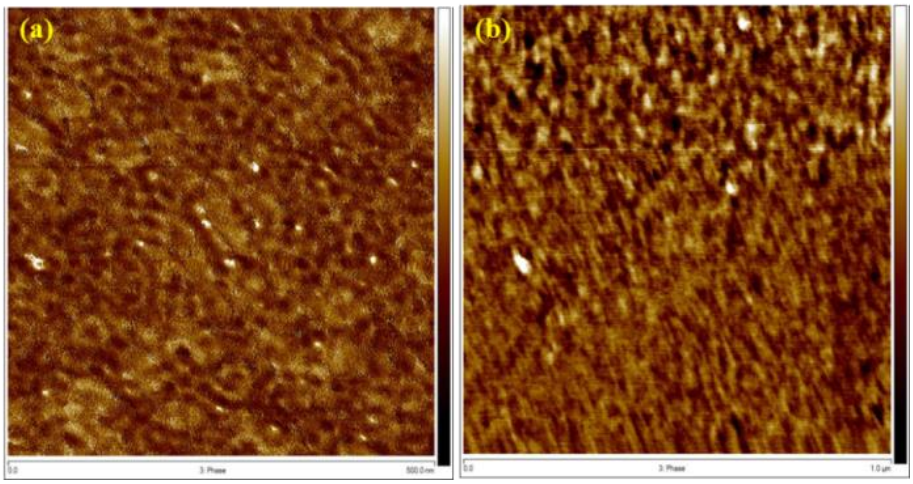

Figure 6.7 AFM tapping mode phase images of (a) SPAES and (b) C-SPAES membrane: Scan size is 500 × 500 nm^2

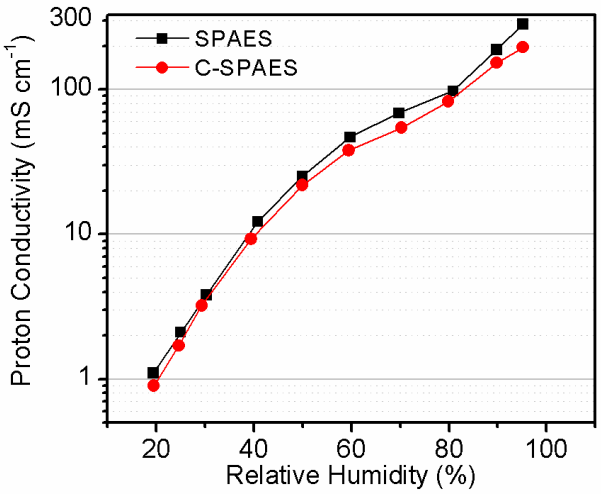

Figure 6.8 Proton conductivity of SPAES and C-SPAES membrane at 90 ℃ as a function of relative humidity.

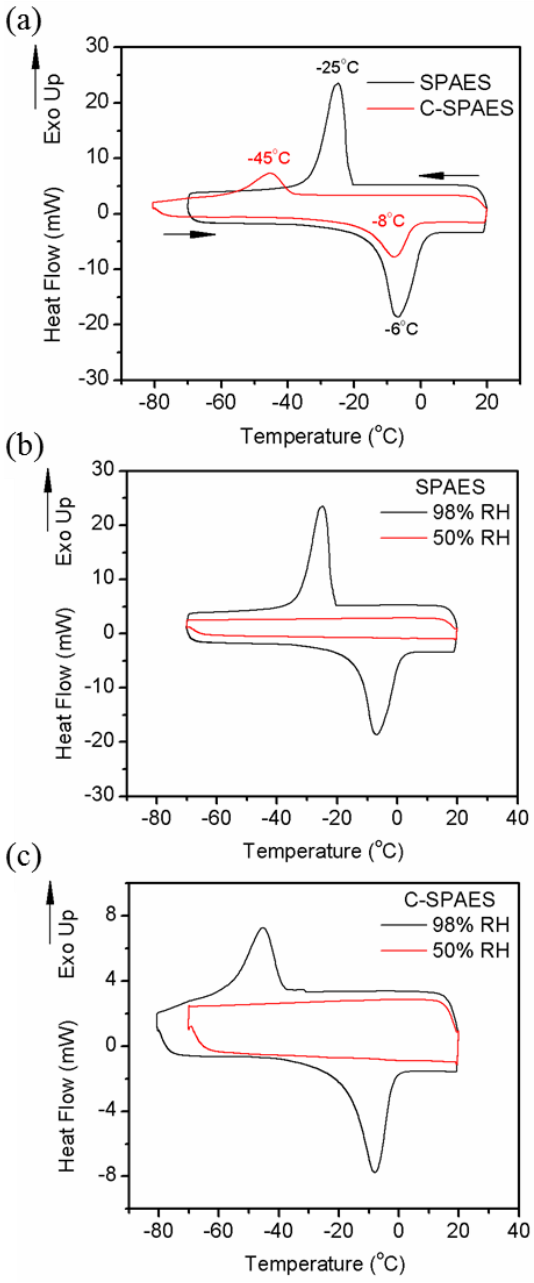

Figure 6.9 Low-temperature DSC thermograms of the membranes: (a) SPAES (black) and C-SPAES (red) membranes equilibrated at 98% RH

prior to measurement, (b) SPAES membrane equilibrated at 98% RH (black) and 50% RH (red), and (c) C-SPAES membrane equilibrated at 98% RH (black) and 50% RH (red).

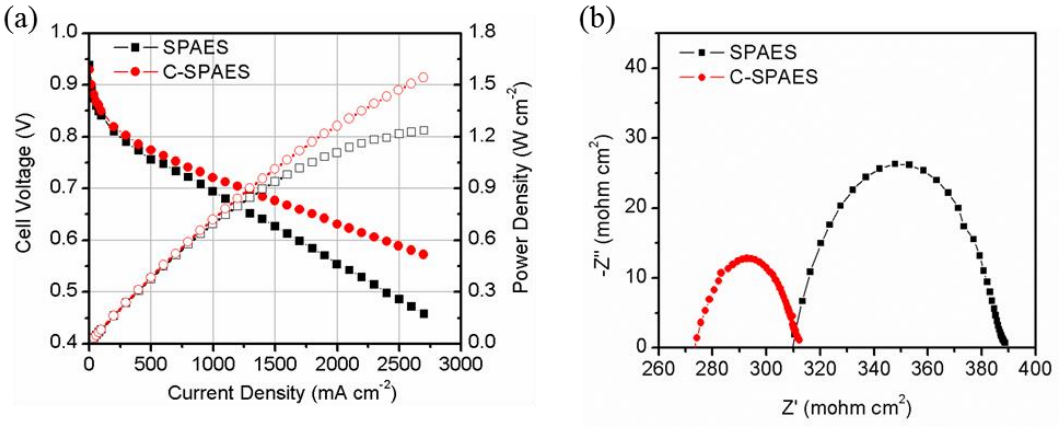

Figure 6.10 (a) Cell performances of MEAs prepared using SPAES, C-SPAES membranes at 90 °C and 50% RH under 150 kPa conditions. Active area of MEA was 25 cm^2 and humidified H_2/air was supplied as feed gases during the measurements. (b) Nyquist plots for cells employing C-SPAES (circle) and SPAES (square) membranes in symmetrical mode with H_2/H_2 at 90 °C and 50% RH under 150 kPa conditions.

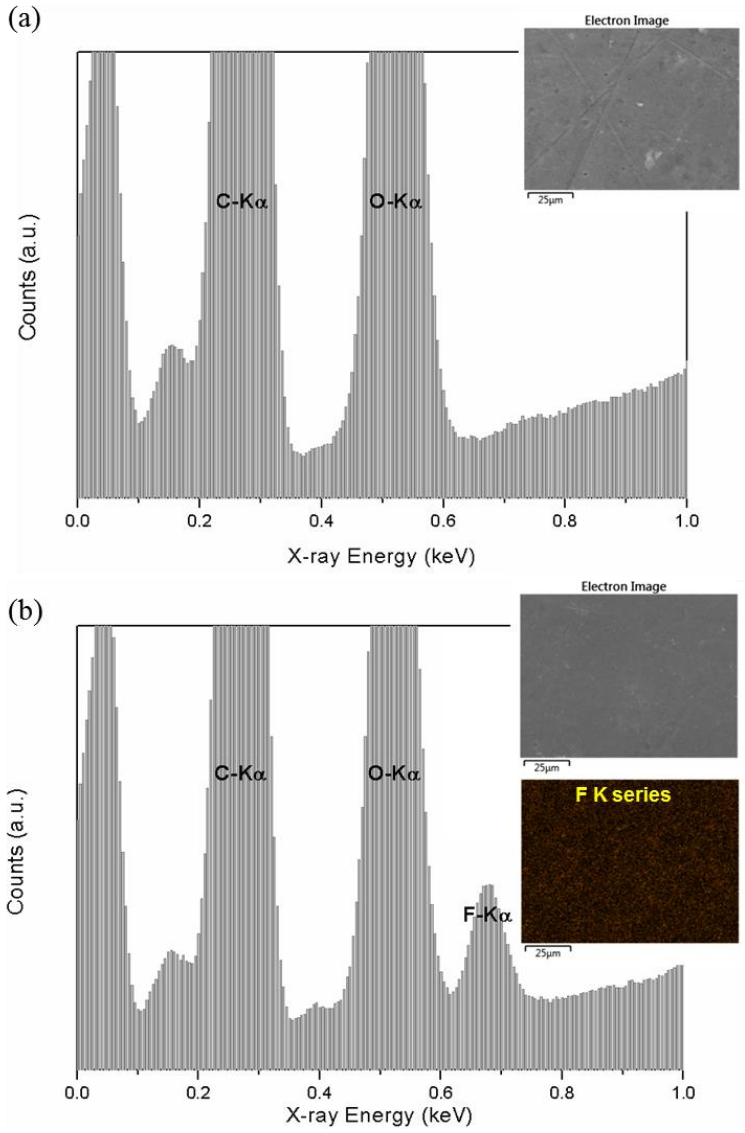

Figure 6.11 EDS spectra of (a) SPAES and (b) C-SPAES membrane. Wherein, surface SEM images and EDS mapping for fluorine of the membranes were included.

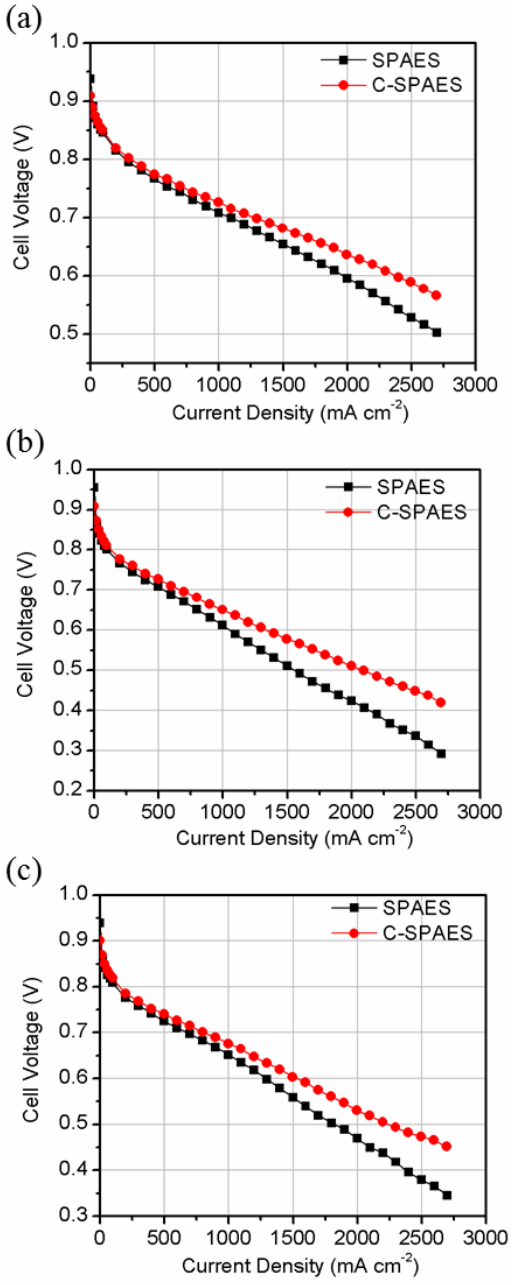

Figure 6.12 Cell performances of MEAs prepared using SPAES and C-SPAES membranes at different operating conditions: (a) 90 °C and 100% RH

under 150 kPa, (b) 60 °C and 50% RH, and (c) 60 °C and 100% RH. Active area of MEA was 25 cm^2 and humidified H_2/air was supplied as feed gases during the measurements.

초 록

본 연구에서는 술포화 폴리(아릴렌 에테르 술폰) (SPAES)을 기반으로 한 고분자 물질의 합성과 분석, 그리고 이를 고온, 저가습 구동용 연료전지 전해질 막으로 응용한 연구에 대하여 기술하였다. 첫째로, SPAES를 기반으로 한 두 종류의 준 관입 망상 구조 (*semi*-IPN)의 전해질 막을 제조하여 고온, 저가습 구동용 연료전지에 사용하고자 하였다. 바이닐포스포닉산 (VPA) 과 SPAES가 녹아있는 *N,N*-디메틸아세트아마이드 용액에 디에틸렌글리콜 디메타크릴레이트 (DEGDMA)와 비스(2-(메타크릴옥실옥시)에틸) 포스페이트 (BMAEP)를 각각 가교제로 사용하여 혼합한 후 캐스팅하고 가열함으로써 가교제의 종류에 따른 두 가지 다른 구조를 갖는 *semi*-IPN 전해질 막을 제조하였다. 제조된 *semi*-IPN 전해질 막의 경우 VPA의 도입을 통해 고온, 저가습 조건에서 전해질 막의 수소 이온 전도도를 크게 향상시켰으며, DEGDMA 혹은 BMAEP와 같은 가교제를 사용하여 안정적인 가교 구조를 도입함으로써 선형 고분자인 폴리바이닐포스포닉산이 형성됨에 따라 발생될 수 있는 물리화학적 안정성의 저하를 큰 폭으로 감소시켰다. 또한 BMAEP를 사용하여

제조된 *semi*-IPN 전해질 막의 경우 BMAEP 자체에 수소 이온을 전달 할 수 있은 작용기가 도입되어 있어 가교 구조 도입으로 인한 전해질 막의 수소 이온 전도도 저하 문제를 개선 할 수 있었다. DEGDMA와 BMAEP를 사용하여 만들어진 각각의 *semi*-IPN 전해질 막을 이용하여 막-전극 접합체를 제조한 후 120 °C, 40% 가습 조건에서 셀 성능을 측정 해 보았을 때, SPAES 단일 전해질 막을 이용한 막-전극 접합체보다 훨씬 향상된 셀 성능을 구현 할 수 있었다. 장기 내구성 실험 결과 두 종류의 *semi*-IPN 전해질 막 모두 SPAES 단일 전해질 막에 비해 낮은 수소 투과도 및 높은 셀 성능을 장 시간 유지하는 것을 확인하였으며, 이를 통해, 실제 고온, 저가습 구동 조건에서 *semi*-IPN 전해질 막의 우수한 성능 및 전기화학적 안정성을 확인할 수 있었다.

두번째로, 가교된 벤족사진-벤즈이미다졸 공중합체를 기반으로 한 다공성 지지체에 술폰화도가 다양한 SPAES를 충진하여 술폰화도가 다른 SPAES가 각각 충진 된 다공 충진 전해질 막들을 제조하고, 이를 고온, 저가습 구동용 연료전지의 전해질 막으로 사용하고자 하였다. SPAES 고분자의 경우 4,4′-디하이드록시바이페닐 단량체

대비 디플루오루 작용기를 갖는 두 종류의 단량체인 4,4′-디플루오루디페닐술폰과 디술포네이트 4,4′-디플루오루디페닐술폰의 몰비율 조절을 통해 다양한 술폰화도를 갖도록 합성되었다. 가교된 벤족사진-벤즈이미다졸 공중합체 기반의 다공성 지지체의 경우, 폴리벤즈이미다졸 (PBI)과 3-페닐-3,4-디하이드로-6-터트-부틸-2*H*-1,3-벤족사진 (*p*BUa) 에 포로젠 물질인 디부틸프탈레이트를 혼합 한 후, 캐스팅 및 열처리 과정과 포로젠을 제거하는 단계를 거쳐 제조되었다. 가교된 벤족사진-벤즈이미다졸 공중합체 기반의 다공성 지지체에 다양한 술폰화도를 갖는 SPAES 고분자를 충진하여 만들어진 다공 충진 전해질 막들의 경우, SPAES 단일 전해질 막들에 비해 매우 향상된 기계적 강도 및 체적 안정성을 나타내었으나, 수소 이온 전도도의 경우 SPAES 단일 전해질 막에 비하여 낮은 수치를 나타내었다. 하지만, 다공 충진 전해질 막들의 경우 향상된 기계적 강도로 인하여 매우 얇으면서도 안정적인 전해질 막을 제조할 수 있었고, 실제 막-전극 접합체를 제조하는 과정에서 매우 얇은 두께의 막을 이용함에 따라 고온, 저가습 (120 °C, 40%) 조건에서 셀 구동시 전해질 막의 두께에 의해 영향을 받는 막 저항을 크게 줄일 수 있어

SPAES 단일 전해질 막을 이용한 막-전극 접합체보다 크게 향상된 셀 성능을 구현 할 수 있었다.

세번째로, 수소 이온 전달 능력이 있는 가교된 벤족사진-벤즈이미다졸 공중합체 구조의 다공성 지지체를 개발하고 이를 기반으로 다공 충진 전해질 막을 제조하여 고온, 저가습 구동용 연료전지의 전해질 막으로 사용하고자 하였다. 수소 이온 전달 능력이 있는 다공성 지지체의 경우, PBI 와 소듐 3-(4-술포나토페닐)-3,4-디하이드로-2*H*-1,3 벤족사진-6-술포네이트 (*p*S) 에 포로젠 물질인 디부틸프탈레이트를 혼합 한 후, 캐스팅 및 열처리 과정과 포로젠을 제거하는 단계를 거쳐 제조되었다. 개발된 다공성 지지체의 경우 친수성도 조절이 용이하였으며 구동 조건에서 수소 이온 전도 특성을 나타내었다. 다공 충진 전해질 막은 개발된 다공성 지지체에 술폰화도가 70몰%인 SPAES를 충진하여 제조되었다. 제조된 다공 충진 전해질 막의 경우 SPAES 단일 전해질 막에 비해 매우 향상된 체적 안정성 및 기계적 강도를 나타내었으며, 수소 이온 전도성이 없는 가교된 벤족사진-벤즈이미다졸 공중합체 구조의 다공성 지지체를 기반으로 한 다공 충진 전해질 막에 비해, 높은 수소 이온 전도도를 나타내었다. 실제 수소 이온 전도성이 있는 다공성 지지체를 기반으로 한 다공 충진 전해질

막을 이용하여 막-전극 접합체를 제조한 후 고온, 저가습 (120 °C, 40%) 구동 조건에서 셀 성능을 측정하였을 경우, 수소 이온 전도성이 없는 다공성 지지체를 기반으로 한 다공 충진 전해질 막을 이용한 막-전극 접합체에 비해 향상된 셀 성능을 구현 할 수 있었다.

마지막으로, 퍼플루오루폴리에테르 (PFPE)를 가교제로 사용하여 고온, 저가습 구동조건에서 우수한 셀 성능 구현이 가능한 가교된 SPAES (C-SPAES) 전해질 막을 제조 할 수 있는 간단하면서도 효과적인 가교 방법을 제시하고자 하였다. C-SPAES 전해질 막의 경우 클로로메틸기가 도입된 SPAES가 녹아있는 용액에 가교제인 PFPE를 혼합한 후, 캐스팅 및 열처리 과정을 거쳐 제조되었다. 매우 소수성이며 유연한 사슬 구조를 갖는 PFPE를 이용하여 가교 구조가 형성됨에 따라 C-SPAES 전해질 막의 경우 뚜렷한 미세 상분리 구조가 형성되었고, 이로 인해 SPAES 단일 전해질 막과 비교시, 이온 전도도 저하가 거의 없이 향상된 물리화학적 안정성을 나타내었다. 또한 불소계 가교제인 PFPE를 도입함에 따라 전극과의 계면 접합 특성이 크게 향상되어 C-SPAES 전해질 막을 이용한 막 전극 접합체를 제조한 후 고온, 저가습 (90 °C, 50%, 150 kPa) 구동

조건에서 셀 성능을 측정하였을 경우, SPAES 단일 전해질 막을 이용하여 제조된 막-전극 접합체에 비해 매우 향상된 셀 성능을 구현할 수 있었다.

주요어: 술포네이트 폴리(아릴렌 에테르 술폰), 고분자 전해질 막 연료전지, 관입 망상 구조 전해질 막, 다공 충진 전해질 막, 가교 구조 전해질 막.

학번: 2013-30277 성명: 김기현